

DEPARTMENT OF PHYSICS AND ASTRONOMY
UNIVERSITY OF HEIDELBERG

THE NEUTRINOLESS DOUBLE BETA DECAY AT THE LHC:
ANALYZING THE LAMBDA-DIAGRAM

MASTER THESIS
IN PHYSICS

submitted by

PHILIPP SEBASTIAN GERNANDT
born in Kastl, Germany

Heidelberg
2017

Acknowledgements

I want to thank Dr. Werner Rodejohann for the opportunity to carry out my master thesis under his supervision, Dr. Buphal Dev for his support and answers regarding neutrino physics, as well as Prof. Dr. Manfred Linder and the whole staff of the MPIK for supplying this friendly, scientific environment at the Astroparticle Physics division at the Max Planck Institute for Nuclear Physics Heidelberg.

I thank my colleagues and group members for the interesting and amusing discussions and coffee breaks. I appreciated the time very much. Furthermore, I gratefully thank Max Hartmann, Nils Mößner, Sebastian Weber, Daniel Jimenez Tejero, Moritz Platscher, Thomas Rink and Thomas Hügler for proof reading this thesis.

Finally I would like to thank my girlfriend Franziska Rother for her support during the writing of this work and my mother for her love, care and helpful advises for more than a quarter of a century.

MASTER THESIS

carried out by

Philipp Gernandt

at the

MAX PLANCK INSTITUTE FOR NUCLEAR PHYSICS
Saupfercheckweg 1, 69117 Heidelberg

submitted to the

DEPARTMENT OF PHYSICS AND ASTRONOMY

University of Heidelberg

on March 7, 2017

SUPERVISOR: Dr. rer. nat. Werner Rodejohann

Abstract

In this work the cross section of the high energy equivalent to the neutrinoless double beta decay is investigated for the λ diagram contribution on the level of quark-quark interaction. As a theoretical framework the Left Right symmetric model has been adopted and is presented in the thesis. The cross sections are derived by analytical considerations combined with numerical simulations with the particle interaction simulator Mad Graph 5. As a result, upper limits on the expected signals are derived by applying the restrictions resulting from the non observation of neutrinoless double beta decay of xenon and electroweak precision measurements. The focus of this work is on the t -channel diagram and it is found that the cross section in the quark-quark interaction involving light neutrino propagators can be as large as 10^{-11} pb, whereas the heavy neutrino contribution can reach up to 10^{-7} pb. For the case of a resonantly produced W_R^- boson in the s -channel, a cross section $\sigma \leq \mathcal{O}(10 \text{ pb})$ is possible in the most promising case.

Zusammenfassung

In dieser Arbeit wird der Beitrag des λ -Diagrams zum Wirkungsquerschnitt des neutrinolosen Doppel-Betazerfalls bei hohen Energien untersucht. Die Wechselwirkung wird auf Parton-Niveau betrachtet und der Fokus liegt auf dem t -Kanal. Als theoretisches Model wird das Links Rechts symmetrische Model verwendet, welches in der Arbeit ausführlich eingeführt wird. Die Näherungen für die Wirkungsquerschnitte werden mit Hilfe analytischer Betrachtungen, unterstützt von numerischen Simulationen hergeleitet. Hierfür wird der Monte Carlo Simulator Mad Graph 5 verwendet. Aus den Ergebnissen und unter Verwendung der Limits auf die Halbwertszeit von Xenon, sowie den Daten aus Präzisionsmessungen zur elektroschwachen Wechselwirkung werden obere Grenzen für das Signal berechnet.

Für den t -Kanal ergibt sich unter Einbezug von leichten Neutrinos ein Wirkungsquerschnitt von maximal 10^{-11} pb, werden schwere Neutrinos berücksichtigt, erhöht sich dieser auf höchstens 10^{-7} pb. Im Falle eines resonant produzierten, schweren W_R^- Bosons im s -Kanal ist $\sigma \leq \mathcal{O}(10 \text{ pb})$ möglich.

Table of contents

Table of contents	I
1 Introduction	1
2 Theory	7
2.1 The Standard Model of particle physics and massive fermions	7
2.2 Extending the Standard Model: seesaw mechanisms	10
2.2.1 Type-I seesaw	11
2.2.2 Type-II seesaw	13
2.2.3 Type-III seesaw	14
2.3 The Left Right symmetric model	16
2.3.1 Particle content, couplings and symmetry	16
2.3.2 Generating masses	20
2.3.3 Charged weak interactions with neutrinos	29
2.3.4 Limits and constraints	31
3 Neutrinoless double beta decay	35
3.1 Contributing amplitudes in the Left Right symmetric model	35
3.2 Nuclear matrix elements and half lives	41
4 Analysing the lambda diagram at the Large Hadron Collider	43
4.1 Limits on the t -channel cross section σ_{λ}^t	48
4.2 Estimates on the s -channel cross section σ_{λ}^{sRL} mediated by light neutrinos	52
4.3 Summary and conclusions	54
A Relevant particle decay widths	57
B Analytical approximations for the λ diagram cross sections	59
B.1 t -channel cross section	60
B.2 s -channel cross section with left-handed final state quarks	66
C Mad Graph 5: a monte carlo simulator	71
C.1 The program	71
C.2 The model file for the Left Right symmetric model	75

Table of contents

Bibliography	89
Statement of authorship	95

Chapter 1

Introduction

The Standard Model of Particle Physics successfully describes most of the phenomena that we observe regarding particles and fundamental interactions. Many experiments in low and high energy physics have formed this theory throughout the last century and finally confirmed its validity up to high precision. The discovery of predicted particles like the Z - and the Higgs boson [1–3], as well as other mechanisms, have established it beyond any doubt. Nevertheless, some questions still remain open: What is dark matter, for example, how did Baryogenesis happen and how can gravity be quantized? Scientists around the world work with great effort to solve these and many other problems.

The question we want to address in this thesis is another one: How do neutrinos acquire their mass and why is it so small? The Standard Model does not include a mass term for the three neutrinos ν_e , ν_μ and ν_τ . By the time the theory was formed, it was believed that they are massless and experiments found that these particles have negative helicity [4] in agreement with the V-A structure of the Standard Model's weak interaction. Consequently, neutrinos are strictly left-handed particles in the Standard Model which forbids the usual mass term.

However, in the 1970s the solar neutrino problem arose with the measurements of the Homestake experiment [5, 6]. It stated a deficit of electron neutrinos arriving from the sun with respect to the theoretical expectations from calculations based on the standard solar model. Further experiments were carried out: Super-Kamiokande measured flavour-oscillations in atmospheric neutrinos [7], KamLAND announced the disappearance of reactor neutrinos [8, 9] and the K2K Collaboration examined oscillations in neutrinos emitted from accelerators[10]. The idea of oscillating neutrinos was actually not new – Pontecorvo suggested it already in 1957 [11, 12]. However, a necessary criterion for oscillation is neutrino mass. This was finally established by the SNO experiment in 2002 which measured a total solar neutrino flux compatible with theory[13]. The discovery was just recently awarded with the Nobel Prize for physics in 2015[14].

Today the absolute masses of the three standard model neutrinos are still unknown, but already constrained to be at most of $\mathcal{O}(\text{eV})$ [15, 16]. The question therefore is, by which mechanism such small masses are generated. In principle, the well known Higgs Mechanism could give mass to the neutrinos just like to the other fermions. However,

as neutrinos are lighter than their electroweak partners e , μ and τ by at least a factor of 10^{-6} , this is regarded as unnatural as it would require very small Yukawa Couplings.

Many attempts have been made to find a model that can describe neutrino masses in an elegant way. A common approach is to use an effective theory which reflects the low energy manifestation of the high energy physics that is not accessible to us in full detail. This means that some heavy field mediates the interaction but is not produced on-shell and only acts on short distances — just like in the case of Fermi interaction. Assuming order one couplings, the scale of the new physics is determined by the mass of the heavy field which has to be integrated out. The operators of such effective field theories are of dimension $d > 4$ and thus are not renormalizable. Furthermore they are suppressed by the new energy scale Λ as they are proportional to Λ^{-1} .

Weinberg showed that the only dimension 5 operator being both invariant under the Standard Model gauge groups and Lorentz invariant is the well-known Weinberg operator [17–19]

$$\mathcal{L}_{\text{eff}}^{d=5} = -\frac{c_{ij}}{\Lambda} \overline{L_{Li}^c} \tilde{\Phi}^* \tilde{\Phi}^\dagger L_{Lj} + \text{h.c.} \xrightarrow{\text{SSB}} -c_{ij} \frac{v^2}{2\Lambda} \overline{\nu_{Li}^c} \nu_{Lj} + \text{h.c.}, \quad (1.1)$$

with L_L being the left-handed lepton doublet and L_L^c its charge conjugate. $\tilde{\Phi}$ is the conjugate Higgs doublet and c_{ij} the coupling coefficients in the lepton flavour space.¹ After spontaneous symmetry breaking (SSB) the Higgs field acquires a non-vanishing vacuum expectation value $v/\sqrt{2}$ and generates mass terms $(m_\nu)_{ij} = c_{ij}v^2/\Lambda$ for the neutrinos as given above.

Equation (1.1) suggests that this operator could couple neutrinos ν with its antiparticles ν^c to form a mass term. In Section 2.3 we will see that this essentially leads to so-called Majorana neutrinos, which are fermions and anti-fermions at the same time — as opposed to usual Dirac Neutrinos which can be distinguished from their anti-particles. The question about neutrino masses is therefore not only a question about the exact value of their mass, but rather connects to many other topics such as Lepton Number Violation, CP-Violation or the Hierarchy Problem.

With $v \approx 246$ GeV being fixed by the Standard Model, two ways to generate small neutrino masses from the above operator are possible: Either the coefficients c_{ij} are small or the energy scale Λ is large — or something in-between. There are three different types of high energy tree level interactions that can lead to the Weinberg operator at low energies[19]: The so-called seesaw mechanisms of type I, II and III which are schematically shown in Figure 1.1.

In the type-I seesaw model, heavy right-handed neutrinos couple to the left-handed Standard Model Neutrinos; the energy-scale in this case can be identified with the heavy

¹ The nomenclature and conventions are rigorously explained in the introduction of the Left Right symmetric model in Section 2.3. Note that a left handed charge conjugate spinor behaves like a right handed spinor.

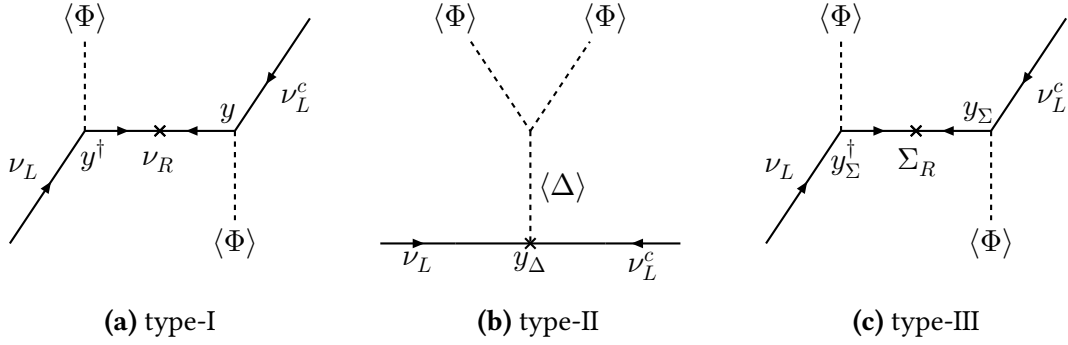


Fig. 1.1 – Type I, II and III seesaw mechanisms: The light neutrino ν_L acquires a mass through the coupling to the Higgs field Φ and the heavy particle ν_R , Δ or Σ_R , respectively. By means of this mechanism the neutrino is connected to its antiparticle ν_L^c . The corresponding Yukawa couplings are indicated as y_i .

neutrino mass $\Lambda \sim M_N$. The type-II seesaw mechanism makes use of heavy scalar triplet fields Δ coupling to the left handed fermions with $\Lambda \sim M_\Delta$ and the type-III seesaw mechanism uses heavy fermionic triplets Σ ; $\Lambda \sim M_\Sigma$ in the last case. More rigorous calculations and explanations concerning the three types of seesaw mechanisms are presented in Section 2.2.

Unfortunately, it is very difficult to probe small masses or very high energies experimentally. Therefore, it is important to analyse the different scenarios both theoretically and by means of simulations in order to be able to predict promising channels and expected signals. One of these possible channels to investigate the origin of the neutrino masses is the neutrinoless double beta decay ($0\nu\beta\beta$) [20, 21]. This process is only possible if the neutrino is a Majorana particle. In that case it can trigger the decay of certain nuclei analogous to the usual beta decay, with the difference being that no neutrino is emitted but only two electrons:

$${}^A_Z X \xrightarrow{0\nu\beta\beta} {}^A_{Z+2} X' + 2e^-.$$

As Nature also allows for the $2\nu\beta\beta$ decay, in which two electrons and two neutrinos are emitted and which is hard to distinguish from the above process due to the difficulties in detecting neutrinos, there are only a few isotopes that are regarded candidates for the observation of the $0\nu\beta\beta$ decay. The SNO+ experiment uses ${}^{130}\text{Te}$ for example [22], a ${}^{76}\text{Ge}$ detector is used in GERDA [23] and SuperNEMO [24] studies ${}^{82}\text{Se}$ decays. However, so far no decay has been detected. The lower limits on the half-lives of the isotopes in this decay thus result in stringent constraints on the physical quantities in seesaw models [21].

The underlying particle interaction in the $0\nu\beta\beta$ decay involves quarks and can thus be probed at particle colliders such as the Large Hadron Collider at high energies. The goal

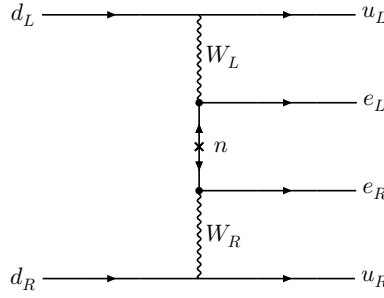


Fig. 1.2 – The λ -diagram contribution to the neutrinoless double beta decay at quark level. Here, n is the intermediate Majorana neutrino which interacts with one left-handed electron e_L and one right-handed electron e_R . W_L and W_R are the gauge bosons mediating the interaction.

of this work is to analyse one specific channel of the high energy equivalent of the $0\nu\beta\beta$ decay, namely the so-called λ -diagram which describes the interaction of two quarks with different chiralities in the desired process. The corresponding Feynman diagram is shown in Fig. 1.2.

As a theoretical framework for this process, we choose the Left Right symmetric model[25–29], which is a well understood and conceptually beautiful extension of the Standard Model. Although it naturally contains the type-I and -II seesaw mechanisms, we will restrict our calculations to the type-I case by choosing the parameters accordingly.²

In order to predict the cross section of the λ -diagram at high energies, we make use of the Monte Carlo simulator Mad Graph 5 [30] and hereby derive an approximative expression for the respective cross sections. Finally, we analyse the parameter space of the neutrino mixing matrices and masses in order to find limits on the signal.

The structure of this thesis is as follows:

Chapter 2 reviews the Standard Model particle content and mass generation mechanism very briefly. Also an overview about the three types of seesaw models is presented and a detailed discussion of the Left Right symmetric model including mass generation, mixing and leptonic the weak interaction Lagrangian is given. The topic of Chapter 3 will be the low energy $0\nu\beta\beta$ decay. Here we list the relevant decay channels including the constraints resulting from xenon experiments. Our main analysis is carried out in Chapter 4. We first give the expressions for the cross sections determined by analytical considerations, combined with the numerical simulations, and then discuss the different scenarios relevant for the high energy cross section and derive upper limits for the dif-

² This is done in order to avoid fine-tuning in the Higgs potential parameters [29], but also to simplify the analysis.

ferent cases under consideration. Hereby we focus on the t -channel contribution. Our results and conclusions are summarized in Section 4.3.

The Appendix is reserved for formulae used in our analysis, as well as the derivation of the cross section approximation. Furthermore, a short introduction to the Monte Carlo simulator Mad Graph 5 and details on the simulations carried out are given there.

Chapter 2

Theory

In this chapter we describe the theoretical framework this work is based on. First, we will very briefly review the Standard Model of particle physics (SM) and sketch how fermion masses are generated by the Higgs mechanism. The reader interested in a complete and rigorous treatment of this theory is referred to [31, 32] and also to Section 2.3 which explains the analogous details in the extended Left Right Symmetric Model (LRSM).

After that, we give an overview of the different types of seesaw mechanisms that could give rise to the desired neutrino mass term and finally we describe the Left-Right Symmetric Model in detail as it will serve as the theoretical framework in this thesis. For the latter we will derive the expression for the fermionic and bosonic mass terms. The mixing between different neutrino flavours is examined, as well as that between the heavy gauge bosons. To conclude we give the expression for the leptonic weak interaction which will be used in the following chapters.

2.1 The Standard Model of particle physics and massive fermions

The Standard Model of particle physics describes the fundamental particles and their interactions among each other. The particles, as well as their anti-particles are distinguished by their spin: fermions carry half-integer spin, scalars are spin-0 particles and vector bosons are spin-1 particles. The latter are the force carriers and are also called gauge bosons as they appear due to the special structure of the SM as a gauge theory.

The fermions can be grouped into four categories: charged leptons ℓ^- , neutrinos ν , up-type quarks u and down-type quarks d . Each of them appears in a three-fold way, that is in three families, e.g. $\ell = e, \mu, \tau$ for the charged leptons. The gauge bosons contained in the SM are one massless photon γ , 8 massless gluons g and three massive vector bosons: W^\pm and Z . The only scalar in the SM is the Higgs-Boson Φ which is responsible for the particles to acquire their masses. The SM particle content is depicted in Fig. 2.1.

As the SM is a gauge theory, the particles can be identified with the representations of their group. The gauge group of the model is a product group of three subgroups:

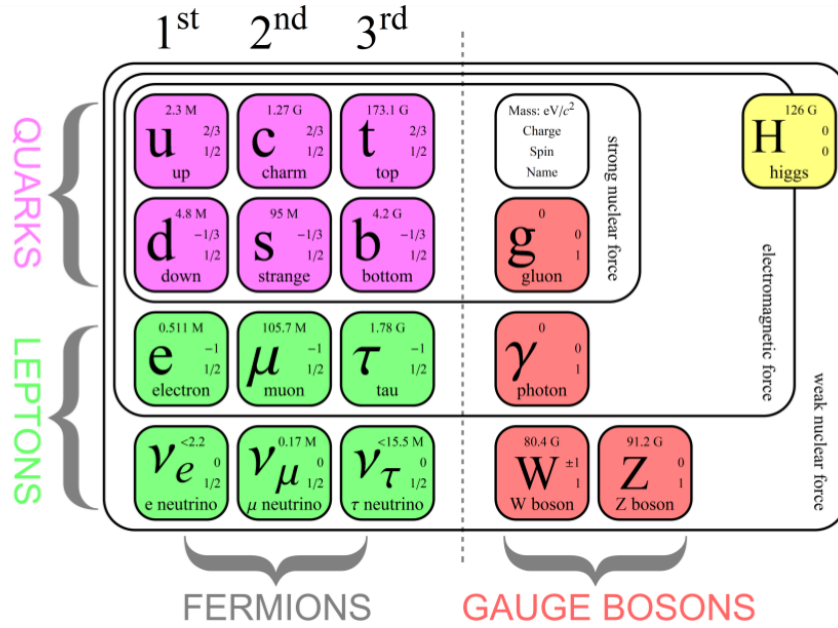


Fig. 2.1 – The Standard Model particle content

$SU(3)_C \times SU(2)_L \times U(1)_Y$. $SU(3)_C$ incorporates the quark color-representations and their interactions via gluons. As this part of the theory is of no interest for us, we will ignore it in what follows. $SU(2)_L$ describes the behaviour of the left-handed (LH)¹ particles and $U(1)_Y$ is called the hypercharge group.

The structure of $SU(2)_L$ requires LH fermions to be placed into doublets, whereas right-handed (RH) spinors are singlets under $SU(2)_L$ transformations, e.g.

$$L_e = \begin{pmatrix} \nu_e \\ e^- \\ e_R^- \end{pmatrix}_L \quad \sim (\mathbf{2}, -\mathbf{1}) \quad (2.1)$$

$$e_R^- \quad \sim (\mathbf{1}, -\mathbf{2})$$

Here, we already gave the conventional way to label the group-elements: $(\mathbf{2}, -\mathbf{1})$ indicates that this object transforms as a doublet ($\mathbf{2}$) under $SU(2)_L$ transformations, i.e. the components of the vector L_e mix with each other under the group transformation – similar to a usual two-dimensional vector under rotations. Its hypercharge eigenvalue is given by $-\mathbf{1}$, which means that the spinors acquires a complex phase $e^{-i\alpha}$ under $U(1)_Y$ gauge transformations. On the other hand, RH particles do not transform under $SU(2)_L$ gauge transformations; this is indicated by $\mathbf{1}$ which is used for singlets.

¹ The chirality of a fermion spinor is defined via the eigenvalues of the γ^5 matrix. This property divides the space of spinors in two separate subspaces of left-handed and right-handed particles, which are not connected via Lorentz transformations. Therefore they are the building-blocks of any fermion spinor. For relativistic particles the chirality is equal to its helicity, i.e. the projection of its spin onto its direction of motion.

The mass term of a fermion, e.g. the electron, is given by the interaction between one LH and one RH particle spinor:

$$\mathcal{L}_m \propto -m_e \bar{e}_L e_R + \text{h.c.} \quad (2.2)$$

However, as \bar{e}_L changes under $SU(2)_L$ transformations, but e_R does not, this term is not invariant under gauge transformations and thus cannot be simply inserted into the Lagrangian without spoiling gauge-invariance of the theory.²

Fortunately, the Higgs mechanism gives an elegant solution to this problem. If we introduce a complex scalar field Φ , which transforms as $SU(2)_L$ doublet and carries hypercharge 1, we can add the following, invariant term into the Lagrangian:

$$\mathcal{L}_Y = -y \bar{L}_e \Phi e_R + \text{h.c.} = -y (\bar{\nu}_L \quad \bar{e}_L) \Phi e_R + \text{h.c.} \quad (2.3)$$

with

$$\Phi = \begin{pmatrix} \phi^+ \\ \phi^0 \end{pmatrix} \sim (\mathbf{2}, \mathbf{1}). \quad (2.4)$$

Terms like these, which couple fermions to scalar fields, are called Yukawa coupling terms. The constant y is the Yukawa coupling.

The neutral scalar component ϕ^0 can acquire a vacuum expectation value (VEV), which means that the field's value is different from zero even in the ground state:

$$\langle \phi^0 \rangle = \frac{v}{\sqrt{2}} > 0. \quad (2.5)$$

This is possible only for electrically neutral fields for obvious reasons. In general, the value of the VEV depends on the scalar potential of the corresponding fields $V_{Sc}(\Phi)$ and was found to be $v_{SM} \approx 246$ GeV in the case of the standard model Higgs boson.

We then can rewrite the scalar field as

$$\Phi = \begin{pmatrix} \phi^+ \\ \phi^0 \end{pmatrix} = \begin{pmatrix} \phi^+ \\ \frac{v+h}{\sqrt{2}} \end{pmatrix} = \begin{pmatrix} 0 \\ \frac{v}{\sqrt{2}} \end{pmatrix} + \Phi' \quad (2.6)$$

The new field h is referred to as the physical Higgs field and has a vanishing VEV $\langle h \rangle = 0$, but now new terms arise in the Lagrangian, Equation (2.3):

$$\mathcal{L}_Y = -\frac{yv}{\sqrt{2}} \bar{e}_L e_R + y \bar{L}_e \Phi' e_R + \text{h.c.} \quad (2.7)$$

² Note that $\bar{e}_L = e_L^\dagger \gamma^0$ corresponds to the anti-fundamental representation and therefore carries $U(1)_Y$ hypercharge +1. Thus, this term is indeed invariant under $U(1)_Y$ -rotations.

Comparing this result with Equation (2.2), we find that we have just recovered the electron-mass term with $m_e = yv/\sqrt{2}$.

This procedure, which we presented in a rather simplified way, reflects the so-called spontaneous symmetry breaking (SSB) and happens when the scalar field Φ undergoes a phase transition from high to low energy.³ Although this is not obvious, the Lagrangian as a whole is still gauge invariant; by choosing the explicit parametrisation of Equation (2.6) we have just rewritten it in a basis where this is not visible anymore. In the SM the Higgs mechanism is not only responsible for generating the masses of all massive fermions, but in a similar way also for the massive vector bosons W^\pm and Z and the Higgs field h itself.

However, the Standard Model does not comprise RH particles for all the fermions: As mentioned before, the neutrino is contained in the SM as LH particle only. Thus, it cannot become massive in this framework.⁴

Nevertheless, oscillation experiments showed [13] that neutrinos possess a very small, but not vanishing mass. One could therefore demand to simply add a RH neutrino to the SM and adopt the same mechanism as explained above. In principle this is possible, but it would raise another question: Why is the neutrino mass so small?

2.2 Extending the Standard Model: seesaw mechanisms

As already pointed out in the introduction, the answer at hand is an effective low energy theory with the mass term of the neutrino being suppressed by some high energy scale. The corresponding operator of mass dimension 5 is called Weinberg operator [17]; it reads

$$\mathcal{L}_{\text{eff}}^{d=5} = -\frac{c_{ij}}{\Lambda} \overline{L_{Li}^c} \tilde{\Phi}^* \tilde{\Phi}^\dagger L_{Lj} + \text{h.c.} \quad (2.8)$$

with $L_L^c = \hat{C} \overline{L_L^T}$ being the Dirac charge conjugate LH lepton doublet and $\tilde{\Phi} = i\sigma^2 \Phi^*$ the conjugate Higgs doublet.⁵ The Pauli matrices are

$$\sigma^1 = \begin{pmatrix} 0 & 1 \\ 1 & 0 \end{pmatrix}, \quad \sigma^2 = \begin{pmatrix} 0 & -i \\ i & 0 \end{pmatrix}, \quad \sigma^3 = \begin{pmatrix} 1 & 0 \\ 0 & -1 \end{pmatrix}. \quad (2.9)$$

³ In a thermal bath the potential $V_{\text{sc}}(\Phi)$ depends on the temperature. At high energies it is symmetric around $|\Phi| = 0$, whereas at low energy it develops a manifold of minima at $\phi^0 = ve^{i\alpha}$.

⁴ As was pointed out in the introduction, it is the smallness of neutrino masses and the $V - A$ structure of the weak interaction that made scientists believe that neutrinos exist as massless LH particles only.

⁵ $\nu_L^c = (\nu_L)^c = (\nu^c)_R$ in our convention. See Equation (2.35) and the discussion below for further useful relations and identities.

After the Higgs field Φ acquired its vacuum expectation value v from Equation (2.6), this term gives rise to a neutrino mass term of the form

$$\mathcal{L}_m^\nu = -c_{ij} \frac{v^2}{2\Lambda} \bar{\nu}_{Li}^c \nu_{Lj} + \text{h.c.} \quad (2.10)$$

The flavour-dependent coefficients c_{ij} are typically proportional to the Yukawa couplings of some underlying interaction; the relevant energy scale can be identified with the mass of some heavy particle $\Lambda \sim M$. Therefore, we find the simple relation that gives its name to this so-called seesaw mechanism:

$$m_\nu \propto \frac{v^2}{M} \quad (2.11)$$

It is easy to see that a larger mass M results in a smaller neutrino mass m_ν and vice versa.

Equation (2.10) implies that the neutrino mass can be generated through a coupling of ν_L to its charge conjugate spinor ν_L^c . This is possible for neutrinos only as they are electrically neutral particles; particles that receive their mass through such terms are referred to as Majorana particles whereas Equation (2.2) generates Dirac particles. For an electron and all the other SM leptons a Majorana mass term would obviously violate charge conservation and thus cannot be realized in Nature.

The possibility of such a Majorana neutrino is very interesting in many ways as it explicitly violates lepton number by two units and thus could mediate non-standard processes which result in interesting signals. Furthermore, it is not clear whether Equation (2.10) is invariant under CP conjugation. This depends on the complex phases of the coefficients c_{ij}/Λ and is also of interest in different scenarios.

We now want to understand the different types of seesaw mechanisms in more detail. In the remainder of the section we therefore follow the descriptions of [18, 19, 33].

2.2.1 Type-I seesaw

The relevant particle in this case is indeed a RH neutrino ν'_R that is a singlet under the SM $SU(2)_L \times U(1)_Y$ gauge group. As it does not interact with the SM particles in an other way than the following, it is often called sterile neutrino. Here and in the following, primes denote that we are working in the flavour- or gauge-eigenbasis, as opposed to unprimed spinors, which are supposed to be mass eigenstates as derived in the following. The mass mechanism in this case is schematically visualized in Figure 1.1a.

We introduce three copies of the new fields ν'_{Ri} ($i = 1, 2, 3$) as for each light neutrino

mass one heavy counterpart is needed.⁶ The resulting Yukawa interaction term is completely analogous to the SM term in Equation (2.3), except for the necessary replacement $\Phi \rightarrow \tilde{\Phi}$. For the RH neutrinos we can however add an additional Majorana mass term which does not violate gauge invariance as these RH particles do not transform under $SU(2)_L$, neither under $U(1)_Y$. Although the origin of this term can be explained by theories like the LRSM, here we simply take it as given.

After symmetry breaking the Lagrangian reads

$$\begin{aligned} \mathcal{L}_m &= -\frac{v}{\sqrt{2}} \overline{\nu'_{Li}} \tilde{y}_{ij} \nu'_{Rj} - \frac{1}{2} \overline{\nu'_{Ri}} (M_R)_{ij} \nu'_{Rj} + \text{h.c.} \\ &= -\frac{1}{2} \underbrace{\begin{pmatrix} \overline{\nu'_L} & \overline{\nu'^c_R} \end{pmatrix}}_{=n'_L} \underbrace{\begin{pmatrix} 0 & \tilde{y}v/\sqrt{2} \\ \tilde{y}^T v/\sqrt{2} & M_R \end{pmatrix}}_{=M_\nu} \underbrace{\begin{pmatrix} \nu'_L \\ \nu'^c_R \end{pmatrix}}_{=n'^c_L} + \text{h.c.} \end{aligned} \quad (2.12)$$

We can now transform into the mass eigenbasis whose eigenvectors correspond to those linear combinations of neutrino fields that have a definite mass and thus describes its propagation through spacetime.

To do this, we diagonalize the mass matrix M_ν by a unitary 6×6 matrix W^7 and label the resulting mass eigenstates by ν for the light particles and N for the heavier ones. They are combined in the 6-vector n :

$$n_L = \begin{pmatrix} \nu_L \\ N_L \end{pmatrix} = W^\dagger n'_L = W^\dagger \begin{pmatrix} \nu'_L \\ \nu'^c_R \end{pmatrix}, \quad n_R = n'_L = W^T n'^c_L. \quad (2.13)$$

With $\hat{M}_\nu = W^\dagger M_\nu W^*$ being diagonal, the Lagrangian (2.12) takes a simple form:

$$\begin{aligned} \mathcal{L}_m &= -\frac{1}{2} n_L \hat{M}_\nu n_R + \text{h.c.} \\ &= -\frac{1}{2} \sum_{\substack{i=1 \\ \text{light}}}^3 m_i \overline{\nu_{Li}} \nu_{Ri} - \frac{1}{2} \sum_{\substack{i=1 \\ \text{heavy}}}^3 M_i \overline{N_{Li}} N_{Ri} + \text{h.c.} \end{aligned} \quad (2.14)$$

Block-diagonalizing M_ν gives the famous seesaw-formula for the light and heavy neutrino masses and is correct up to mixing within the light and heavy neutrinos, respectively. It is therefore a useful indication for the expected order of magnitude of the

⁶ Of course it is possible to investigate the addition of only one heavy particle or even more than three. Our choice is motivated by means of symmetry: The left right symmetric model studied in the next section naturally requires one RH partner for each LH neutrino. Note furthermore that the observed neutrino oscillations call for at least two massive light neutrinos and thus two RH partners in this scenario.

⁷ For the case of the LRSM, the explicit form of W will be given below.

masses.

$$m \sim \frac{1}{2} \left(M_R - \sqrt{M_R^2 - 4 M_D M_D^T} \right) \approx -M_D M_R^{-1} M_D^T, \quad (2.15)$$

$$M \sim \frac{1}{2} \left(M_R + \sqrt{M_R^2 - 4 M_D M_D^T} \right) \approx M_R + M_D M_R^{-1} M_D^T \approx M_R. \quad (2.16)$$

Here, $M_D = \tilde{y}v/\sqrt{2}$ is the Dirac mass matrix from the usual SM mass term. Comparing this result with the mass term in Equation (2.10) stemming from the Weinberg operator, we find that indeed

$$m_\nu \sim \frac{v^2 \tilde{y}^2}{2M_R}. \quad (2.17)$$

Finally, it is worth noting how the Majorana nature of the neutrino is manifested in the seesaw scenarios: The mass term in Equation (2.14) is built out of a LH spinor n_L and its charge conjugate $n_R = n_L^c$. Therefore, the combined particle spinor $n = n_L + n_R$ represents both, particle and antiparticle:

$$n^c = n_L^c + n_R^c = n_R + n_L = n. \quad (2.18)$$

This is precisely what makes the Majorana neutrino so special: By propagating through spacetime, it can interact either as particle or antiparticle. As we will see later, processes in which it interacts both as particle and antiparticle, are suppressed by its mass term due to the insertion of the propagator.

2.2.2 Type-II seesaw

The type-II seesaw mechanism is conceptually somewhat simpler than the type-I. Instead of a massive fermion which couples to the neutrino, a heavy scalar triplet $\Delta \sim (3, 2)$ with an electrically neutral component δ^0 is used. δ^0 can then develop a VEV v_Δ similar to the SM Higgs boson. This essentially generates the neutrino mass; it is indicated in Figure 1.1b.

Canonically, the triplet is given by

$$\vec{\Delta} = \begin{pmatrix} \Delta^1 \\ \Delta^2 \\ \Delta^3 \end{pmatrix} \quad (2.19)$$

However, to couple it to the $SU(2)_L$ leptonic doublets, it is more convenient to use the

2×2 matrix representation:

$$\Delta = \vec{\sigma} \cdot \vec{\Delta} = \begin{pmatrix} \Delta^3 & \Delta^1 - i\Delta^2 \\ \Delta^1 + i\Delta^2 & \Delta^3 \end{pmatrix} = \sqrt{2} \begin{pmatrix} \delta^+/\sqrt{2} & \delta^{++} \\ \delta^0 & -\delta^+/\sqrt{2} \end{pmatrix}, \quad (2.20)$$

where we used the Pauli matrices σ^i and the triplet charge eigenstates $\delta^+ = \Delta^3$ and $\delta^{\pm\pm} = (\Delta^1 \mp i\Delta^2)/\sqrt{2}$.

The invariant Yukawa coupling term and the resulting mass term after SSB with $\langle \delta^0 \rangle = v_\Delta/\sqrt{2}$ reads⁸

$$\mathcal{L}_Y = -(y_\Delta)_{ij} \overline{L_{Li}^c} i\sigma^2 \Delta L'_{Lj} + \text{h.c.} \xrightarrow{\text{SSB}} -\frac{1}{2} \overline{\nu'_L} \underbrace{2y_\Delta^* v_\Delta}_{=m_\nu} \nu'_L + \text{h.c.} \quad (2.21)$$

In order to recover a mass term of the form predicted by the Weinberg operator (Equation (2.10)), one has to take into account that the triplet couples to the SM Higgs boson in the scalar potential $V_{Sc}(\Phi, \Delta)$. [19, 34] give the hereof resulting relation $v_\Delta = \mu v^2/2M_\Delta^2$ with M_Δ being the triplet mass μ the coupling between Φ and Δ .⁹

Using this, the neutrino mass matrix reads

$$m_\nu = \frac{\mu v^2}{M_\Delta^2} y_\Delta^* \quad (2.22)$$

and the the energy scale Λ and the coupling coefficients c_{ij} are given by $\Lambda = M_\Delta^2/\mu v^2$ and $c_{ij} = y_{\Delta ij}^*$.

Although the theory of type-II seesaw is quite simple, it has a richer phenomenology to offer: The components of the scalar triplet Δ also couple to the charged leptons and gauge bosons and can thus mediate lepton number violating interactions at tree level. This opens up attractive possibilities, but as it has not been observed yet, it also places strong limits on the couplings and masses of the triplet (see [19, 34, 35] for constraints and limits).

2.2.3 Type-III seesaw

In this type of seesaw mechanism, illustrated in Figure 1.1c, we re-encounter heavy neutrinos suppressing the light neutrino mass similar to type-I seesaw. They couple to the SM particles as RH triplets $\Sigma \sim (\mathbf{1}, \mathbf{0})$.

⁸ Note that the Yukawa coupling becomes conjugate by use of the hermitian conjugate h.c.: $(\nu'_L y_\Delta \nu'_L)^\dagger = \overline{\nu'_L} y_\Delta^* \nu'_L + \text{h.c.}$

⁹ This relation is true if $M_\Delta \gg v \gg v_\Delta$ [34].

We introduce three copies of the new field ($j = 1, 2, 3$) just like in the type-I case and rewrite them in the 2×2 representation in the charge eigenbasis as we have done for the scalar triplet Δ :

$$\vec{\Sigma}_j = \begin{pmatrix} \Sigma_j^1 \\ \Sigma_j^2 \\ \Sigma_j^3 \end{pmatrix} \quad (2.23)$$

$$\Sigma_j = \vec{\sigma} \cdot \vec{\Sigma}_j = \begin{pmatrix} \Sigma_j^3 & \Sigma_j^1 - i \Sigma_j^2 \\ \Sigma_j^1 + i \Sigma_j^2 & -\Sigma_j^3 \end{pmatrix} = \begin{pmatrix} \Sigma_j^0 & \sqrt{2} \Sigma_j^+ \\ \sqrt{2} \Sigma_j^- & -\Sigma_j^0 \end{pmatrix}.$$

Again, we used $\Sigma_j^\pm = (\Sigma_j^1 \mp i \Sigma_j^2)/\sqrt{2}$ and $\Sigma_j^0 = \Sigma_j^3$. The charged fermions Σ_j^\pm form Dirac particles E'_j , whereas the neutral components are of Majorana nature and will be called ν'_{Rj} in analogy to type-I seesaw. They are defined as

$$E'_j = \Sigma_j^- + \Sigma_j^+ \quad \nu'_{Rj} = \Sigma_j^0. \quad (2.24)$$

The different triplets can now be coupled among each other via a Majorana mass term

$$\mathcal{L}_M^\Sigma = -\frac{1}{2} (M_\Sigma)_{ij} \overline{\vec{\Sigma}_i^c} \vec{\Sigma}_j + \text{h.c.} \quad (2.25)$$

$$= -\frac{1}{2} (M_\Sigma)_{ij} \overline{\nu'_{Ri}{}^c} \nu'_{Rj} - \frac{1}{2} (M_\Sigma)_{ij} \overline{E'_i} E'_j + \text{h.c.}, \quad (2.26)$$

and to the LH SM doublets via a Yukawa coupling

$$\mathcal{L}_Y = -(y_\Sigma)_{ij} \overline{L'_L i} (\vec{\sigma} \cdot \vec{\Sigma}_j) \tilde{\Phi} + \text{h.c.} \quad (2.27)$$

$$\xrightarrow{\text{SSB}} -\frac{(y_\Sigma)_{ij} v}{\sqrt{2}} \overline{\nu'_{Li}} \nu'_{Rj} - (y_\Sigma)_{ij} v \overline{\ell'_{Li}} E'_{Rj} + \text{h.c.} \quad (2.28)$$

Using equations (2.26) and (2.28), we arrive at a neutrino mass term which looks very much like in the type-I case:

$$\mathcal{L}_m^\nu = -\frac{1}{2} \begin{pmatrix} \overline{\nu'_L} & \overline{\nu'_R{}^c} \end{pmatrix} \begin{pmatrix} 0 & y_\Sigma v/\sqrt{2} \\ y_\Sigma^T v/\sqrt{2} & M_\Sigma \end{pmatrix} \begin{pmatrix} \nu'_L{}^c \\ \nu'_R \end{pmatrix} + \text{h.c.} \quad (2.29)$$

Diagonalizing this Lagrangian results in expressions for the mass eigenstates and their masses analogous to equations (2.13), (2.15) and (2.16).

Although the new charged leptons couple to the SM particles, they do not mix with them as one might have guessed.¹⁰ In fact they decouple from most processes due to

¹⁰In our case we find $\mathcal{L}^\ell \supset -(\overline{\ell'_L} \ \overline{E'_L}) \begin{pmatrix} y v/\sqrt{2} & v y_\Sigma \\ 0 & M_\Sigma \end{pmatrix} \begin{pmatrix} \ell'_R \\ E'_R \end{pmatrix} + \text{h.c.}$. Due to the zero matrix in the left bottom corner of the mixing matrix, the upper right couplings $v y_\Sigma$ do not contribute to the

their heaviness. Therefore, the resulting mass mixing and particle content in the effective low energy theory is basically identical to the type-I seesaw case and type III is rarely considered.

In the above we demonstrated three different mechanisms leading to small neutrino masses via suppression through some heavy intermediate particle. One crucial ingredient shared by all of these models is the mixing matrix W mentioned in Equation (2.13). Its elements determine the interaction strength of both, light and heavy neutrinos with the SM gauge bosons. Consequently, they also appear in the context of neutrino oscillations and are already being measured for the LH sector.

In the subsequent section we introduce the LRSM including the type-I and -II seesaw mechanisms. In this context we will further discuss the mixing and coupling to gauge bosons. However, in our actual calculations in Chapter 4 we work with the type-I seesaw only.

2.3 The Left Right symmetric model

The Left Right Symmetric Model was originally introduced in order to explain parity violation by restoring a symmetry between LH and RH sector at higher energies [25–27]. Fortunately, it also implements the seesaw I and II mechanisms to generate the tiny neutrino masses in a very elegant way.

In the following we introduce the model with its particle content. We discuss the neutrino and gauge boson mass generation, their mixing as well as the weak interaction Lagrangian. The section is mainly based on [29] and [28] which give a very detailed introduction into the model.

2.3.1 Particle content, couplings and symmetry

The gauge group of the LRSM is $SU(2)_L \times SU(2)_R \times U(1)_Y$ ¹¹ with the electric charge being defined as $Q_{el} = T_L^3 + T_R^3 + Y/2$.¹² The model extends the Standard Model particle content such that for each LH particle a RH counterpart exists. Therefore, RH gauge bosons are introduced and RH fermions are organized into doublets in complete analogy to the LH sector.

mass eigenvalues. This might be different if further particle content and/or symmetries are included.

¹¹Note that we are mainly interested in the weak sector of the model. Therefore we will not include strong interactions into our discussion.

¹² $T_{L/R}^a = \sigma^a/2$ ($a = 1, 2, 3$) are the generators of $SU(2)_{L/R}$; Y is the hypercharge operator.

Fermions

The fermion gauge eigenstates read as follows:

$$\begin{aligned} L'_{Li} &= \begin{pmatrix} \nu'_L \\ \ell'_L \end{pmatrix}_i \sim (\mathbf{2}, \mathbf{1}, -\mathbf{1}), & L'_{Ri} &= \begin{pmatrix} \nu'_R \\ \ell'_R \end{pmatrix}_i \sim (\mathbf{1}, \mathbf{2}, -\mathbf{1}), \\ Q'_L &= \begin{pmatrix} u'_L \\ d'_L \end{pmatrix}_i \sim (\mathbf{2}, \mathbf{1}, 1/3), & Q'_R &= \begin{pmatrix} u'_R \\ d'_R \end{pmatrix}_i \sim (\mathbf{1}, \mathbf{2}, 1/3). \end{aligned} \quad (2.30)$$

As usual, the index i runs over the three flavours¹³ and ' denotes flavour-eigenstates. Similar to the discussion in Section 2.1, the representation is indicated by the values in the parenthesis. They are ordered according to the gauge groups as $(\mathbf{L}, \mathbf{R}, \mathbf{Y})$.

Combining the LH and RH particle spinors, $\psi = \psi_L + \psi_R$, one can define projection operators, recovering the LH or RH part respectively:

$$\begin{aligned} P_L &= \frac{1-\gamma^5}{2}, & P_L \psi &= \psi_L, \\ P_R &= \frac{1+\gamma^5}{2}, & P_R \psi &= \psi_R, \\ P_L \cdot P_R &= 0, & P_{L/R} \gamma^\mu &= \gamma^\mu P_{R/L}. \end{aligned} \quad (2.31)$$

The Dirac charge-conjugate spinor ψ^c is defined as $\psi^c = \hat{C} \bar{\psi}^T$, with \hat{C} being the charge conjugation operator which fulfils the following relations:

$$\hat{C}^{-1} = \hat{C}^\dagger = -\hat{C} \quad \text{and} \quad \hat{C}^\dagger \gamma^\mu \hat{C} = -\gamma^{\mu T}. \quad (2.32)$$

In the above, γ^μ are the gamma matrices which can be written in terms of the Pauli matrices in Equation (2.9) as

$$\gamma^0 = \begin{pmatrix} \mathbb{1}_2 & 0 \\ 0 & -\mathbb{1}_2 \end{pmatrix}, \quad \gamma^i = \begin{pmatrix} 0 & \sigma^i \\ -\sigma^i & 0 \end{pmatrix} \quad (i = 1, 2, 3), \quad (2.33)$$

$$\gamma^5 = i\gamma^0\gamma^1\gamma^2\gamma^3.$$

The charge conjugation operator is then explicitly given by

$$\hat{C} = i\gamma^2\gamma^0. \quad (2.34)$$

Note especially that LH spinors become RH spinors under charge conjugation and vice

¹³I.e. $i = 1, 2, 3$ or $i = e, \mu, \tau$. The latter is sometimes used in combination with the charged leptons and the light neutrinos to stress that they are part of the flavour eigenbasis.

versa; our convention for the definition of $\psi_{L/R}^c$ is as follows:

$$\begin{aligned}\psi_{L/R}^c &= (\psi_{L/R})^c = \hat{C} \overline{\psi_{L/R}}^T = \hat{C} P_{R/L} \overline{\psi}^T = P_{R/L} \hat{C} \overline{\psi}^T = (\psi^c)_{R/L}, \\ \overline{\psi_{L/R}^c} &= \overline{(\psi_{L/R})^c} = \overline{(\psi^c)_{R/L}} = \overline{P_{R/L} (\psi^c)} = \overline{(\psi^c)} P_{L/R}.\end{aligned}\tag{2.35}$$

Frequently used identities, relating fermion currents to the charge conjugate ones, are

$$\overline{\psi} \varphi = \overline{\varphi^c} \psi^c, \quad \overline{\psi} \gamma^\mu \varphi = -\overline{\varphi^c} \gamma^\mu \psi^c.\tag{2.36}$$

Scalars

The scalar sector is also augmented with respect to the SM. The SM Higgs doublet is promoted to be an hypercharge-0 Higgs bidoublet ϕ which couples to both LH and RH fermions. Furthermore, two heavy scalar triplets Δ_L and Δ_R are introduced, one for each chirality:

$$\begin{aligned}\Delta_L &= \begin{pmatrix} \delta_L^+/\sqrt{2} & \delta_L^{++} \\ \delta_L^0 & -\delta_L^+/\sqrt{2} \end{pmatrix} && \sim (\mathbf{3}, \mathbf{1}, \mathbf{2}), \\ \Delta_R &= \begin{pmatrix} \delta_R^+/\sqrt{2} & \delta_R^{++} \\ \delta_R^0 & -\delta_R^+/\sqrt{2} \end{pmatrix} && \sim (\mathbf{1}, \mathbf{3}, \mathbf{2}), \\ \phi &= \begin{pmatrix} \phi_1^0 & \phi_2^+ \\ \phi_1^- & \phi_2^0 \end{pmatrix} && \sim (\mathbf{2}, \mathbf{2}, \mathbf{0}), \\ \tilde{\phi} &= \sigma^2 \phi^* \sigma^2 = \begin{pmatrix} \phi_2^{0*} & -\phi_1^+ \\ -\phi_2^- & \phi_1^{0*} \end{pmatrix} && \sim (\mathbf{2}, \mathbf{2}, \mathbf{0}).\end{aligned}\tag{2.37}$$

Gauge Bosons and Covariant Derivatives

In order to make the theory gauge-invariant, gauge bosons are introduced which couple through covariant derivatives to the scalars and fermions. For both $SU(2)_L$ and $SU(3)_R$ three vector bosons, $W_{L\mu}^a$ and $W_{R\mu}^a$ ($a = 1, 2, 3$), are present, whereas $U(1)_Y$ contributes one gauge field B_μ . The covariant derivatives are:

$$\begin{aligned}D_\mu \psi_L &= \partial_\mu \psi_L - ig_L W_{L\mu} \psi_L - ig_Y B_\mu \frac{Y}{2} \psi_L, \\ D_\mu \psi_R &= \partial_\mu \psi_R - ig_R W_{R\mu} \psi_R - ig_Y B_\mu \frac{Y}{2} \psi_R, \\ D_\mu \Delta_L &= \partial_\mu \Delta_L - ig_L [W_{L\mu}, \Delta_L] - ig_Y B_\mu \Delta_L, \\ D_\mu \Delta_R &= \partial_\mu \Delta_R - ig_R [W_{R\mu}, \Delta_R] - ig_Y B_\mu \Delta_R, \\ D_\mu \phi &= \partial_\mu \phi - ig_L W_{L\mu} \phi + ig_R \phi W_{R\mu}.\end{aligned}\tag{2.38}$$

Here, g_R is the RH coupling constant, g_L the LH one and g_Y the $U(1)_Y$ gauge coupling, with the latter two being inherited from the SM. W_μ is the sum over the gauge bosons times their associated generators T^a which act as operators:¹⁴

$$W_\mu = \sum_{a=1}^3 W_\mu^a T_\mu^a = \sum_{a=1}^3 W_\mu^a \frac{\sigma^a}{2} = \frac{1}{\sqrt{2}} \begin{pmatrix} W_\mu^3/\sqrt{2} & W_\mu^+ \\ W_\mu^- & -W_\mu^3/\sqrt{2} \end{pmatrix}. \quad (2.39)$$

In the last equality we used the definition of the charged W -Bosons: $W_\mu^\pm = (W_\mu^1 \mp iW_\mu^2)/\sqrt{2}$.

Parity symmetry

Finally, the LRSM allows to define a discrete symmetry between the RH and LH sectors. In this thesis we work with a discrete parity symmetry, that is:¹⁵

$$\begin{aligned} x^\mu = \begin{pmatrix} t \\ \vec{x} \end{pmatrix} &\xrightarrow{\hat{P}} x_P^\mu := \begin{pmatrix} t \\ -\vec{x} \end{pmatrix} \\ \psi_{L/R}(x) &\xrightarrow{\hat{P}} \psi_{R/L}(x_P) \\ \phi(x) &\xrightarrow{\hat{P}} \phi^\dagger(x_P) \\ \Delta_{L/R}(x) &\xrightarrow{\hat{P}} \Delta_{R/L}(x_P) \\ B_\mu(x) &\xrightarrow{\hat{P}} \epsilon(\mu) B_\mu(x_P) \\ W_{L/R\mu}^a(x) &\xrightarrow{\hat{P}} \epsilon(\mu) W_{R/L\mu}^a(x_P) \end{aligned} \quad \epsilon(\mu) = \begin{cases} +1, & \mu = 0 \\ -1, & \mu = 1, 2, 3 \end{cases} \quad (2.40)$$

Lagrangian

The most general Lagrangian invariant under gauge transformations and respecting Lorentz invariance can be decomposed as:

$$\mathcal{L} = \mathcal{L}_Y + \mathcal{L}_F + \mathcal{L}_{Sc} + \mathcal{L}_{gauge} - V_{Sc} \quad (2.41)$$

The Yukawa-Lagrangian $\mathcal{L}_Y = \mathcal{L}_Y^L + \mathcal{L}_Y^q$ describes the coupling of the various fermions with the scalar fields and will be responsible for the generation of fermion masses in the following. In \mathcal{L}_F the fermions' kinetic terms, as well as their interaction with the gauge

¹⁴ Wherever a statement is valid for both sectors, LH and RH, we drop the subscripts L and R .

¹⁵ Note that one could instead impose a discrete charge symmetry[28]: $C: W_L \rightarrow W_R^\dagger, \psi_L \rightarrow \psi_R^c$.

bosons is defined. \mathcal{L}_{S_c} contains the scalar kinetic terms and their coupling to gauge bosons; gauge-boson mass terms arise from this Lagrangian after symmetry breaking. \mathcal{L}_{gauge} is responsible for the kinetic terms of the gauge bosons and their coupling among each other. Finally, V_{S_c} is the scalar potential which contains the interaction between the various scalar fields, including their mass terms. Minimizing this part of the Lagrangian gives the vacuum expectation values of the neutral scalar fields.

Details about \mathcal{L}_{gauge} and the potential V_{S_c} are given in [29]. We are mainly interested in \mathcal{L}_Y and \mathcal{L}_F as these parts give rise to neutrino masses and mixing. For the gauge bosons this is determined by \mathcal{L}_{S_c} which will therefore also be subject to our investigation.

The procedure is as follows: first we give expressions for the scalar VEVs. We then derive the neutrino mass eigenvalues and -states, as well as their mixings. After commenting on neutrino oscillations, we continue examining the gauge bosons in their mass eigenbasis and finally the leptonic weak interactions.

2.3.2 Generating masses

The Vacuum Expectation Values

When the fields enter the low energy regime, the LRSM gauge groups are broken spontaneously,

$$\begin{aligned} SU(2)_L \times SU(2)_R \times U(1)_Y &\xrightarrow{\text{SSB}} SU(2)_L \times U(1)_Y \\ &\xrightarrow{\text{SSB (SM)}} U(1)_{em}, \end{aligned} \quad (2.42)$$

and the minimum of the scalar potential V_{S_c} determines the value of the neutral scalar components in the vacuum. This can be parametrised by four phases $\theta_1, \theta_2, \theta_L$ and θ_R and $\kappa_1, \kappa_2, v_L, v_R \in \mathbb{R}_0^+$ as follows:

$$\begin{aligned} \langle \Delta_L \rangle &= \frac{1}{\sqrt{2}} \begin{pmatrix} 0 & 0 \\ v_L e^{i\theta_L} & 0 \end{pmatrix}, & \langle \phi \rangle &= \frac{1}{\sqrt{2}} \begin{pmatrix} \kappa_1 e^{i\theta_1} & 0 \\ 0 & \kappa_2 e^{i\theta_2} \end{pmatrix}, \\ \langle \Delta_R \rangle &= \frac{1}{\sqrt{2}} \begin{pmatrix} 0 & 0 \\ v_R e^{i\theta_R} & 0 \end{pmatrix}, & \langle \tilde{\phi} \rangle &= \frac{1}{\sqrt{2}} \begin{pmatrix} \kappa_2 e^{-i\theta_2} & 0 \\ 0 & \kappa_1 e^{-i\theta_1} \end{pmatrix}. \end{aligned} \quad (2.43)$$

As we have seen in Section 2.2, the triplet VEVs v_L and v_R induce a Majorana mass term through the type-II seesaw for the the LH and RH neutrinos, respectively. The bidoublets VEVs κ_1 and κ_2 then mediate the coupling between LH and RH sector and thereby result in the type-I seesaw mechanism.

It is now possible to eliminate two of the four complex phases by fixing the $SU(2)_L$ and $SU(2)_R$ gauges and absorbing the resulting overall phases in the fermion-sector into the definition of the particle spinors. By convention θ_R and θ_1 are set to zero,

$$\theta_R = 0 = \theta_1. \quad (2.44)$$

Furthermore, the authors of [29] argue that the vacuum expectation value v_L and the complex phase θ_2 have to vanish unless the various parameters of the potential are fine-tuned. This will make the LH type-II seesaw mechanism impossible in our model and reduce the discussion to type-I seesaw. For the remainder of this chapter we will keep v_L and θ_2 finite, but set it to zero in our actual calculations in Chapter 4.

The Yukawa Lagrangian

As the scalar triplets Δ have $U(1)_Y$ hypercharge 2, they can only couple to leptons, more specifically to one lepton and one charge conjugate lepton. ϕ and $\tilde{\phi}$ on the other hand couple equally to quarks and leptons. Yukawa matrices $h_L, h_R, f, \tilde{f}, f_q$ and \tilde{f}_q are introduced to parametrise the coupling to the different fermion flavours:¹⁶

$$\begin{aligned} \mathcal{L}_Y^L = & -\overline{L'_L} i\sigma^2 \Delta_L h_L L'_L - \overline{L'_R} i\sigma^2 \Delta_R h_R L'_R - \\ & - \overline{L'_L} (f\phi + \tilde{f}\tilde{\phi}) L'_R + \text{h.c.}, \end{aligned} \quad (2.45)$$

$$\mathcal{L}_Y^q = -\overline{Q'_L} (f_q\phi + \tilde{f}_q\tilde{\phi}) Q'_R + \text{h.c.} \quad (2.46)$$

Requiring the Lagrangian to be invariant under parity transformations of Equation (2.40) yields the following relations for the Yukawa matrices and the $SU(2)$ couplings [21, 29]:

$$\begin{aligned} h_L &= h_R^*, & g &= g_L = g_R, \\ f &= f^\dagger, & f_q &= f_q^\dagger, \\ \tilde{f} &= \tilde{f}^\dagger, & \tilde{f}_q &= \tilde{f}_q^\dagger. \end{aligned} \quad (2.47)$$

After spontaneous symmetry breaking, when the scalar fields acquire their VEVs of

¹⁶The matrix notation in the following denotes a summation over the flavour indices, i.e. $\overline{L'_L} f \phi L'_R = \sum_{i,j=1}^3 \overline{L'_{Li}} f_{ij} \phi L'_{Rj}$

Equation (2.43), the above Lagrangian contains mass terms for the fermions:

$$\begin{aligned} \mathcal{L}_m^\nu = & -\frac{1}{\sqrt{2}} \left(\overline{\nu'_L{}^c} \nu_L e^{i\theta_L} h_L \nu'_L + \overline{\nu'_R{}^c} \nu_R h_R \nu'_R + \right. \\ & \left. + \overline{\nu'_L} \left(f\kappa_1 + \tilde{f}\kappa_2 e^{-i\theta_2} \right) \nu'_R \right) + \text{h.c.} \end{aligned} \quad (2.48)$$

$$\mathcal{L}_m^\ell = -\frac{1}{\sqrt{2}} \overline{\ell'_L} \left(f\kappa_2 e^{i\theta_2} + \tilde{f}\kappa_1 \right) \ell'_R + \text{h.c.} \quad (2.49)$$

$$\begin{aligned} \mathcal{L}_m^q = & -\frac{1}{\sqrt{2}} \overline{u'_L} \left(f_q \kappa_1 + \tilde{f}_q \kappa_2 e^{-i\theta_2} \right) u'_R - \\ & - \frac{1}{\sqrt{2}} \overline{d'_L} \left(f_q \kappa_2 e^{i\theta_2} + \tilde{f}_q \kappa_1 \right) d'_R + \text{h.c.} \end{aligned} \quad (2.50)$$

The Yukawa matrices are in general not diagonal and the mass eigenstates are therefore not equal to the gauge eigenstates. To find the physical states with definite masses, which describe the propagation of the fields, the mass matrices have to be diagonalized via (bi-)unitary matrices.

Neutrinos

As we are mainly interested in neutrinos in this work, we proceed with their mass matrix in detail and continue with the charged leptons and quarks afterwards.

The neutrino mass Lagrangian (2.48) can be written in a more compact form as

$$\mathcal{L}_m^\nu = -\frac{1}{2} \overline{n'_L} M_\nu n'_R + \text{h.c.} \quad (2.51)$$

The 6-component vector n'_L , its charge conjugate $n'_R = n'^c_L$ and the 6×6 mass matrix M_ν are

$$n'_L = \begin{pmatrix} \nu'_L \\ \nu'^c_R \end{pmatrix}, \quad n'_R = n'^c_L = \begin{pmatrix} \nu'^c_L \\ \nu'_R \end{pmatrix}, \quad (2.52)$$

$$M_\nu = \begin{pmatrix} M_L & M_D \\ M_D^T & M_R \end{pmatrix}, \quad n' = n'_L + n'_R = n'^c. \quad (2.53)$$

with

$$\begin{aligned} M_L &= \sqrt{2} \nu_L e^{-i\theta_L} h_L^*, & M_R &= \sqrt{2} \nu_R h_R \\ M_D &= \left(f\kappa_1 + \tilde{f}\kappa_2 e^{-i\theta_2} \right) / \sqrt{2} \end{aligned} \quad (2.54)$$

In this notation the Majorana nature of the neutrino becomes obvious: Equation (2.53) indicates that the neutrino is identical to its own anti-particle. The same will be true for the mass eigenstates as we will see later.

The LH and RH mass matrices are symmetric: $M_L^T = M_L$ and $M_R^T = M_R$.¹⁷ Therefore M_ν is also symmetric:

$$M_\nu^T = M_\nu \quad (2.55)$$

It can be diagonalized by a unitary 6×6 matrix W , from which we get the masses of the physical states:

$$\hat{M}_\nu := W^\dagger M_\nu W^* = \text{diag}(m_1, m_2, m_3, M_1, M_2, M_3) = \text{diag}(m, M) \quad (2.56)$$

with m and M being the light and heavy diagonal 3×3 mass matrices. To distinguish notationally between the masses of the light and heavy neutrinos, we denote the light masses by m_i , whereas the heavy masses are denoted by M_i .

Plugging Equation (2.56) into Equation (2.51) yields

$$\mathcal{L}_m^\nu = -\frac{1}{2} \overline{n'_L} W \hat{M}_\nu W^T n'_R + \text{h.c.} = -\frac{1}{2} \overline{n_L} \hat{M}_\nu n_R + \text{h.c.}, \quad (2.57)$$

and the physical neutrino fields therefore read

$$n_L = W^\dagger n'_L, \quad n_R = n_L^c = W^T n'_R. \quad (2.58)$$

A useful parametrisation of the mixing matrix W which frequently will be used in the following can be found in [36]:¹⁸

$$\begin{aligned} W &= \begin{pmatrix} V_L^\nu \\ V_R^\nu \end{pmatrix} = \begin{pmatrix} U & S \\ T & V \end{pmatrix} \\ &\simeq \underbrace{\begin{pmatrix} 1 - \frac{1}{2} R R^\dagger & R \\ -R^\dagger & 1 - \frac{1}{2} R^\dagger R \end{pmatrix}}_{=O_R} \begin{pmatrix} U_L & 0 \\ 0 & U_R \end{pmatrix} \end{aligned} \quad (2.59)$$

V_L^ν and V_R^ν are the 6×3 unitary matrices describing the composition of the LH and RH flavour neutrinos in terms of the six mass eigenstates respectively. R is a small-valued 3×3 complex matrix, parametrising the mixing between LH and RH neutrinos and U_L and U_R are unitary matrices mixing the LH and RH neutrinos within their chiral sector. The latter are the well-known PMNS¹⁹ matrix and its RH analogue. They are usually

¹⁷ This follows from $i\sigma^2 \Delta$ in Equation (2.45) being symmetric.

¹⁸ More accurately, it can be parametrised as $W = \begin{pmatrix} \sqrt{1 - \rho \rho^\dagger} & \rho \\ -\rho^\dagger & \sqrt{1 - \rho^\dagger \rho} \end{pmatrix} \begin{pmatrix} U_L & 0 \\ 0 & U_R \end{pmatrix}$, with some small matrix ρ and the square root being understood as a Taylor series.

¹⁹ Pontecorvo – Maki – Nakagawa – Sakata

parametrised as follows:²⁰

$$\begin{aligned}
 U_{L/R} &= \begin{pmatrix} 1 & 0 & 0 \\ 0 & c_{23} & s_{23} \\ 0 & -s_{23} & c_{23} \end{pmatrix} \begin{pmatrix} c_{13} & 0 & s_{13}e^{-i\delta} \\ 0 & 1 & 0 \\ -s_{13}e^{i\delta} & 0 & c_{13} \end{pmatrix} \begin{pmatrix} c_{12} & s_{12} & 0 \\ -s_{12} & c_{12} & 0 \\ 0 & 0 & 1 \end{pmatrix} \\
 &= \begin{pmatrix} c_{12}c_{13} & s_{12}c_{13} & s_{13}e^{-i\delta} \\ -s_{12}c_{23} - c_{12}s_{23}s_{13}e^{i\delta} & c_{12}c_{23} - s_{12}s_{23}s_{13}e^{i\delta} & s_{23}c_{13} \\ s_{12}s_{23} - c_{12}c_{23}s_{13}e^{i\delta} & -c_{12}s_{23} - s_{12}c_{23}s_{13}e^{i\delta} & c_{23}c_{13} \end{pmatrix}.
 \end{aligned} \tag{2.60}$$

Here, $s_{ij} = \sin \theta_{ij}$ and $c_{ij} = \cos \theta_{ij}$ are used as abbreviations and δ is the CP-violating complex Dirac phase. For $\delta \notin \{0, \pi\}$ CP symmetry is violated directly in the neutrino sector.

The unitarity-relations $W^\dagger W = \mathbb{1}_3$ and $WW^\dagger = \mathbb{1}_3$ give interesting relations among U, S, T and V :

$$\begin{aligned}
 UU^\dagger + SS^\dagger &= \mathbb{1}_3 & TT^\dagger + VV^\dagger &= \mathbb{1}_3 \\
 U^\dagger U + T^\dagger T &= \mathbb{1}_3 & S^\dagger S + V^\dagger V &= \mathbb{1}_3 \\
 UT^\dagger + SV^\dagger &= 0 & U^\dagger S + T^\dagger V &= 0
 \end{aligned} \tag{2.61}$$

From Equation (2.59) it is clear that the absolute value of the elements of U and V must be close to one, whereas the elements of S and T are of the same order of magnitude as the elements of R , which we will find to be $\mathcal{O}(10^{-2})$ at most. More accurate analyses of this will be the subject of Chapter 4.

To distinguish between light and heavy mass eigenstates, we denote them by ν_i and N_i , respectively. The transformation between flavour and mass eigenstates then reads

$$\begin{aligned}
 n'_L &= \begin{pmatrix} \nu'_L \\ \nu'_R \end{pmatrix} = W n_L = \begin{pmatrix} V_L^\nu \\ V_R^\nu \end{pmatrix} n_L = \begin{pmatrix} U & S \\ T & V \end{pmatrix} \begin{pmatrix} \nu_L \\ N_L \end{pmatrix}, \\
 n'_R &= n'^c_L = \begin{pmatrix} \nu'^c_L \\ \nu'^c_R \end{pmatrix} = W^* n_R = \begin{pmatrix} V_L^{\nu*} \\ V_R^{\nu*} \end{pmatrix} n_R = \begin{pmatrix} U^* & S^* \\ T^* & V^* \end{pmatrix} \begin{pmatrix} \nu_R \\ N_R \end{pmatrix}.
 \end{aligned} \tag{2.62}$$

(2.63)

As only the light neutrinos have been experimentally observed up to now, it is worth commenting on the light neutrino part separately from the heavy one. Using Equation (2.59) once more, it is possible to express the neutrino mass term in Equation (2.51) as

²⁰Possible Majorana phases can be taken to be included in R here for simplicity.

block diagonalized:

$$\begin{aligned}\mathcal{L}_m^\nu &\simeq -\frac{1}{2} \overline{n'_L} O_R \begin{pmatrix} m_\nu & 0 \\ 0 & m_N \end{pmatrix} O_R^T n'_R + \text{h.c.} \\ &= -\frac{1}{2} \overline{\nu_L} U_L^\dagger m_\nu U_L \nu_R - \frac{1}{2} \overline{N_L} U_R^\dagger m_N U_R N_R + \text{h.c.}\end{aligned}\quad (2.64)$$

The matrices m_ν and m_N are not diagonal, but result from block diagonalizing M_ν in Equation (2.53). Thus they can be expressed through the seesaw formula, Equations (2.15) and (2.16):

$$m_\nu \approx M_L - M_D M_R^{-1} M_D^T, \quad m_N \approx M_R - M_D M_R^{-1} M_D^T \approx M_R. \quad (2.65)$$

Finally, U_L is precisely the matrix responsible for light neutrino oscillations. It therefore links the experimental values with the fundamental masses and parameters from the LRSM:²¹

$$\begin{aligned}\text{diag}(m_1, m_2, m_3) &= U_L^\dagger m_\nu U_L = U_L^\dagger (M_L - M_D M_R^{-1} M_D^T) U_L, \\ R &\approx M_D M_R^{-1} + \mathcal{O}(M_D^3 M_R^{-3}).\end{aligned}\quad (2.66)$$

The last equation can be found by considering $M_\nu = O_R \text{diag}(m_\nu, m_N) O_R^T$ together with the seesaw relations above.

Charged Lepton and Quark Masses

We are now going to briefly repeat the procedure of deriving the mass eigenstates for the charged leptons and quarks. The mass term for the charged leptons in Equation (2.49) can be written in matrix form as

$$\mathcal{L}_m^\ell = -\overline{\ell'_L} M_\ell \ell'_R + \text{h.c.} = -\overline{\ell_L} \hat{M}_\ell \ell_R + \text{h.c.} \quad (2.67)$$

with the mass matrix and the bi-unitary transformation used to diagonalize it being defined by

$$M_\ell = \frac{1}{\sqrt{2}} (f \kappa_2 e^{i\theta_2} + \tilde{f} \kappa_1), \quad \hat{M}_\ell = \text{diag}(m_e, m_\mu, m_\tau) = V_L^{\ell\dagger} M_\ell V_R^\ell. \quad (2.68)$$

The corresponding eigenvectors read

$$\ell'_L = V_L^\ell \ell_L, \quad \ell'_R = V_R^\ell \ell_R. \quad (2.69)$$

The 3×3 matrices V_L^ℓ and V_R^ℓ are unitary and describe the composition of the LH and

²¹ See Equation (2.109) and Equation (2.110) for the corresponding best-fit values.

RH charged lepton flavour states in terms of their corresponding mass eigenstates.

As will be understood when examining the weak interaction in the mass basis, the matrices V_L^ℓ and V_R^ℓ itself have no physical meaning. It's rather the combination $V_L^\ell V_L^{\nu\dagger}$ that is a physically observable. Therefore, we will absorb the charged lepton mixing matrices into the neutrino mixing matrices by an appropriate redefinition of $V_{L/R}^\nu$ and will afterwards regard $V_{L/R}^\ell$ as being equal to unity.

Finally, the mass terms for the quarks in Equation (2.50) are given by the matrix equation

$$\mathcal{L}_m^q = -\overline{u'_L} M_q^u u'_R - \overline{d'_L} M_q^d d'_R + \text{h.c.} = -\overline{u_L} \hat{M}_q^u u_R - \overline{d_L} \hat{M}_q^d d_R + \text{h.c.}, \quad (2.70)$$

where we used

$$\begin{aligned} M_q^u &= \frac{1}{\sqrt{2}} \left(f_q \kappa_1 + \tilde{f}_q \kappa_2 e^{-i\theta_2} \right), & \hat{M}_q^u &= V_L^{u\dagger} M_q^u V_R^u = \text{diag} (m_u, m_c, m_t), \\ M_q^d &= \frac{1}{2} \left(f_q \kappa_2 e^{i\theta_2} + \tilde{f}_q \kappa_1 \right), & \hat{M}_q^d &= V_L^{d\dagger} M_q^d V_R^d = \text{diag} (m_d, m_s, m_b), \end{aligned} \quad (2.71)$$

and

$$\begin{aligned} u'_L &= V_L^u u_L, & d'_L &= V_L^d d_L, \\ u'_R &= V_R^u u_R, & d'_R &= V_R^d d_R. \end{aligned} \quad (2.72)$$

The mixing in the quark sector is analogous to the mixing in the neutrino sector, except for the quarks not being of Majorana nature.

Vector Boson Masses

After spontaneous symmetry breaking, the gauge boson mass terms arise from the scalar kinetic Lagrangian

$$\mathcal{L}_{Sc} = \text{Tr} \left[(D_\mu \phi)^\dagger (D^\mu \phi) \right] + \text{Tr} \left[(D_\mu \Delta_L)^\dagger (D^\mu \Delta_L) \right] + \text{Tr} \left[(D_\mu \Delta_R)^\dagger (D^\mu \Delta_R) \right]. \quad (2.73)$$

Using the covariant derivatives given in Equation (2.38) and the VEVs from Equation (2.43), one can extract the terms coupling two gauge bosons (e.g. $W_{L\mu}^{3\dagger} W_{R\mu}^3$) from Equa-

tion (2.73). For the charged bosons $W_{L/R\mu}^\pm$ they can be organized as

$$\begin{aligned}\mathcal{L}_m^{W^\pm} &= \begin{pmatrix} W_{L\mu}^+ & W_{R\mu}^+ \end{pmatrix} M_W^2 \begin{pmatrix} W_L^{-\mu} \\ W_R^{-\mu} \end{pmatrix} \\ &= \begin{pmatrix} W_{1\mu}^+ & W_{2\mu}^+ \end{pmatrix} \begin{pmatrix} m_{W_1}^2 & \\ & m_{W_2}^2 \end{pmatrix} \begin{pmatrix} W_{1\mu}^{-\mu} \\ W_{2\mu}^{-\mu} \end{pmatrix},\end{aligned}\quad (2.74)$$

with the mass matrix and the transformation, leading to the eigenvectors $W_{1/2\mu}^\pm$ reading

$$M_W^2 = \frac{g^2}{4} \begin{pmatrix} \kappa_+^2 + 2v_L^2 & -2\kappa_1\kappa_2 e^{i\theta_2} \\ -2\kappa_1\kappa_2 e^{-i\theta_2} & \kappa_+^2 + 2v_R^2 \end{pmatrix}, \quad (2.75)$$

$$\begin{pmatrix} W_{L\mu}^\pm \\ W_{R\mu}^\pm \end{pmatrix} = \begin{pmatrix} \cos \xi & \sin \xi e^{\pm i\theta_2} \\ -\sin \xi e^{\mp i\theta_2} & \cos \xi \end{pmatrix} \begin{pmatrix} W_{1\mu}^\pm \\ W_{2\mu}^\pm \end{pmatrix}. \quad (2.76)$$

Here we introduced $\kappa_+^2 = \kappa_1^2 + \kappa_2^2$ which has to be equal to the Standard Model VEV in the case of Standard Model alignment $\kappa_+ \approx v_{\text{SM}} \approx 246$ GeV. The mixing angle and the physical masses of the W bosons are then found to be

$$\tan 2\xi = -\frac{2\kappa_1\kappa_2}{v_R^2 - v_L^2}, \quad (2.77)$$

$$m_{W_{1/2}}^2 = \frac{g^2}{4} \left(\kappa_+^2 + v_R^2 + v_L^2 \mp \sqrt{4\kappa_1^2\kappa_2^2 + v_R^4 + v_L^4 - 2v_R^2v_L^2} \right). \quad (2.78)$$

For $v_R^2 \gg \kappa_+^2$ and negligible v_L^2 , these values can be approximated as

$$\xi \approx -\frac{\kappa_1\kappa_2}{v_R^2}, \quad m_{W_1}^2 \approx \frac{g^2}{4} \kappa_+^2 \left(1 - 2\frac{\kappa_1\kappa_2}{\kappa_+^2 v_R^2} \right), \quad m_{W_2}^2 \approx \frac{g^2}{2} v_R^2. \quad (2.79)$$

If we additionally require $\kappa_2 \gg \kappa_1$, the mixing parameter becomes

$$\xi \approx -2 \frac{\kappa_2}{\kappa_1} \frac{m_{W_1}^2}{m_{W_2}^2} \ll 1. \quad (2.80)$$

For the neutral gauge bosons the same procedure yields

$$\begin{aligned}\mathcal{L}_m^{B,W^3} &= \frac{1}{2} \begin{pmatrix} W_{L\mu}^3 & W_{R\mu}^3 & B_\mu \end{pmatrix} M_0^2 \begin{pmatrix} W_L^{3\mu} \\ W_R^{3\mu} \\ B^\mu \end{pmatrix} \\ &= \frac{1}{2} \begin{pmatrix} Z_{1\mu} & Z_{2\mu} & A_\mu \end{pmatrix} \begin{pmatrix} m_{Z_1}^2 & & \\ & m_{Z_2}^2 & \\ & & 0 \end{pmatrix} \begin{pmatrix} Z_1^\mu \\ Z_2^\mu \\ A^\mu \end{pmatrix},\end{aligned}\quad (2.81)$$

with the massless SM photon A_μ and

$$M_0^2 = \frac{1}{2} \begin{pmatrix} g^2 \left(2v_L^2 + \frac{\kappa_+^2}{2} \right) & -g^2 \frac{\kappa_+^2}{2} & -2gg_Y v_L^2 \\ -g^2 \frac{\kappa_+^2}{2} & g^2 \left(2v_R^2 + \frac{\kappa_+^2}{2} \right) & -2gg_Y v_R^2 \\ -2gg_Y v_L^2 & -2gg_Y v_R^2 & 2g_Y^2 (v_L^2 + v_R^2) \end{pmatrix}, \quad (2.82)$$

$$m_{Z_{1/2}}^2 = \frac{1}{4} \left[g^2 \kappa_+^2 + 2g_+^2 v_+^2 \mp \sqrt{(g^2 \kappa_+^2 + 2g_+^2 v_+^2)^2 - 4g^2 (g_+^2 + g_Y^2) (4v_L^2 v_R^2 + \kappa_+^2 v_+^2)} \right]. \quad (2.83)$$

As abbreviation we defined $g_+ = g^2 + g_Y^2$ and $v_+^2 = v_L^2 + v_R^2$. The rotation leading to the mass eigenbasis in Equation (2.81) can be found in [29]:

$$\begin{pmatrix} W_{L\mu}^3 \\ W_{R\mu}^3 \\ B_\mu \end{pmatrix} = \begin{pmatrix} c_W c & c_W s & s_W \\ -s_W s_M c - c_M s & -s_W s_M s + c_M c & c_W s_M \\ -s_W c_M c + s_M s & -s_W c_M s - s_M c & c_W c_M \end{pmatrix} \begin{pmatrix} Z_{1\mu} \\ Z_{2\mu} \\ A_\mu \end{pmatrix}. \quad (2.84)$$

With e being the electric charge and θ_W the SM Weinberg angle, the mixing angles are given by

$$\begin{aligned} s_W &= \sin \theta_W = \frac{e}{g}, & c_W &= \cos \theta_W, \\ s_M &= \tan \theta_W, & c_M &= \frac{\sqrt{\cos 2\theta_W}}{\cos \theta_W} = \frac{e}{g_Y c_W}, \\ s &= \sin \phi, & c &= \cos \phi. \end{aligned} \quad (2.85)$$

The angle ϕ parametrises the mixture between the different chiralities and is given in terms of the mass-squared difference $\Delta m^2 = m_{Z_2}^2 - m_{Z_1}^2$:

$$\sin 2\phi = \frac{g^2}{2\Delta m^2 c_W^2} (4s_W^2 v_L^2 - \cos 2\theta_W \kappa_+^2). \quad (2.86)$$

Again, for $v_L \approx 0$ and $v_R \gg \kappa_+^2$, we have

$$m_{Z_1}^2 \approx \frac{g^2}{4} \frac{g^2 + 2g_Y^2}{g^2 + g_Y^2} \kappa_+^2, \quad m_{Z_2}^2 \approx (g^2 + g_Y^2) v_R^2, \quad (2.87)$$

$$\sin 2\phi \approx \frac{-g^2 \kappa_+^2 \cos 2\theta_W}{2\Delta m^2 c_W^2}. \quad (2.88)$$

2.3.3 Charged weak interactions with neutrinos

Having derived the general expressions relevant for the generation of mass and mixing, we are now able to derive expressions for the charged weak interactions involving neutrinos. For this we will separate the interaction part included in the fermion Lagrangian in Equation (2.41) which reads

$$\mathcal{L}_F = \underbrace{\overline{L}'_L i\rlap{/}\partial L'_L + \overline{L}'_R i\rlap{/}\partial L'_R}_{=\mathcal{L}_F^L} + \underbrace{\overline{Q}'_L i\rlap{/}\partial Q'_L + \overline{Q}'_R i\rlap{/}\partial Q'_R}_{=\mathcal{L}_F^q}. \quad (2.89)$$

Here, the slash denotes a contraction with the Dirac γ matrices: $\rlap{/}\partial = D_\mu \gamma^\mu$.

Now, the covariant derivatives given in Equation (2.38) can be inserted and $\mathcal{L}_F^{L/q}$ can be split into the kinetic terms $\mathcal{L}_{kin}^{L/q}$, neutral current interactions (NC) $\mathcal{L}_{NC}^{L/q}$ and charged current interactions (CC) $\mathcal{L}_{CC}^{L/q}$. As Equation (2.89) contains a sum over the the flavour indices, the mixing matrices derived above in general make the expression complicated when changing to the mass basis. However, in the following we show that the NC part,²² and the kinetic part are free of mixing and then focus on the more interesting flavour changing CC interactions.

First, consider the kinetic term for LH charged leptons in combination with the transformations given in Equation (2.69):

$$\overline{\ell}'_L i\rlap{/}\partial \ell'_L = \overline{\ell}_L V_L^{\ell\prime\dagger} i\rlap{/}\partial V_L^\ell \ell_L = \overline{\ell}_L i\rlap{/}\partial \ell_L. \quad (2.90)$$

The calculation is analogous for ℓ'_R and the quarks. For neutrinos, however, we have to consider both chiralities simultaneously, because they are Majorana particles:

$$\begin{aligned} \overline{\nu}'_L i\rlap{/}\partial \nu'_L + \overline{\nu}'_R i\rlap{/}\partial \nu'_R &= \overline{\nu}'_L i\rlap{/}\partial \nu'_L + \overline{\nu}'_R{}^c i\rlap{/}\partial \nu'^c_R \\ &= \overline{n}'_L i\rlap{/}\partial n'_L = \overline{n}_L i\rlap{/}\partial n_L = \frac{1}{2} \overline{n} i\rlap{/}\partial n, \end{aligned} \quad (2.91)$$

where we used $\overline{\nu}'_R i\rlap{/}\partial \nu'_R = -\overline{\partial}_\mu \nu'^c_R i\gamma^\mu \nu'_R$ and Equation (2.36) in the first line and the transformations from Equation (2.62) in the second line.

We can thus conclude that the kinetic terms do not depend on the mixing parameters. Similarly, the neutral current interactions are free from mixing and do not change the

²²For the more complicated expression of the neutral current in the mass eigenbasis, we refer to [29].

interacting flavour:

$$\begin{aligned}
 \mathcal{L}_{\text{NC}} &\supseteq \frac{1}{2} \left(\overline{\nu}'_L \quad \overline{\ell}'_L \right) \gamma^\mu \left[gW_{L\mu}^3 \begin{pmatrix} 1 & 0 \\ 0 & -1 \end{pmatrix} - g_Y B_\mu \right] \begin{pmatrix} \nu'_L \\ \ell'_L \end{pmatrix} \\
 &= \frac{1}{2} \overline{\nu}'_L \gamma^\mu [gW_{L\mu}^3 - g_Y B_\mu] \nu'_L - \frac{1}{2} \overline{\ell}'_L \gamma^\mu [gW_{L\mu}^3 + g_Y B_\mu] \ell'_L \\
 &= \frac{1}{2} \overline{n}_L \gamma^\mu [gW_{L\mu}^3 - g_Y B_\mu] n_L - \frac{1}{2} \overline{\ell}_L \gamma^\mu [gW_{L\mu}^3 + g_Y B_\mu] \ell_L \\
 &= \frac{1}{2} \overline{L}_L \gamma^\mu \left[gW_{L\mu}^3 \begin{pmatrix} 1 & 0 \\ 0 & -1 \end{pmatrix} - g_Y B_\mu \right] L_L.
 \end{aligned} \tag{2.92}$$

For the charged current, however, the situation is different. In the case of LH flavour eigenstates the CC Lagrangian for the leptons reads

$$\begin{aligned}
 \mathcal{L}_{\text{CC}} &\supseteq \frac{g}{\sqrt{2}} \left(\overline{\nu}'_L \quad \overline{\ell}'_L \right) \gamma^\mu \begin{pmatrix} 0 & W_{L\mu}^+ \\ W_{L\mu}^- & 0 \end{pmatrix} \begin{pmatrix} \nu'_L \\ \ell'_L \end{pmatrix} \\
 &= \frac{g}{\sqrt{2}} \overline{\ell}'_L \gamma^\mu \nu'_L W_{L\mu}^- + \text{h.c.} \\
 &= \frac{g}{\sqrt{2}} \overline{\ell}_L \gamma^\mu V_L^{\ell\dagger} V_L^\nu n_L W_{L\mu}^- + \text{h.c.}
 \end{aligned} \tag{2.93}$$

As was mentioned before, the physically observable parameters connected to mixing are not the elements of $V_{L/R}^\nu$, but rather the combination $V_{L/R}^{\ell\dagger} V_{L/R}^\nu$ above. Therefore we define

$$K_L = V_L^{\ell\dagger} V_L^\nu, \quad K_R = V_R^{\ell\dagger} V_R^{\nu*}. \tag{2.94}$$

Note that for the RH sector the matrix V_R^ν appears as conjugate because of the charge conjugation in the definition of N_R in Equation (2.63).

Although $K_{L/R}$ is the relevant quantity in processes involving mixing, for the actual calculations we can nevertheless regard $V_{L/R}^\ell$ as being equal to unity and thus work with $V_{L/R}^\nu$ only and use the parametrisation given in Equation (2.59). This is possible as all remaining parts of the Lagrangian are diagonal in the charged leptons. Because of that, deviations from $V_{L/R}^\ell = \mathbb{1}$ cannot be detected.

Finally, we also use Equation (2.76) to express the gauge bosons in their mass eigenbasis and give the complete expression for the leptonic charged current with both helicities

in the mass eigenbasis of all participating particles:

$$\mathcal{L}_{CC}^L = \frac{g}{\sqrt{2}} \bar{\ell} \gamma^\mu (W_{L\mu}^- K_L P_L + W_{R\mu}^- K_R P_R) n + \text{h.c.} \quad (2.95)$$

$$\begin{aligned} &= \frac{g}{\sqrt{2}} \bar{\ell} \gamma^\mu P_L (U\nu + SN) (\cos \xi W_{1\mu}^- + \sin \xi e^{-i\theta_2} W_{2\mu}^-) \\ &+ \frac{g}{\sqrt{2}} \bar{\ell} \gamma^\mu P_R (T^* \nu + V^* N) (\cos \xi W_{2\mu}^- - \sin \xi e^{i\theta_2} W_{1\mu}^-) + \text{h.c.} \end{aligned} \quad (2.96)$$

For completeness we note here that the mixing also occurs in the charged currents containing quarks. The analogue to the K_L and K_R matrices above, is the familiar CKM-matrix,²³ which results from the mixing matrices V_L^u and V_L^d in Equation (2.72):

$$U_L^{\text{CKM}} = V_L^{u\dagger} V_L^d, \quad U_R^{\text{CKM}} = V_R^{u\dagger} V_R^d. \quad (2.97)$$

For the LH sector this effect is already well known from the SM; the RH extension in the LRSM further satisfies [29].

$$(U_L^{\text{CKM}})_{ij} = \pm (U_R^{\text{CKM}})_{ij}. \quad (2.98)$$

2.3.4 Limits and constraints

To conclude this chapter, we give a short overview over the constraints on the parameters of the LRSM that are relevant for this work.

In order to be in agreement with the Standard Model and the experimental observations, the mixing between the two charged gauge bosons must be small. From the universality in weak decays and non-leptonic Kaon decays an upper limit on the mixing angle ξ in Equation (2.77) can be derived [37]:

$$|\xi| \lesssim 10^{-3}. \quad (2.99)$$

Thus, for all practical purposes the approximation

$$\cos \xi \approx 1 \quad \text{and} \quad \sin \xi \approx \xi \quad (2.100)$$

can be used, e.g. in the expression of the charged current interaction (2.96). Because of the small mixing, the notation is frequently abused and the educated reader should be aware that

$$\begin{aligned} W_1^\pm &\simeq W_L^\pm, & W_2^\pm &\simeq W_R^\pm, \\ m_{W_1} &\simeq m_L, & m_{W_2} &\simeq m_R. \end{aligned} \quad (2.101)$$

²³Cabbibo - Kobayashi - Maskawa

As we consider the case of very small mixing $\xi \approx 0$ in our analysis, we will adopt this notation in the following chapters as well.

Theoretical considerations on the vacuum stability require [38]

$$m_{W_2} > M_i, \quad (2.102)$$

with M_i being the mass of any of the three heavy neutrinos; CP violation in meson mixing results in a lower limit on the mass m_{W_2} [39]:

$$m_{W_2} \gtrsim 4 \text{ TeV}. \quad (2.103)$$

Furthermore, the hierarchy in the quark masses requires a hierarchy in the scalar VEVs of Equation (2.43) [39]:

$$v_L \ll \kappa_2 < \kappa_1 \ll v_R; \quad (2.104)$$

from neutral Kaon and B-meson mixing, the ratio of the bi-doublet VEVs is limited as [39, 40]²⁴

$$1 \gg \frac{\kappa_2}{\kappa_1} \gtrsim 0.02. \quad (2.105)$$

However, to reproduce the Standard Model, it is necessary to have

$$\kappa_+^2 = \kappa_1^2 + \kappa_2^2 = v_{\text{SM}} \approx 246 \text{ GeV}. \quad (2.106)$$

with v_{SM} being the vacuum expectation value of the SM.

Observations show [15, 16], that the light neutrino masses have to be smaller than 1 eV. This constraints the combination of heavy neutrino masses and mixings[41]:

$$\left| \sum_{k=1}^3 S_{\ell k}^* M_k S_{\ell' k}^* \right| \lesssim 1 \text{ eV}, \quad \ell, \ell' \in \{e, \mu, \tau\}. \quad (2.107)$$

From electroweak precision experiments, the elements of the matrix R in Equation (2.59) which mediates the mixing between LH and RH sector, are constrained as follows[41]:

$$|\eta_{ij}| \leq \begin{pmatrix} 2.0 \times 10^{-3} & 0.6 \times 10^{-4} & 1.6 \times 10^{-3} \\ 0.6 \times 10^{-4} & 0.8 \times 10^{-3} & 1.0 \times 10^{-3} \\ 1.6 \times 10^{-3} & 1.0 \times 10^{-3} & 2.6 \times 10^{-3} \end{pmatrix}_{ij}, \quad RR^\dagger = -2\eta = SS^\dagger \quad (2.108)$$

²⁴This applies in the case of parity as the discrete symmetry, which we haven chosen above.

Oscillation experiments constrain the values of the light neutrino mixing matrix U_L in Equation (2.59). The best-fit values in the parametrisation given in Equation (2.60) are [42]:

$$\begin{aligned}
 \sin^2\theta_{12} &= 2.97 \times 10^{-1} \quad (\text{NH \& IH}), \\
 \sin^2\theta_{13} &= 2.14 \times 10^{-2} \quad (\text{NH}), & \sin^2\theta_{13} &= 2.18 \times 10^{-2} \quad (\text{IH}), \\
 \sin^2\theta_{23} &= 4.37 \times 10^{-1} \quad (\text{NH}), & \sin^2\theta_{23} &= 5.69 \times 10^{-1} \quad (\text{IH}), \\
 \delta &= 1.35 \pi \quad (\text{NH}), & \delta &= 1.32 \pi \quad (\text{IH}).
 \end{aligned} \tag{2.109}$$

As indicated above, the values depend on the hierarchy of the masses of the light neutrinos. In the case of normal hierarchy (NH) the masses are ordered as $m_1 < m_2 < m_3$, whereas an inverted hierarchy (IH) implies $m_3 < m_1 < m_2$.

The squared mass differences $\delta m^2 = m_2^2 - m_1^2$ and $\Delta m^2 = m_3^2 - (m_1^2 + m_2^2)$ of the light neutrino masses m_i fit the experimental values best if they are

$$\begin{aligned}
 \delta m^2 &= 7.37 \times 10^{-5} \text{ eV}^2 \quad (\text{NH \& IH}), \\
 \Delta m^2 &= 2.50 \times 10^{-3} \text{ eV}^2 \quad (\text{NH}), & \Delta m^2 &= 2.46 \times 10^{-3} \text{ eV}^2 \quad (\text{IH}).
 \end{aligned} \tag{2.110}$$

Further constraints and considerations, e.g. about the scalar components, can be found in [34, 35, 43–45].

Chapter 3

Neutrinoless double beta decay

In this chapter we give a short overview over the neutrinoless double beta decay contributions in the LRSM. We first list the different amplitudes with their characteristics and limits and then show how they combine to the resulting half life of the decay. As we are mainly interested in the λ diagram, we will stress how the respective limit is obtained from the half life. The information in this chapter are taken from [21], combined with the current lower limit on the half life of xenon from [46].

Similarly to the ordinary beta decay, in which a neutron decays into a proton, an electron and an anti electron neutrino, in the $0\nu\beta\beta$ decay two neutrons decay. However, in this case, the decay products are two protons and two electrons, but no neutrino. This is only possible if the neutrino interacts as Majorana particle. Roughly speaking, the neutrino emitted from one neutron can interact as anti neutrino with the other neutron. Therefore, the discovery of this process would unambiguously prove the Majorana nature of the neutrino.

In the low energy regime, the interaction happens inside an nucleus. Therefore, nuclear physical aspects have to be included, such as transition matrix elements. The results of the corresponding calculations vary by $\mathcal{O}(1)$ factors depending on the calculation scheme. Thus the limits obtained by the following considerations have to be taken with care.

3.1 Contributing amplitudes in the Left Right symmetric model

At the particle physics level, the relevant constituents of the $0\nu\beta\beta$ decay are weakly interacting quarks, which have to be described by the Lagrangian given in Equation (2.96). In the Left Right symmetric model different amplitudes give rise to the $0\nu\beta\beta$ decay. One main difference between these contributions is the chirality of the external particles involved. Furthermore mass mixing in the bosonic currents can lead to different amplitudes with same chiralities, although in general they are suppressed due to the smallness of the mixing (see Equation (2.99)).

In order to estimate the cross section of the respective channel, one has to take into account the W propagators $\sim m_{L/R}^{-2}$, the neutrino propagator as described below and the coupling of the neutrinos to the gauge bosons parametrised by the mixing matrices $K_L = (U, S)$ and $K_R = (T^*, V^*)$ given in Equation (2.94). Furthermore, the gauge boson mixing $\sim \tan \xi$ might be included (2.76).

The chiralities of the outgoing electrons are connected to the neutrino propagator contribution:

$$\mathcal{A} \propto P_{L/R} \frac{\not{q} + m}{q^2 - m^2} P_{L/R}, \quad (3.1)$$

with q being the four-momentum carried by the neutrino, m its mass (heavy or light) and $P_{L/R}$ the chirality projection operators introduced in Equation (2.31). The latter depend on the chiralities of the outgoing electrons. First we consider them to be equal. The expression simplifies as follows:

$$\mathcal{A} \propto P_L \frac{\not{q} + m}{q^2 - m^2} P_L = \frac{m}{q^2 - m^2} P_L. \quad (3.2)$$

As the momentum dependency of the nominator vanishes by use of the identities in Equation (2.31), processes like this are called mass-dependent. In theories without RH gauge bosons, e.g. minimal extensions to the SM, these are the only contributions to the $0\nu\beta\beta$ decay.

For the case of two different chiralities in the outgoing electrons, we find

$$\mathcal{A} \propto P_L \frac{\not{q} + m}{q^2 - m^2} P_R = \frac{\not{q}}{q^2 - m_i^2} P_R, \quad (3.3)$$

and call such amplitudes momentum-dependent.

For neutrinoless double beta decay in nuclei, the energies involved are rather small and as an estimate we can use $q^2 \approx 10^4 \text{ MeV}^2$. Depending on whether we are considering light or heavy neutrinos in the propagator – both have to be summed up in general – the amplitude might be larger for momentum-dependent or mass-dependent mechanisms.

Standard left handed diagram \mathcal{A}^L

In the simplest extension to the Standard Model a Majorana neutrino couples to two LH gauge bosons as shown in Figure 3.1a. The amplitude is then given by

$$\mathcal{A}^L \simeq G_F^2 \left(\sum_{i=1}^3 U_{ei} \frac{m_i}{q^2} U_{ei} + \sum_{i=1}^3 S_{ei} \frac{M_i}{q^2 - M_i^2} S_{ei} \right), \quad (3.4)$$

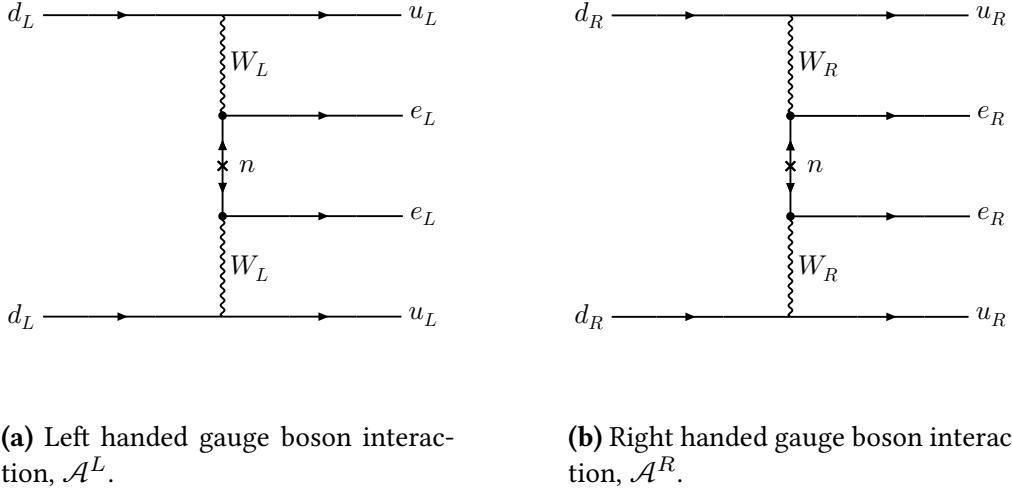


Fig. 3.1 – Feynman diagrams for the contributions to the neutrinoless double beta decay with equal chiralities in the outgoing electrons.

with $G_F = \sqrt{2}g^2/8m_L^2$ being the Fermi Constant of Weak Interaction. The two contributions can be characterized separately as

$$\mathcal{A}_\nu \simeq G_F^2 \left(\sum_{i=1}^3 U_{ei} \frac{m_i}{q^2} U_{ei} \right) = G_F^2 \frac{\langle m_{ee} \rangle}{q^2}, \quad (3.5)$$

$$\mathcal{A}_{N_R}^L \simeq G_F^2 \sum_{i=1}^3 \frac{S_{ei}^2}{M_i^2}. \quad (3.6)$$

For \mathcal{A}_ν the physically interesting quantity describing the contribution of this process is the effective mass $|\langle m_{ee} \rangle| = |\sum U_{ei}^2 m_i|$. In order to express this parameter in terms of a dimensionless quantity, $\langle m_{ee} \rangle$ is rescaled by the electron mass:

$$|\eta_\nu| = \frac{|\langle m_{ee} \rangle|}{m_e} \leq 3.0 \times 10^{-7}. \quad (3.7)$$

The limit given here, as well as in the case of the amplitudes below, is obtained from the experimental limit on the half life of the nucleus under consideration as described in Section 3.2 below.

The corresponding parameter for $\mathcal{A}_{N_R}^L$ is

$$|\eta_{N_R}^L| = m_p \left| \sum_{i=1}^3 \frac{S_{ei}^2}{M_i} \right| \leq 2.9 \times 10^{-9}. \quad (3.8)$$

Here, m_p is the mass of the proton.

If we additionally include the possibility of gauge boson mixing¹, we can summarize the amplitude for two LH electrons being emitted as

$$\mathcal{A}_{LL} \simeq G_F^2 (1 + 2\tan \xi + \tan^2 \xi) \sum_{i=1}^3 \left(\frac{U_{ei}^2 m_i}{q^2} - \frac{S_{ei}^2}{M_i} \right). \quad (3.9)$$

Standard right handed diagram \mathcal{A}^R

Figure 3.1b shows the Feynman diagram that is obtained from replacing all LH particles in the \mathcal{A}_ν diagram with RH particles. Its amplitude reads

$$\mathcal{A}^R \simeq G_F^2 \frac{m_L^4}{m_R^4} \left(\sum_{i=1}^3 T_{ei}^* \frac{m_i}{q^2} T_{ei} + \sum_{i=1}^3 V_{ei}^* \frac{M_i}{q^2 - M_i^2} V_{ei} \right). \quad (3.10)$$

Here, the light neutrino exchange can be neglected, as it is suppressed by both the light neutrino mass m_i as well as the small mixing $T_{ei} \ll V_{ei}$. The heavy neutrino contribution is approximately given by

$$\mathcal{A}_{NR}^R \approx -G_F^2 \frac{m_L^4}{m_R^4} \sum_{i=1}^3 \frac{V_{ei}^{*2}}{M_i}, \quad (3.11)$$

and as a dimensionless parameter for this process we can define

$$|\eta_{NR}^R| = m_p \frac{m_L^4}{m_R^4} \left| \sum_{i=1}^3 \frac{V_{ei}^{*2}}{M_i} \right| \leq 2.9 \times 10^{-9}. \quad (3.12)$$

For two RH electrons emitted we thus find the overall amplitude including boson mixing up to $\mathcal{O}(\tan^2 \xi)$ as follows

$$\mathcal{A}_{RR} \simeq G_F^2 \left(\frac{m_L^4}{m_R^4} + 2 \frac{m_L^2}{m_R^2} \tan \xi + \tan^2 \xi \right) \sum_{i=1}^3 \left(\frac{T_{ei}^{*2} m_i}{q^2} - \frac{V_{ei}^{*2}}{M_i} \right). \quad (3.13)$$

Triplet exchange diagrams $\mathcal{A}_{\delta_{L/R}}$

The Left Right symmetric model also includes doubly charged heavy scalar triplets resulting from the type-II seesaw mechanism. These particles can also mediate the $0\nu\beta\beta$ decay. The corresponding Feynman diagrams are shown in Figure 3.2.

¹ In this case the quarks coupled the boson may not have the same chirality as the electron.

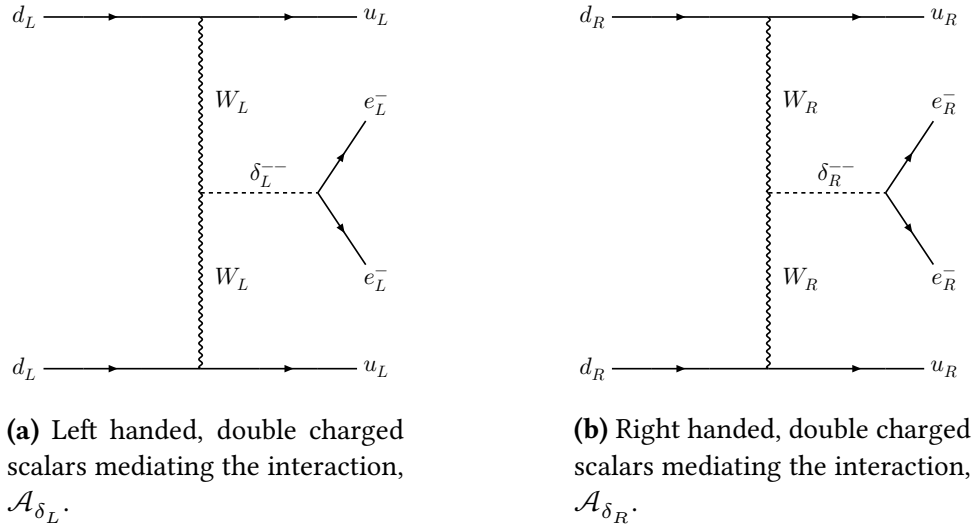


Fig. 3.2 – Contribution from the $SU(2)_{L/R}$ triplets of the Left Right symmetric model.

In the case of the RH triplet (Fig. 3.2b), the amplitude is given by

$$\mathcal{A}_{\delta_R} \simeq G_F^2 \frac{m_L^4}{m_R^4} \sum_{i=1}^3 \frac{V_{ei}^2 M_i}{m_{\delta_R^{--}}^2}, \quad (3.14)$$

and the corresponding particle physics parameter reads

$$|\eta_{\delta_R}| = \frac{m_p}{G_F^2} \frac{|\sum_{i=1}^3 V_{ei}^2 M_i|}{m_{\delta_R^{--}}^2 m_R^4} \leq 2.9 \times 10^{-9}, \quad (3.15)$$

where the relation $\sqrt{2}v_R(h_R)_{ee} = \sum V_{ei}^2 M_i$ has been used.

For the LH triplet, the expression reads

$$\mathcal{A}_{\delta_L} \simeq G_F^2 \frac{(h_L)_{ee} v_L}{m_{\delta_L^{--}}^2}. \quad (3.16)$$

Here, h is the the Yukawa coupling matrix given in Equation (2.45). This amplitude is suppressed by a factor of $q^2/m_{\delta_L^{--}}^2$ compared to the other diagrams and can thus be neglected.

Momentum dependent diagrams

After having presented the mass-dependent mechanisms above, we now explain the two most important momentum dependent amplitudes.

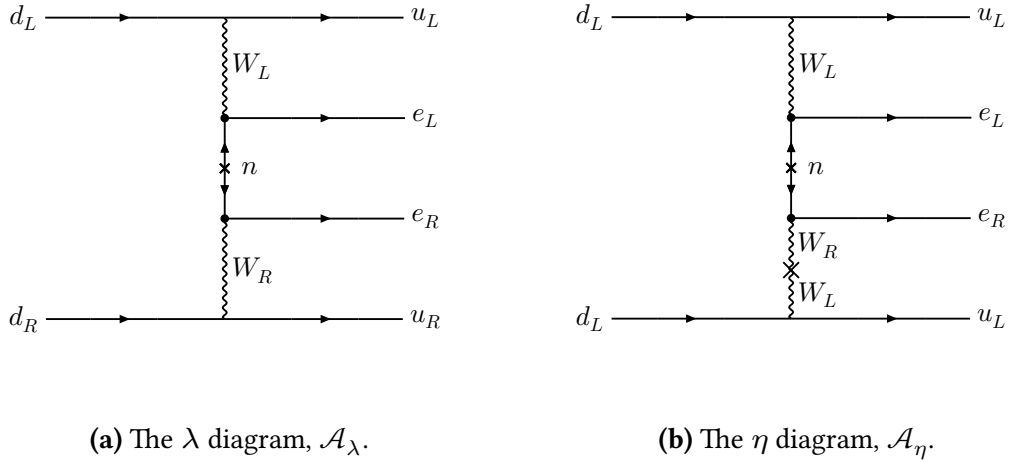


Fig. 3.3 – Contributions with different helicities in the outgoing electrons.

In these channels the emitted electrons have different helicities. This requires to couple the neutrino to two gauge bosons of different helicities W_L^- and W_R^- . In the simplest case, without gauge boson mixing, the result is the λ diagram shown in Figure 3.3a. Its amplitude reads

$$\mathcal{A}_\lambda \simeq G_F^2 \frac{m_L^2}{m_R^2} \left(\sum_{i=1}^3 \frac{U_{ei} T_{ei}^*}{q} + \sum_{i=1}^3 S_{ei} V_{ei}^* \frac{q}{q^2 - M_i^2} \right). \quad (3.17)$$

In the low energy $0\nu\beta\beta$ decay, the heavy neutrino contribution is suppressed by its mass; as we want to consider this diagram at high energies, we nevertheless derive an approximate expression including the heavy neutrino propagators. Therefore we use an approximation from [41], which was originally introduced for the standard mass-dependent mechanism \mathcal{A}_{NR}^L :

$$\mathcal{A}_\lambda \simeq \frac{G_F^2}{q} \frac{m_L^2}{m_R^2} \left(\sum_{i=1}^3 U_{ei} T_{ei}^* - \sum_{i=1}^3 F(A, M_i) S_{ei} V_{ei}^* \right), \quad (3.18)$$

with $F(A, M_i)$ resulting from the integration over the small transferred momentum q . It reads

$$F(A, M_i) \approx \frac{M_a^2}{M_i^2} f(A), \quad M_a \approx 0.9 \text{ GeV}, \quad (3.19)$$

and depends on the considered nucleus with atomic number A through the value $f(A)$. For ^{136}Xe , which we use for our calculations, we have $f(^{136}\text{Xe}) \approx 0.068$. The values for other nuclei can be taken from [41].

The particle physics parameter in this case reads

$$|\eta_\lambda| = \frac{m_L^2}{m_R^2} \left| \sum_{i=1}^3 U_{ei} T_{ei}^* - \sum_{i=1}^3 F(A, M_i) S_{ei} V_{ei}^* \right| \leq 2.4 \times 10^{-7}. \quad (3.20)$$

This value will be used in the following chapter to derive upper limits on the cross section of the high energy equivalent.

Finally, the light neutrino part of the η diagram (Fig. 3.3b) also contributes to the momentum-dependent amplitude.² It is given by

$$\mathcal{A}_\eta \simeq G_F^2 \tan \xi \sum_{i=1}^3 \frac{U_{ei} T_{ei}^*}{q}, \quad (3.21)$$

and can be described by the dimensionless particle physics parameter

$$|\eta_\eta| = \tan \xi \left| \sum_{i=1}^3 U_{ei} T_{ei}^* \right| \leq 1.3 \times 10^{-9}. \quad (3.22)$$

The general expression for the momentum-dependent amplitude, including mixing up to second order, reads

$$\mathcal{A}_{LR} \simeq G_F^2 \left(\frac{m_L^2}{m_R^2} + \tan \xi + \frac{m_L^2}{m_R^2} \tan \xi + \tan^2 \xi \right) \sum_{i=1}^3 \left(\frac{U_{ei} T_{ei}^*}{q} - S_{ei} V_{ei}^* \frac{q}{M_i^2} \right). \quad (3.23)$$

3.2 Nuclear matrix elements and half lives

The lifetime $T_{1/2}^{0\nu}$ of the nucleus under consideration in the $0\nu\beta\beta$ decay has to be calculated including the nuclear matrix elements \mathcal{M}_i which describe the interaction of the constituent quarks in the environment of the nucleus. For our analysis we consider ^{136}Xe , although the following considerations are analogous for other nuclei with the appropriate replacements (see [21] for details).

The general expression for $T_{1/2}^{0\nu}$ resulting from the contribution of all diagrams above can be written as

$$\begin{aligned} (T_{1/2}^{0\nu})^{-1} = G_{01}^{0\nu} & \left(|\mathcal{M}_\nu^{0\nu}|^2 |\eta_\nu|^2 + |\mathcal{M}_N^{0\nu}|^2 |\eta_{N_R}^L|^2 + |\mathcal{M}_N^{0\nu}|^2 |\eta_{N_R}^R + \eta_{\delta_R}|^2 + \right. \\ & \left. + |\mathcal{M}_\lambda^{0\nu}|^2 |\eta_\lambda|^2 + |\mathcal{M}_\eta^{0\nu}|^2 |\eta_\eta|^2 \right) + \text{interference terms.} \end{aligned} \quad (3.24)$$

² We neglect the heavy neutrino propagator here as it is suppressed by the heavy neutrino mass M_i and we are not further interested in details about this diagram.

$G_{01}^{0\nu}$ is the phase space factor resulting from the integration over the available momentum space. Following the notation of [21], the $\mathcal{M}_i^{0\nu}$ contain the actual nuclear matrix elements \mathcal{M}_i as well as kinematical factors and some weight that takes into account that different approaches have been adopted to calculate the matrix elements for the different processes.

Given the limit on the neutrinoless double beta decay, one can finally extract a limit on the parameter of interest by assuming that the amplitude under consideration is mainly responsible for the decay. In our case – we are interested in the λ diagram– we can therefore assume

$$\left(T_{1/2}^{0\nu}\right)^{-1} \approx G_{01}^{0\nu} |\mathcal{M}_\lambda^{0\nu}|^2 |\eta_\lambda|^2. \quad (3.25)$$

Among various other values, [21] quotes the value for $G_{01}^{0\nu}$ and a range for $\mathcal{M}_\lambda^{0\nu}$ in the case of xenon:

$$\mathcal{M}_\lambda^{0\nu} = 1.96 - 2.49 \quad \text{and} \quad G_{01}^{0\nu} \approx 4.24 \times 10^{-14} \text{ yrs}^{-1}. \quad (3.26)$$

The current half life limit for ^{136}Xe from the experiment is [46]:

$$T_{1/2}^{0\nu} \geq 1.07 \times 10^{26} \text{ yrs} \quad (3.27)$$

Equation (3.25) then yields

$$|\eta_\lambda| \approx \left(G_{01}^{0\nu}\right)^{-1/2} |\mathcal{M}_\lambda^{0\nu}|^{-1} \left(T_{1/2}^{0\nu}\right)^{-1/2} \lesssim 2.4 \times 10^{-7}. \quad (3.28)$$

The same procedure can be done for the other diagrams, giving the limits presented in Section 3.1.

Chapter 4

Analysing the lambda diagram at the Large Hadron Collider

In this chapter we perform our analysis of the λ diagram cross section in the high energy scenario and derive upper limits for the respective signal. We first summarise the scenario we are considering, i.e. we give the relevant model parameters we used for our simulations and the constraints we will use for the discussion. Then we consider the t -channel process (Fig. 3.3a) and afterwards the s -channel process for the case where the incoming quarks couple to the W_R^- (Fig. 4.1). As we are working in the ultra-relativistic limit the interference between the different channels can be neglected.¹

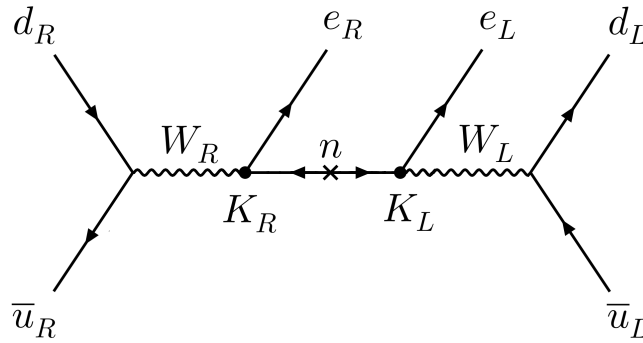


Fig. 4.1 – The s -channel λ diagram contribution with right-handed incoming quarks. The mixing matrices contributing to the coupling between the neutrino propagator n and the W bosons are indicated by $K_L \simeq (U, S)$ and $K_R \simeq (T^*, V^*)$, respectively.

We stress that we consider the interaction in the center of mass frame of the participating quarks only, i.e. we did not take any parton distribution into account. The center of mass energy \sqrt{s} corresponds therefore to the energy resulting from the two quarks

¹ The interference terms are proportional to the mass m of the incoming quark as $\sum P_L \psi_s \bar{\psi}_s \gamma^\mu P_R = m \gamma^\mu P_R$, whereas the pure, non-interfering amplitudes are proportional to its momentum $q \gg m$: $\sum P_L \psi_s \bar{\psi}_s \gamma^\mu P_L = \not{q} \gamma^\mu P_L$; here, ψ denotes the spinor of the incoming quark and the sum is taken over its spin $s = \pm \frac{1}{2}$.

only:

$$s = (p_{q1} + p_{q2})^2, \quad (4.1)$$

with p_{q1} and p_{q2} the momenta of the quarks. It is connected to the center of mass energy in the proton-proton collision $\sqrt{s_{pp}}$ via

$$\sqrt{s} = x_1 \cdot x_2 \cdot \sqrt{s_{pp}}. \quad (4.2)$$

Here, x_1 and x_2 characterize the fraction of the proton momenta carried by the interacting quarks. In general it is necessary to include the parton distribution function² in order to calculate the correct cross section in terms of $\sqrt{s_{pp}}$. However, as a rough estimate, one can use the averaged momentum fractions $\langle x_i \rangle$. For the valence quarks (d and u) and sea quarks (the remaining quarks and anti quarks), these are approximately [47]

$$\langle x_V \rangle \approx 0.12 \quad \text{and} \quad \langle x_S \rangle \approx 0.04. \quad (4.3)$$

The cross section in a proton-proton collision can then be calculated by summing up all contributions, that is, of all combinations of quarks in the protons that can lead to the interaction. In the case of the t -channel diagram this gives

$$\begin{aligned} \sigma(s) &= \sigma_{dd}(s) + \sigma_{\bar{u}\bar{u}}(s) + \sigma_{d\bar{u}}(s) + \sigma_{\bar{u}d}(s) \\ &= \sigma_{dd}(s) + \sigma_{\bar{u}\bar{u}}(s) + 2\sigma_{d\bar{u}}(s) \\ &\approx \sigma(0.12^2 s_{pp}) + \sigma(0.04^2 s_{pp}) + 2\sigma(0.12 \cdot 0.04 s_{pp}). \end{aligned} \quad (4.4)$$

For the s -channel, it reads

$$\sigma(s) \approx 2\sigma(4.8 \times 10^{-3} s_{pp}). \quad (4.5)$$

In the following we will continue working with the center of mass energy in the quark-quark interaction \sqrt{s} . However, we stress that the above reduces the signal of interactions involving heavy neutrinos by several orders of magnitude as

$$\sigma \propto s^2 \approx 10^{-4} s_{pp}^2. \quad (4.6)$$

The simulations which resulted in the approximative expressions for the cross sections given below, were carried out with the Monte Carlo simulator Mad Graph 5. Technical details about the implementation of the LRSM and the simulations as well as a short introduction to this program can be found in Appendix C. The model parameters we used for the simulations were chosen such that they fulfil the constraints given in Subsection

² The parton distribution function describes how the values of x are distributed, i.e. how probable it is that a quark has momentum $p_q = x \cdot p$.

2.3.4; they are summarised as follows:

We restrict ourselves to the scenario where the mixing between the gauge bosons (see Equation (2.77)) is negligible, we thus set the bi-doublet VEVs accordingly:

$$\kappa_1 \simeq 245.9 \text{ GeV} \quad \text{and} \quad \kappa_2 \simeq 7.4 \text{ GeV}. \quad (4.7)$$

This results in vanishing mixing in the gauge boson sector, as can be understood by use of Equation (2.80).

For the left handed unitary neutrino mixing matrix U_L from Equation (2.59) we used the best-fit PMNS-matrix parameters for the normal hierarchy scenario given in Equation (2.109). The right handed analogue U_R was randomly chosen in the full parameter space, i.e.

$$\sin \theta_R \in \{-1, 1\} \quad \text{for} \quad \theta_R \in \{\theta_{R12}, \theta_{R13}, \theta_{R23}\} \quad \text{and} \quad \delta_R \in \{0, \pi\}. \quad (4.8)$$

The complex elements of the matrix R which is responsible for heavy-light mixing in the neutrinos, were drawn within the constraints given by the electroweak precision data in Equation (2.108).

Finally, different combinations for the heavy neutrino masses M_i , the heavy W boson mass m_R and the center of mass energy \sqrt{s} have been simulated and evaluated separately. Only such combinations of the above mentioned parameters have been accepted that fulfilled the constraints given by electroweak precision measurements (Equation (2.108)) and the requirement of small neutrino masses (Equation (2.107)). As the latter constrains the combination of heavy neutrino masses M_i and their mixing matrix elements S_{ei} quite strongly, the resulting values of the R_{ij} were rather small in most cases.

However, the conclusion we draw in the following are unaffected hereof as the effect of the mixing matrix elements can be factored out by analytical considerations (see Chapter B). In this way it is possible to recover expressions for the cross sections valid for arbitrary R .

The values for m_R , \sqrt{s} and M_i spanned the ranges

$$\begin{aligned} 0.5 \text{ TeV} &\lesssim m_R \lesssim 50 \text{ TeV}, \\ 1 \text{ TeV} &\lesssim \sqrt{s} \lesssim 20 \text{ TeV}, \\ 50 \text{ GeV} &\lesssim M_i \lesssim 4 \text{ TeV}, \end{aligned} \quad (4.9)$$

but were mainly taken near $m_R \approx 4 \text{ TeV}$, $\sqrt{s} \approx 13 \text{ TeV}$ and around $500 \text{ GeV} \lesssim M_i \lesssim 2 \text{ TeV}$ as this part of the parameter space is most promising due to the small masses; much larger values of \sqrt{s} are not accessible today. The conclusions we draw in the following should be considered valid for regions of the parameter space near these reference values mainly.

In the following we are interested in investigating how the results of the low energy $0\nu\beta\beta$ decay constrain the high energy cross section. Thus we will work with the constraint on the parameter η_λ from Equation (3.18), which we recall being

$$\left| \sum_{i=1}^3 U_{ei} T_{ei}^* + \sum_{i=1}^3 S_{ei} V_{ei}^* \frac{M_a^2}{M_i^2} f(A) \right| \leq \frac{m_R^2}{m_L^2} \eta_0, \quad M_a \approx 0.9 \text{ GeV}. \quad (4.10)$$

In the case of ^{136}Xe , which we used in our analysis, we have

$$f(A) \simeq 0.068 \quad \text{and} \quad \eta_0 \leq 2.41 \times 10^{-7}. \quad (4.11)$$

In the generic case where the $S_{ei} V_{ei}^*$ are of the same order of magnitude as the $U_{ei} T_{ei}^*$ we find $f(A) M_a^2/M_i^2 \ll 1$ and the heavy neutrino contribution in the low energy case can be neglected.³ More generally, if $U_{ei} T_{ei}^* \gg S_{ei} V_{ei}^* f(A) M_a^2/M_i^2$, or if the heavy neutrinos do not contribute at low energy for any other reason, the constraint in Equation (4.10) affects only the light neutrino couplings $\sum U_{ei} T_{ei}^* \approx -R_{11}$ and we can write

$$\left| \sum_{i=1}^3 U_{ei} T_{ei}^* \right| \approx |R_{11}| \leq \frac{m_R^2}{m_L^2} \eta_0. \quad (4.12)$$

Similarly, if the light neutrinos do not contribute, e.g. if $R_{11} \approx 0$, we have

$$\left| \sum_{i=1}^3 \frac{S_{ei} V_{ei}^*}{M_i^2} \right| \leq \frac{m_R^2}{m_L^2 M_a^2} \frac{\eta_0}{f(A)}. \quad (4.13)$$

However, this is a very weak constraint as the heavy neutrino mass in the denominator suppresses the matrix elements by some orders of magnitude, which can be understood as the $0\nu\beta\beta$ decay happens at relatively low energies of $\mathcal{O}(100 \text{ MeV})$; at this energy, the heavy neutrino contribution is strongly suppressed and consequently the limit resulting from the non-observation of xenon decays does not constrain the heavy neutrino parameters. Thus, it is fulfilled in almost all cases under consideration.

Furthermore, from Subsection 2.3.4 we know that the various parameters of the model are constrained by theory as well as by experimental data. Below we will mainly use

³ Note that this is true for the λ diagram, but not necessarily for mass-dependent mechanisms (see Section 3.1) where the heavy neutrino mass dependency is different.

three conditions and constraints thereof, namely

$$\sum_{i=1}^3 U_{ei} T_{ei}^* = - \sum_{i=1}^3 S_{ei} V_{ei}^* \approx R_{11}, \quad (4.14)$$

$$\left| \sum_{i=1}^3 S_{ei}^{*2} M_i \right| \leq 1 \text{ eV} \approx 0 \quad (4.15)$$

$$\text{and } |\eta_{ij}| \leq \begin{pmatrix} 2.0 \times 10^{-3} & 0.6 \times 10^{-4} & 1.6 \times 10^{-3} \\ 0.6 \times 10^{-4} & 0.8 \times 10^{-3} & 1.0 \times 10^{-3} \\ 1.6 \times 10^{-3} & 1.0 \times 10^{-3} & 2.6 \times 10^{-3} \end{pmatrix}_{ij}, \quad (4.16)$$

with the matrix η being defined as

$$\eta = -\frac{1}{2} R R^\dagger = -\frac{1}{2} S S^\dagger. \quad (4.17)$$

Equation (4.14) results from the unitarity of the mixing matrix W when neglecting terms of $\mathcal{O}(R^3)$; this approximation will be used frequently without explicitly mentioning it in the following. Equation (4.15) has to be fulfilled in order to get small neutrino masses and is meaningful only when considering all three heavy neutrinos contributing to the signal, in other cases it can generally be argued that the non-contributing neutrinos can compensate the terms in the constraint coming from the interacting neutrino. Although we will use it only at the end of the chapter, we already give it here to summarize the important constraints.

Finally, Equation (4.16) is extracted from electroweak precision measurements. In particular it implies

$$|R_{11}|^2 \leq 4.0 \times 10^{-3} \text{ and } |S_{ei}|^2 \leq 4.0 \times 10^{-3} \text{ for } i = 1, 2, 3. \quad (4.18)$$

This result, together with Equation (4.12), determines the upper limit for any signal, as we will see in a moment. Note that we can also use $|S_{ei} V_{ei}^*|^2 \leq 4 \times 10^{-3}$ as the matrix V is of order one (see Equation (2.59)).

The constraints on R_{11} are shown in Figure 4.2a; we also indicate how the allowed parameter space for $|R_{11}|$ changes if the future limit on the half life of xenon in the neutrinoless double beta decay is improved by a factor of 2 or 10, respectively.

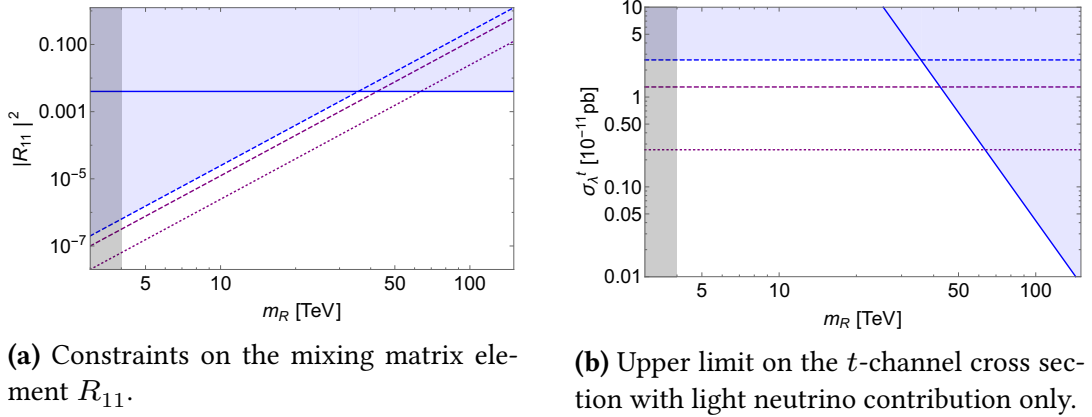


Fig. 4.2 – Constraints for negligible heavy neutrino contribution in the low energy $0\nu\beta\beta$ decay. The blue lines indicate current constraints from electroweak precision data (solid line) and the non-observation of low energy $0\nu\beta\beta$ decay of xenon (dashed line); the purple lines correspond to improved $0\nu\beta\beta$ limits, i.e. if the lower limit on the half life doubles (dashed) or increases by a factor of 10 (dotted). The gray-shaded region is excluded by the limit on the heavy W boson mass of $m \gtrsim 4$ TeV.

4.1 Limits on the t -channel cross section σ_λ^t

For the t -channel, the cross section can be calculated by the formula derived in Section B.1 in the appendix:

$$\sigma_\lambda^t = \frac{s a(s)}{m_R^4} \sum_{i,j=0}^3 \mathcal{M}_i \mathcal{M}_j^* \sigma_0^t(y_i, y_j). \quad (4.19)$$

Here, \sqrt{s} is the center of mass energy, $a(s)$ an $\mathcal{O}(1)$ -function given in Equation (B.14) and the matrix elements and masses have been renamed to shorten the notation as

$$\mathcal{M}_i = \begin{cases} \sum_{j=1}^3 U_{ej} T_{ej}^* \approx -R_{11}, & i = 0, \\ S_{ei} V_{ei}^*, & i = 1, 3, 4, \end{cases} \quad (4.20)$$

$$y_i = \begin{cases} 0, & i = 0 \\ M_i^2/s, & i = 1, 3, 4. \end{cases}$$

The function $\sigma_0^t(y_i, y_j)$ is shown in Figure B.3. It is symmetric in its two arguments and decreases monotonically in both of them. For $y_i \approx 0 \approx y_j$ it takes its maximum of roughly 10^{10} pb, which corresponds to the exchange of light neutrinos. For large values of y_i , the cross section is suppressed by the heavy neutrino mass as expected: $\sigma_0^t \propto M_i^{-2}$ in this limit, and $\sigma_0^t \propto M_i^{-2} M_j^{-2}$ for both y_i and y_j large.

We now want to estimate the maximal possible cross section in the case of different

neutrino contributions in the propagator of the λ diagram. As a concrete example, we work with

$$\begin{aligned} m_R &= 4 \text{ TeV} & \text{and} \\ \sqrt{s} &= 13 \text{ TeV}. \end{aligned} \tag{4.21}$$

For other values, the corresponding calculations can be done by use of Equation (4.19).

Only light neutrinos involved First, consider a scenario where only the light neutrinos ν contribute to the high energy cross section σ_λ^t . This can be the case if the masses of the heavy neutrinos are much larger than the accessible energy \sqrt{s} , if the mixing matrix elements $S_{ei}V_{ei}^*$ are very small, or if the heavy neutrino contribution vanishes due to interference between the three N_i . In this case, the constraints from electroweak precision data (4.18) and the neutrinoless double beta decay (4.12) can be directly translated into an upper limit for the t -channel cross section σ_λ^t which turns out to be of $\mathcal{O}(10^{-11} \text{ pb})$ in the most optimistic case. The limit is shown in Figure 4.2b.

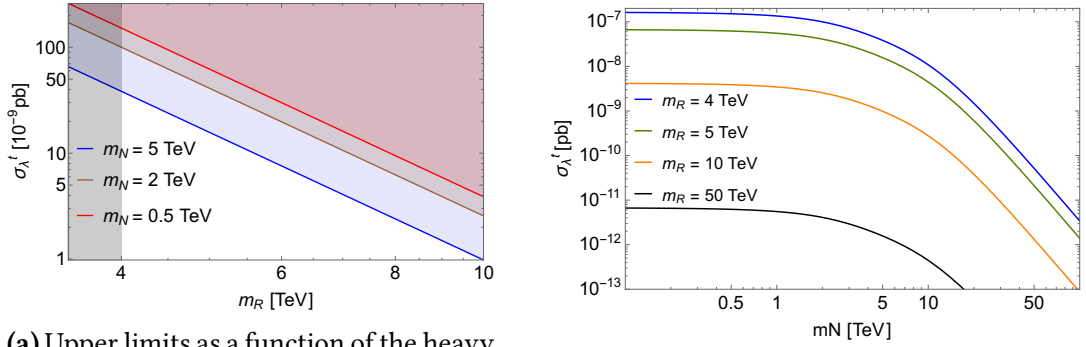
Only one heavy neutrino involved If instead one single heavy neutrino N_i mediates the interaction, but no light neutrinos ν are involved, nor other heavy neutrinos N_j ($j \neq i$), this means that either some interference cancels the contributions from the light and remaining heavy neutrinos, or $R_{11} \ll S_{ei}V_{ei}^*/M_i^2$ as well as $S_{ej}V_{ej}^*/M_j^2 \ll S_{ei}V_{ei}^*/M_i^2$ (e.g. the N_j decouple due to their heavy mass). In either case, the cross section is determined by the properties of N_i , roughly speaking:

$$\sigma_\lambda^t \propto \frac{|S_{ei}V_{ei}^*|^2}{M_i^4}. \tag{4.22}$$

The relevant constraint in this case is given by the electroweak precision data in Equation (4.13). As discussed above, the constraint coming from the $0\nu\beta\beta$ decay turns out to be much weaker here and would apply only for $m_R^4 M_i^4 \lesssim 4 \times 10^{-3} m_L^4 M_a^4 f(A)^2$, which is already ruled out by the lower limits on the heavy neutrino and W_R^- masses (see Equation (2.103)). We find that the signal can be of $\mathcal{O}(10^{-7} \text{ pb})$ in the most promising case, which might be surprising as heavy neutrino contributions should be suppressed compared to light one. However, this is just the result of the light neutrinos being stronger constraint from low energy experiments.

Figure 4.3 shows the resulting limit on σ_λ^t , both as a function of the right handed gauge boson mass m_R for different heavy neutrino masses m_N and vice versa.

One heavy and light neutrinos involved Having understood the rather simple cases of only light neutrinos or one single heavy neutrino contributing to the cross section, we



(a) Upper limits as a function of the heavy W boson mass for different heavy neutrino masses. The gray shaded region is excluded by $m_R \geq 4$ TeV; the colored shaded regions are excluded for the different neutrino masses, respectively.

(b) The cross section limits as a function of the heavy neutrino mass m_N for different W_R^- masses. Values above the curves are excluded for the different m_R cases, respectively.

Fig. 4.3 – Upper limits on the t -channel cross section σ_λ^t of the λ diagram in the case of single heavy neutrino dominance.

can now investigate the scenario in which both light neutrinos ν and one single heavy neutrino N_i mediate the interaction simultaneously. For this, R_{11} must be of the same order of magnitude as $S_{ei}V_{ei}^*/M_i^2$, and $S_{ej}V_{ej}^*/M_j^2$ (which determines the contribution of the remaining heavy neutrinos N_j , $j \neq i$) has to be small compared to the former. In this situation, interference between the light neutrinos and N_i becomes important and it is interesting to consider the extreme case of maximal positive interference. Using Equation (4.19) we can write⁴

$$\sigma_\lambda^t \approx \frac{s a(s)}{m_R^4} \left(|R_{11}|^2 \sigma_0^t(0, 0) - 2 \mathcal{R}e(R_{11}^* S_{ei} V_{ei}^*) \sigma_0^t \left(0, \frac{M_i}{\sqrt{s}} \right) + |S_{ei} V_{ei}^*|^2 \sigma_0^t \left(\frac{M_i}{\sqrt{s}}, \frac{M_i}{\sqrt{s}} \right) \right), \quad (4.23)$$

and find the maximal positive signal by requiring $\mathcal{R}e(R_{11}^* S_{ei} V_{ei}^*) \approx -|R_{11}| |S_{ei} V_{ei}^*|$.

In Figure 4.4 we plot the resulting limit on the cross section as a function of m_R for this rather optimistic case. For comparison we also included the results from above.

The plot shows that for low W_R^- masses, the heavy neutrino contribution dominates. The reason for this is again that the constraint from neutrinoless double beta decay does not apply for the heavy neutrinos. For large boson masses, the situation changes and both contributions, those of the light neutrinos and the heavy neutrino, become equally important. In this regime, the constraint from electroweak precision measurements is the more restricting one. As it equally applies for R_{11} and S_{ei} , the resulting limit in the

⁴ Note that the minus sign in the interference term is due to $\sum U_{ei} T_{ei}^* = -R_{11}$.

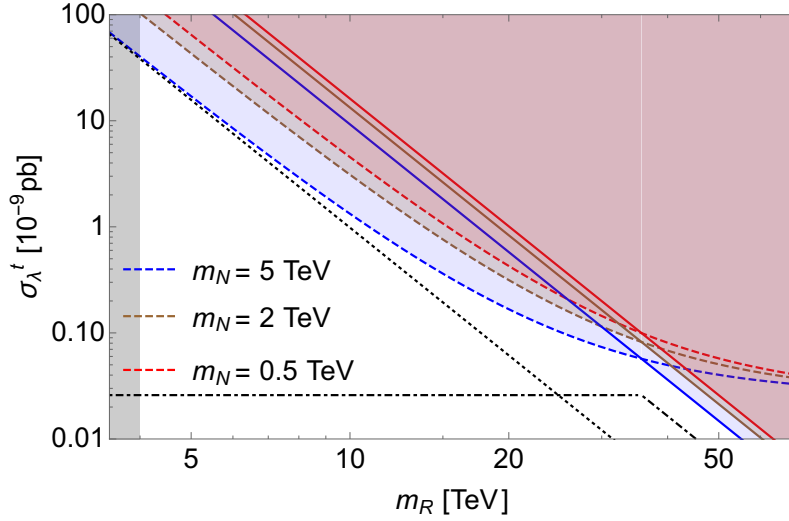


Fig. 4.4 – Upper limit on the t -channel cross section in the case of light neutrinos maximally positive interfering with one heavy neutrino. The limit is shown as function of the heavy gauge boson mass m_R for different heavy neutrino masses m_N . Dashed lines result from $0\nu\beta\beta$ decay constraints, solid lines from the electroweak precision data. For comparison, upper limits in the case of light neutrinos (dash-dotted) and one single heavy neutrino only (dashed), are shown in black. The shaded regions above the curves are ruled out for the respective neutrino mass. The gray shaded region is excluded due to constraints on the W_R^- mass.

case of positive interference is proportional to the limit in the case of light neutrinos only (Fig. 4.2b). The proportionality factor is determined by the dependency of σ_0^t in Equation (4.19) on the mass of the heavy neutrino m_N and can range from 1 for very large m_N (decoupling limit) to 4 (vanishing neutrino mass).

Above we found that the light neutrino contribution is severely restricted due to the $0\nu\beta\beta$ decay constraint in Equation (4.10). The allowed parameter space of the cross section would reach up to $\mathcal{O}(10^{-7})$ pb if it would be possible to avoid this constraint and Equation (4.18) would apply only. Therefore, one could argue that by means of interference the term $\sum U_{ei}T_{ei}^* + \sum S_{ei}V_{ei}^* f(A) M_a^2/M_i^2$ vanishes without $\sum U_{ei}T_{ei}^*$ actually being small. Consequently, this would imply

$$\sum_{i=1}^3 U_{ei}T_{ei}^* \approx - \sum_{i=1}^3 S_{ei}V_{ei}^* f(A) \frac{M_a^2}{M_i^2} \lesssim -4 \times 10^{-3} f(A) \sum_{i=1}^3 \frac{M_a^2}{M_i^2} \quad (4.24)$$

by use of the electroweak precision constraint $S_{ei}V_{ei}^* \lesssim 4 \times 10^{-3}$. Thus, the constraint on R_{11} becomes even more restrictive. On the other hand, we have seen that for heavy neutrinos the parameter space for a signal of that size is not yet ruled out. Therefore, the scenario of a rather light heavy neutrino with a mass of a few hundred GeV is the

most promising scenario for the t -channel at the moment.

More than one heavy neutrino involved In the case of more than one heavy neutrino significantly contributing to the cross section precise calculations become difficult. However, it turns out that the upper limit on the cross section does not significantly change. To understand this, we consider the case of two heavy neutrinos. For both contributions to be significant, their masses must be of the same order of magnitude. Else, the lighter neutrino could be neglected.⁵ In this case, similarly to the case of light neutrinos in combination with one heavy neutrino, the maximal possible cross section increases by an $\mathcal{O}(1)$ factor at most. Furthermore, Equation (4.16) constraints the sum of both mixing matrix elements. Thus, we rather find $|S_{ei}V_{ei}^*|^2 \leq 2 \times 10^{-3}$ than $|S_{ei}V_{ei}^*|^2 \leq 4 \times 10^{-3}$ for each contributing heavy neutrino in the most promising case, which reduces the maximal possible signal by a factor of two.

Similar considerations are true for the case of three heavy neutrinos and also when including the light neutrinos. In the case of all six neutrinos contributing – three light and three heavy – further constraints should be imposed, such as Equation (4.14) and Equation (4.15). This usually restricts the possible signal strength even more.

4.2 Estimates on the s -channel cross section σ_λ^{sRL} mediated by light neutrinos

In the following, we comment very briefly on the s -channel diagram shown in Figure 4.1. In this channel the incoming quarks have RH helicities and produce the heavy W_R boson. If the energy is sufficient ($s \gtrsim m_R^2$) the boson can be produced at resonance which enhances the cross section. In Equation (B.27) in the appendix we give an approximation for the cross section σ_λ^{sRL} :

$$\begin{aligned} \sigma_\lambda^{sRL} = & \frac{a(s) \sqrt{s^3} \text{ GeV}^{-1}}{(s - m_R^2)^2 + \Gamma_R^2 m_R^2} \int_0^\infty f_\lambda^{sRL} \left(\frac{q^2}{s} \right) \times \\ & \times \left| \sum_{\substack{i=1 \\ \text{light}}}^3 U_{ei} T_{ei}^* + \sum_{\substack{i=1 \\ \text{heavy}}}^3 S_{ei} V_{ei}^* \frac{q^2}{q^2 - M_i^2 + i \Gamma_i M_i} \right|^2 \frac{dq^2}{s}, \end{aligned} \quad (4.25)$$

⁵ Note that it is of course possible to have equally contributing heavy neutrinos with different masses, i.e. if the mixing matrices are compensate the difference: $\frac{S_{ei}V_{ei}^*}{M_i^2} \approx \frac{S_{ej}V_{ej}^*}{M_j^2}$. However, the result of the following argumentation would stay the same.

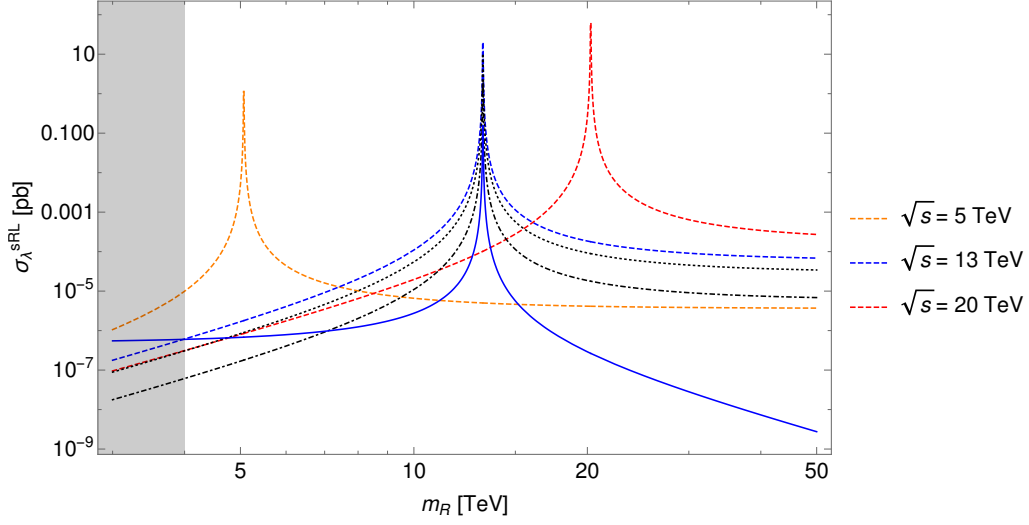


Fig. 4.5 – Limits on the s -channel cross section including light neutrinos only. Colored dashed lines correspond to the limits from $0\nu\beta\beta$ decay, the solid line is obtained by applying the limit obtained by electroweak precision data. In black we give projective future limits for an improvement of the half life of xenon by a factor of 2 (dotted) and 10 (dashed-dotted). The gray shaded region is excluded by the limit on the W_R mass.

with the functions a and f_λ^{sRL} being obtained from simulations:

$$\begin{aligned}
 a(s) &= 1.08 - 0.88 \frac{s}{13 \text{ TeV}^2}, \\
 f_\lambda^{sRL}(x) &= a_0 \frac{e^{-\frac{b_0}{x}}}{(x + c_0)^4}, \quad \text{with } x = q^2/s \text{ and} \\
 a_0 &= 0.0136 \text{ GeV}^2 \text{ pb}, \quad b_0 = 2.7 \times 10^{-3}, \quad c_0 = 0.133.
 \end{aligned} \tag{4.26}$$

Restricting ourselves to light neutrinos in the propagator, yields roughly

$$\begin{aligned}
 \sigma_\lambda^{sRL} &= \frac{a(s) \sqrt{s^3} \text{ GeV}^{-1} |R_{11}|^2}{(s - m_R^2)^2 + \Gamma_R^2 m_R^2} \int_0^\infty f_\lambda^{sRL} \left(\frac{q^2}{s} \right) \frac{dq^2}{s} \\
 &\approx 1.62 |R_{11}|^2 \frac{a(s) \sqrt{s^3} \text{ GeV}^{-1}}{(s - m_R^2)^2 + \Gamma_R^2 m_R^2},
 \end{aligned} \tag{4.27}$$

In order to obtain an upper limit on the signal, we apply the limits given in Equations (4.12) and (4.18) again. The result is shown in Figure 4.5. It shows that the limit from electroweak precision data is more restrictive than the $0\nu\beta\beta$ limit. Furthermore, the cross section could reach $\mathcal{O}(10 \text{ pb})$ in the most promising scenario. However, this is mainly due to the resonance of the W_R boson and depends very much on its mass.

In the appendix we also derive formulae for the case where heavy neutrinos take part

in the interaction (Equation (B.32) and (B.35)). The heavy neutrino contribution is suppressed by its mass, if it is not resonantly produced. However, if they are produced at resonance ($q^2 \approx M_i^2$), our calculations suggest that the cross section is enhanced and interference terms between different heavy neutrinos can be neglected (if their masses are not very similar). The analysis carried out in Section B.2 suggests that including all neutrinos of the Left Right symmetric model (i.e. three light neutrinos and three heavy neutrinos) is approximately equivalent to the case where only heavy neutrinos contribute if it is possible to produce the heavy neutrinos resonantly. This means that the contribution from the heavy states dominates over the light states. However, this outcome is not fully understood and needs further investigation. Therefore, we decided to not discuss the heavy neutrino contributions further; for concrete and reliable statements more data would be needed.

We also mention that another s -channel diagram contributes to the full λ cross section; it is obtained by interchanging all chiralities in Figure 4.1; i.e. the incoming quarks couple to W_L . For this case and with $m_R = 4$ TeV and $\sqrt{s} = 13$ TeV we found cross sections of $\mathcal{O}(10^{-6} \text{ pb}) \times |R_{11}|^2$ if only including light neutrinos and $\mathcal{O}(10^{-5} \text{ pb}) \times |S_{ei} V_{ei}^*|^2$ if a heavy neutrino of mass $M_i \approx 1$ TeV mediates the interaction.

4.3 Summary and conclusions

In this thesis we analysed the possible cross sections of the λ diagram at energies around $\sqrt{s} \approx 13$ TeV. We focused on the quark-quark interaction without parton distribution function. It was found that for the t -channel the cross section cannot be larger than $\mathcal{O}(10^{-11} \text{ pb})$ if only light neutrinos interact and $\mathcal{O}(10^{-7} \text{ pb})$ if heavy neutrinos are contributing significantly. For the s -channel the light neutrino contribution was limited to $\sigma \leq \mathcal{O}(10 \text{ pb})$, which was found for the case of a resonantly produced W_R boson.

In general the light neutrino contribution dominates over the heavy neutrino one. However, we found that the limit from neutrinoless double beta decay only restricts the light neutrinos. Therefore their parameter space is stronger restricted than for heavy neutrinos; in fact, the $0\nu\beta\beta$ limit from the non-observation of xenon decays is only significant in the case of light neutrinos in the t -channel.

The simple approximations we carried out in this work gave an overview over the possible channels and signals. The expected maximal order of magnitude of the cross section was derived; however, for more details and a better understanding how cancellations caused by interference could be important, further analysis is needed for the high energy sector as well at low energies.

Similar studies have been performed by various authors to show that interactions including heavy neutrinos leading to diboson signals can be detected at the LHC if the

cross section is of order $\mathcal{O}(\text{fb})$ [45, 48]. Therefore, we conclude that the above discussed channels cannot be detected at present experiments.

Furthermore we emphasise that the parton distribution has to be taken into account in order to get experimentally meaningful cross sections. However, this will reduce the cross sections above by at least a factor of 10^{-4} , which makes the observation of the signal impossible in the discussed scenarios.

Appendix A

Relevant particle decay widths

In this chapter we give analytical formulae for the relevant particle decay widths we used in our numerical analysis. In the case of the heavy W boson the expressions have been taken from [49]. In the calculation, fermion masses have been neglected, except for the top-mass m_t and the heavy neutrino masses N_i .

$$\Gamma(W_R^- \rightarrow \nu_i \ell_\alpha^-) = \frac{g_R^2}{48\pi} |T_{\alpha i}|^2 m_R, \quad (\text{A.1})$$

$$\Gamma(W_R^- \rightarrow N_i \ell_\alpha^-) = \frac{g_R^2}{48\pi} |V_{\alpha i}|^2 m_R \left(1 + \frac{M_i^2}{2 m_R^2}\right) \left(1 - \frac{M_i^2}{m_R^2}\right)^2, \quad (\text{A.2})$$

$$\Gamma(W_R^- \rightarrow \bar{u}d) = \Gamma(W_R^- \rightarrow \bar{c}s) = \frac{g_R^2}{16\pi} m_R, \quad (\text{A.3})$$

$$\Gamma(W_R^- \rightarrow \bar{t}b) = \frac{g_R^2}{16\pi} m_R \left(1 + \frac{m_t^2}{2 m_R^2}\right) \left(1 - \frac{m_t^2}{m_R^2}\right)^2, \quad (\text{A.4})$$

Here, $T_{\ell i}$ and $V_{\ell i}$ are the mixing matrix elements of the charged leptons $\ell \in \{e, \mu, \tau\}$ with the LH and RH currents respectively (see Equation (2.59)). Note that we did not list the decay channel $\Gamma(W_R^- \rightarrow W_L^- Z_L)$ here, neither $\Gamma(W_R^- \rightarrow W_L^- H)$ as they are negligible due to vanishing mixing in the scenario under consideration. However, in the simulations we included them for completeness. Figure ?? shows the remaining contributions to Γ_{W_R} with normalised mixings $U = 1$.

The decay widths for the heavy neutrinos can be found in [50] and [45]; they read

$$\Gamma(N_i \rightarrow \ell_\alpha^\pm W_L) = \frac{g_L^2}{64\pi} |S_{\alpha i}|^2 \frac{M_i^3}{m_L^2} \left(1 - \frac{m_L^2}{M_i^2}\right)^2 \left(1 + 2 \frac{m_L^2}{M_i^2}\right), \quad (\text{A.5})$$

$$\begin{aligned} \Gamma(N_i \rightarrow \nu_j Z_L) &= \frac{g_L^2}{128\pi} |(S^\dagger U)_{ij}|^2 \frac{M_i^3}{m_{Z_L}^2 \cos^2 \theta_W} \\ &\times \left(1 - \frac{m_{Z_L}^2}{M_i^2}\right)^2 \left(1 + 2 \frac{m_{Z_L}^2}{M_i^2}\right), \end{aligned} \quad (\text{A.6})$$

$$\Gamma(N_i \rightarrow \nu_j H) = \frac{g_L^2}{128\pi} |(S^\dagger U)_{ij}|^2 \frac{M_i^3}{m_L^2} \left(1 - \frac{m_H^2}{M_i^2}\right)^2. \quad (\text{A.7})$$

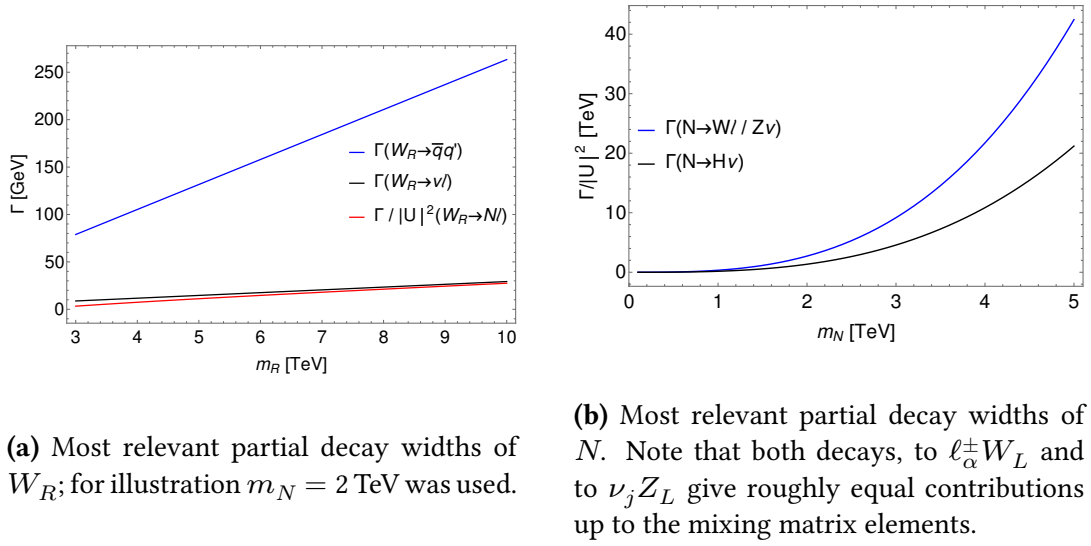


Fig. A.1 – Different partial decay widths of W_R and N ; the respective mixing matrix elements U have been normed to 1 for comparison.

Note that the coupling to the Z boson mass eigenstates in general is rather involved. We used the expression for the vanishing-mixing limit here; the full expression can be found in [29]. Again we did only give the relevant contributions here; the three-body decays $\Gamma(N_i \rightarrow \ell_\alpha^\pm W_R^* \rightarrow \ell^\pm jj)$ and $\Gamma(N_i \rightarrow \nu_j Z_R^* \rightarrow \nu_j jj)$ have been omitted as they are much smaller than the remaining in our case.

Appendix B

Analytical approximations for the λ diagram cross sections

In this section we derive formulae to calculate the cross section of the high-energy equivalent to the neutrinoless double beta decay λ -diagram. The result will not be a simple analytical function. Thus we make use of Monte Carlo simulations to solve the remaining multi-dimensional integrals and to find a simple approximation for the cross section. More concrete, we derive an expression for the differential cross section $d\sigma/dq^2$ in terms of the center of mass energy \sqrt{s} , the square of the four-momentum mediated by the neutrino q^2 and the masses and couplings of the participating particles.

To arrive at the desired function, we first analyse the dimensional dependencies and then rewrite the cross section in a convenient way. This procedure is first done for the t -channel diagram and afterwards repeated for the s -channel with the heavy W boson coupling to the initial particles; as we are working in the ultra-relativistic limit, the three contributions can be regarded as interference-free. The expressions we are deriving here are valid for the hard quark-quark interaction only, i.e. to obtain experimentally sensible values they have to be folded with the parton distribution function. Alternatively, one can approximate the valence-quark contribution by scaling down the proton-proton collision energy $\sqrt{s_{pp}}$ to the average energy carried by the valence quarks as [47]. We adopt the latter approach after deriving the quark-quark cross sections.

We work in the LR-symmetric model without mixing, i.e. we assume that the W -boson mixing angle ξ in Equation (2.77) vanishes:

$$\xi \approx 0 \tag{B.1}$$

Then we can use the following notation without ambiguity:

$$\begin{aligned} W_1 &\simeq W_L, & W_2 &\simeq W_R, \\ m_{W_1} &\simeq m_L, & m_{W_2} &\simeq m_R, \\ g &\equiv g_L = g_R. \end{aligned} \tag{B.2}$$

In the process we are interested in, the neutrino couples to one LH and one RH electron. In the model under consideration the couplings of the neutrino mass eigenstates

in the virtual propagator are proportional to $U_{ei}T_{ei}^*$ and $S_{ei}V_{ei}^*$, respectively. However, the conclusions we are drawing are valid for other models with different couplings as well, as long as the currents are of the same form, i.e. $V \mp A$.

B.1 t -channel cross section

The interesting physics is encapsulated in the transition matrix element \mathcal{A} of the t -channel λ -diagram, which can be obtained from the Lagrangian in Equation (2.96). The corresponding Feynman diagram is depicted in Figure B.1.

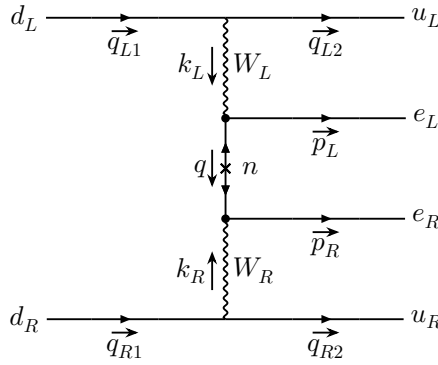


Fig. B.1 – Feynman diagram for the t -channel λ -diagram.

The expression for the amplitude reads

$$\begin{aligned}
 i\mathcal{A} &= \frac{-g_L^2}{2} \bar{u}_L \gamma^{\mu'} P_L d_L \left(\eta_{\mu'\mu} - \frac{k_{L\mu'} k_{L\mu}}{m_L^2} \right) \frac{-i}{k_L^2 - m_L^2} \\
 &\times \frac{-g_R^2}{2} \bar{u}_R \gamma^{\nu'} P_R d_R \left(\eta_{\nu'\nu} - \frac{k_{R\nu'} k_{R\nu}}{m_R^2} \right) \frac{-i}{k_R^2 - m_R^2} \\
 &\times \bar{e}_L \gamma^\mu P_L \left(\sum_{\substack{i=1 \\ \text{light}}}^3 U_{ei} \frac{i(\not{q} + m_i)}{q^2 - m_i^2} T_{ei}^* + \sum_{\substack{i=1 \\ \text{heavy}}}^3 S_{ei} \frac{i(\not{q} + M_i)}{q^2 - M_i^2} V_{ei}^* \right) P_R \gamma^\nu e_R^c.
 \end{aligned} \tag{B.3}$$

Here, $u_{L/R}$, $d_{L/R}$ and $e_{L/R}$ are the fermion spinors of the initial and final states, q^μ is the four-momentum of the exchanged neutrino and k_L^μ and k_R^μ are the four-momenta of the exchanged gauge-bosons. m_i and M_i are the light and heavy neutrino masses, respectively, and $P_{L/R}$ denote the chirality projection operators from Equation (2.31).

Note that the second electron is charged conjugate due to the Majorana nature of the neutrino [51] and q^2 , k_L^2 and k_R^2 are strictly negative because the interaction happens in

the *t*-channel. Thus we do not produce any particle at resonance and need not to include the decay widths into the propagators.

As the light neutrino masses are very small, one can approximate their propagator via

$$\frac{q + m_i}{q^2 - m_i^2} \approx \frac{q + m_i}{q^2}. \quad (\text{B.4})$$

The structure of the λ -diagram now simplifies the expression significantly due to the equality

$$P_L (\not{q} + m) P_R = \not{q} P_R, \quad (\text{B.5})$$

where we used the identities in Equation (2.31).

Because of this, we observe that the light neutrino masses do not enter the matrix element, whereas the heavy neutrino masses appear in the denominator of the propagator only. After factoring out $i\not{q}/q^2$ from the last part of Equation (B.3), we thus find the simple proportionality

$$\mathcal{A} \propto \left(\sum_{\substack{i=1 \\ \text{light}}}^3 U_{ei} T_{ei}^* + \sum_{\substack{i=1 \\ \text{heavy}}}^3 S_{ei} V_{ei}^* \frac{q^2}{q^2 - M_i^2} \right). \quad (\text{B.6})$$

Although we will not use it here, we point out that in the Left Right symmetric model $\sum U_{ei} T_{ei}^* = -\sum S_{ei} V_{ei}^*$ (see Equation (2.61)). Thus, we can also rewrite the amplitude as

$$\mathcal{A} \propto \sum_{\substack{i=1 \\ \text{heavy}}}^3 S_{ei} V_{ei}^* \frac{M_i^2}{q^2 - M_i^2}. \quad (\text{B.7})$$

The elements of the mixing matrices U , S , T and V , as well as the heavy masses M_i appear only in this part of the matrix element. As we are mainly interested in these parameters, expression (B.6) is used various times in the analysis in Chapter 4.

From the above and Equation (B.3), we can express the amplitude as

$$\mathcal{A} = \frac{1}{m_R^2} \times \left(\sum_{\substack{i=1 \\ \text{light}}}^3 U_{ei} T_{ei}^* + \sum_{\substack{i=1 \\ \text{heavy}}}^3 S_{ei} V_{ei}^* \frac{q^2}{q^2 - M_i^2} \right) \times \mathcal{A}_0 \left(\frac{q^2}{s}, \frac{m_L^2}{s}, \frac{m_R^2}{s} \right). \quad (\text{B.8})$$

Here, $\sqrt{s} = |q_{L1}^\mu + q_{R1}^\mu|$ is the center of mass energy and \mathcal{A}_0 a dimensionless function

depending on the quantities m_L^2/s , m_R^2/s and q^2/s .¹ Of course there are also dependencies on the remaining momenta (i.e. of the outgoing quarks and electrons). However, we are interested in the total, spin averaged cross section and therefore will integrate out the momenta in the next step.

The formula for the cross section with the momenta labelled according to Figure B.1 reads

$$\begin{aligned} d\sigma = & \frac{\langle |\mathcal{A}|^2 \rangle}{2q_{L1}^0 2q_{R1}^0} \frac{1}{(2\pi)^{12} \Delta v} \frac{d^3 \vec{q}_{L2}}{2q_{L2}^0} \frac{d^3 \vec{q}_{R2}}{2q_{R2}^0} \frac{d^3 \vec{p}_L}{2p_L^0} \frac{d^3 \vec{p}_R}{2p_R^0} \\ & \times (2\pi)^4 \delta^4(q_{L1} + q_{R1} - q_{L2} - q_{R2} - p_L - p_R). \end{aligned} \quad (\text{B.9})$$

In the center of mass frame in the relativistic limit, we have $2q_L^0 = \sqrt{s} = 2q_R^0$ and the Galilean velocity difference $\Delta v = v_{d_L} - v_{d_R} \approx 2$ (in natural units $c \equiv 1$).² The Lorentz invariant phase space factors $d^3 \vec{p}_i / 2q_i^0$ are proportional to s each and the Dirac delta function can be rescaled to obtain its dimensionality as

$$\delta^4 \left(\sum_i p_i^\mu \right) = \delta^4 \left(\sqrt{s} \sum_i \frac{p_i^\mu}{\sqrt{s}} \right) = \frac{1}{s^2} \delta^4 \left(\sum_i \frac{p_i^\mu}{\sqrt{s}} \right). \quad (\text{B.10})$$

As we are interested in the cross section in terms of its proportionality to the propagator term in Equation (B.6), we need to change the integration variables such that the integral is performed over q^2 . This transformation is taken into account by the Jacobian matrix $J^{q^2} \simeq \partial p_i^{new} / \partial p_i^{old}$.

Explicitly calculating this is rather involved and will not result in an useful expression. Thus, we simply put together our dimensional considerations from above and conclude that we can write

$$d\sigma = \frac{s}{m_R^4} \left| \sum_{\substack{i=1 \\ \text{light}}}^3 U_{ei} T_{ei}^* + \sum_{\substack{i=1 \\ \text{heavy}}}^3 S_{ei} V_{ei}^* \frac{q^2}{q^2 - M_i^2} \right|^2 G \left(\frac{q^2}{s}, \frac{m_L^2}{s}, \frac{m_R^2}{s} \right) \frac{dq^2}{s}. \quad (\text{B.11})$$

Note that we already performed the integrals over the various momenta. The dimensionless function $G(q^2/s, m_L^2/s, m_R^2/s)$ is roughly given by

$$G \simeq C \prod_{i=1}^{11} \left(\int_{-\infty}^{\infty} dp_i \right) \det(J^{q^2}) \delta^4 \left(\sum p_i^\mu \right) \frac{\langle |\mathcal{A}_0|^2 \rangle}{p_i^4}, \quad (\text{B.12})$$

¹ This can be found by reorganizing the terms in Equation (B.3) and considering their dimensionalities: $m_i^2 \sim s$, $q^2 \sim s$ and $\psi \sim s^{\frac{1}{4}}$ with ψ representing the spinors $u_{L/R}$, $d_{L/R}$ and $e_{L/R}$.

² The formula in Equation (B.9) was taken from [52]. They explicitly state that Δv is not a Lorentz invariant quantity and thus is not calculated respecting special relativity.

with p_i being some not further specified rescaled (i.e. divided by \sqrt{s}) momenta resulting from the coordinate transformation discussed above and C a numerical constant.

Now it would be interesting to understand the exact dependencies of G on its variables. As was mentioned before, it is not an easy task to determine it analytically. Therefore we chose another approach: The Monte Carlo simulations carried out by Mad Graph 5 (see Chapter C) are used to calculate both, the cross section σ and the q^2 spectrum of the interaction with the latter being precisely given by $d\sigma/dq^2$.

Exploiting this, we find that in the region of interest, i.e. for $m_R^2 \gtrsim 16 \text{ TeV}$ and $\sqrt{s} \simeq \mathcal{O}(13 \text{ TeV})$, the function G can be approximated as

$$G\left(\frac{q^2}{s}, \frac{m_L^2}{s}, \frac{m_R^2}{s}\right) \simeq \frac{a(s)}{s} f_\lambda^t\left(\frac{q^2}{s}\right). \quad (\text{B.13})$$

Thus, the dependency on the boson masses is very weak and can be neglected.

Fitting numerical data, we constructed the approximation

$$a(s) = 0.16 \text{ GeV}^2 \log\left(1 + 1.3 \times 10^{-8} \left(\frac{s}{\text{TeV}^2}\right)^2\right), \quad (\text{B.14})$$

$$f_\lambda^t(x) = a_0 \frac{e^{\frac{b_0}{x}}}{(x - c_0)^4},$$

with $x = q^2/s$ and

$$a_0 = 1.785 \times 10^9 \text{ GeV}^2 \text{ pb}, \quad b_0 = 2.357 \times 10^{-4}, \quad c_0 = 0.372. \quad (\text{B.15})$$

To illustrate this result, a comparison between the approximation and the numerical values obtained from simulation is given in Figure B.2 for different values of \sqrt{s} .

With this approximation given, we can even perform the integral over q^2 to obtain an expression for the full cross section σ . For deductive reasons we insert the term $q^2/(q^2 - m^2)$ into the light neutrino propagator in Equation (B.11) with the replacement $m \rightarrow 0$ taken later again. This yields

$$d\sigma = \frac{s a(s)}{m_R^4} \left| \sum_{\substack{i=1 \\ \text{light}}}^3 U_{ei} T_{ei}^* \frac{q^2}{q^2 - m^2} + \sum_{\substack{i=1 \\ \text{heavy}}}^3 S_{ei} V_{ei}^* \frac{q^2}{q^2 - M_i^2} \right|^2 f_\lambda^t\left(\frac{q^2}{s}\right) \frac{dq^2}{s}. \quad (\text{B.16})$$

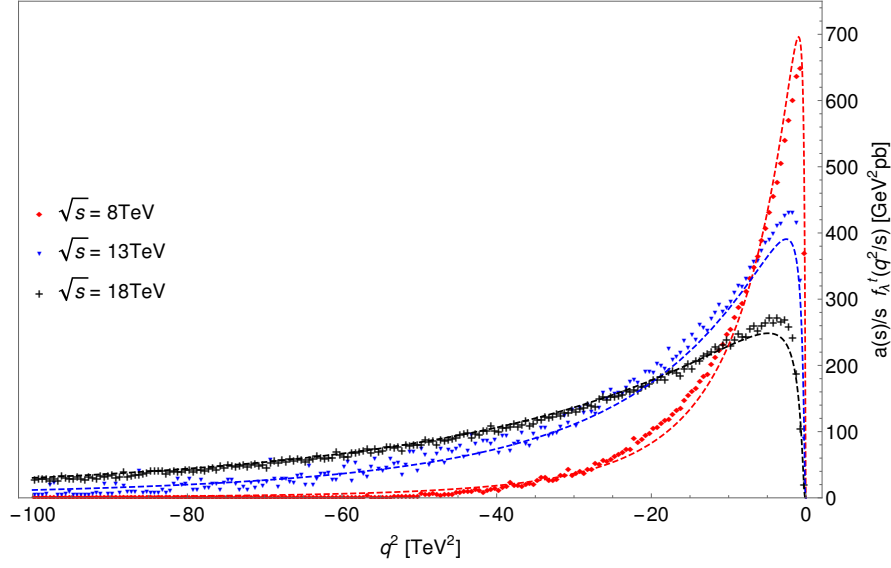


Fig. B.2 – Numerical results for $\frac{a(s)}{s} f_{\lambda}^t(\frac{q^2}{s})$ (dots) and analytical approximation (dashed) for different energies \sqrt{s} .

Next, we ease the notation by use of the redefinitions

$$\begin{aligned} \mathcal{M}_i &= \begin{cases} \sum_{j=1}^3 U_{ej} T_{ej}^*, & i = 0, \\ S_{ei} V_{ei}^*, & i = 1, 3, 4, \end{cases} \\ y_i &= \begin{cases} m^2/s \rightarrow 0, & i = 0, \\ M_i^2/s, & i = 1, 3, 4, \end{cases} \quad \text{and} \\ x &= \frac{q^2}{s}. \end{aligned} \quad (\text{B.17})$$

The cross section then becomes³

$$\begin{aligned} \sigma &= \frac{s a(s)}{m_R^4} \int_{-\infty}^0 \left| \sum_{i=0}^3 \mathcal{M}_i \frac{x}{x - y_i} \right|^2 f_{\lambda}^t(x) dx \\ &= \frac{s a(s)}{m_R^4} \sum_{i,j=0}^3 \mathcal{M}_i \mathcal{M}_j^* \int_{-\infty}^0 \frac{x^2}{(x - y_i)(x - y_j)} f_{\lambda}^t(x) dx \end{aligned} \quad (\text{B.18})$$

$$= \sigma_{\lambda}^t = \frac{s a(s)}{m_R^4} \sum_{i,j=0}^3 \mathcal{M}_i \mathcal{M}_j^* \sigma_0^t(y_i, y_j), \quad (\text{B.19})$$

where we defined the two-dimensional symmetric function $\sigma_0^t(y_i, y_j)$. We want to stress

³ Keep in mind that $q^2 < 0$ in the t -channel.

here, that this result is true for the interaction of the quarks. In order to obtain the cross section for the full proton-proton interaction the parton distribution function has to be taken into account. The integral can be performed numerically for different values of M_i^2/s and M_j^2/s . For the special cases $s \gg M_{i,j}^2$ and $s \ll M_{i,j}^2$, the solution is readily found:

$$\begin{aligned} \sigma_0 &\xrightarrow{M_{i,j}^2 \ll s} 10^{10} \text{ GeV}^2 \text{ pb}, \\ \sigma_0 &\xrightarrow{M_{i,j}^2 \gg s} 8 \times 10^8 \text{ GeV}^2 \text{ pb} \frac{s^2}{M_i^2 M_j^2}. \end{aligned} \quad (\text{B.20})$$

Note that the former corresponds to one light being exchanged, whereas the latter is used for very heavy neutrinos. Figure B.3 shows the numerical values of the integration for the cases $M_i = M_j$, $M_i = 0$ and $M_i = 500 \text{ GeV}$, as well as a contour plot of the region $M_{i,j} \leq 5 \text{ TeV}$; both for $\sqrt{s} = 13 \text{ TeV}$.

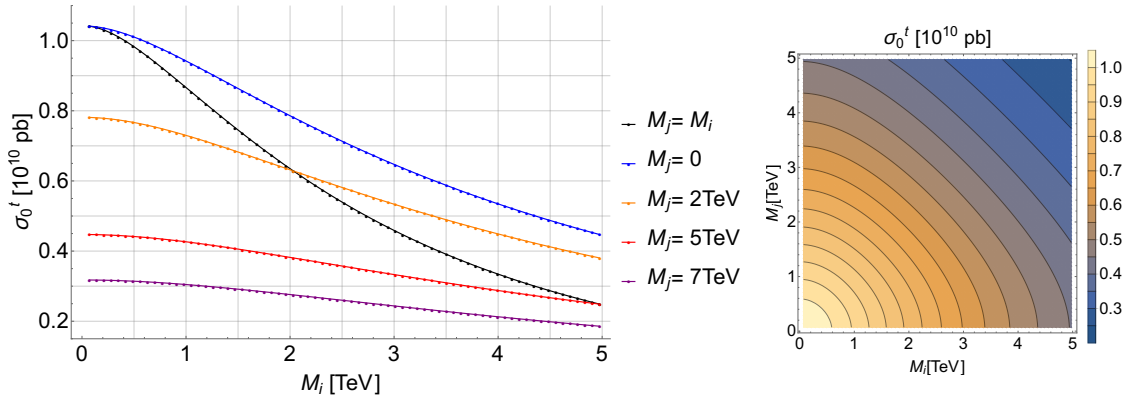


Fig. B.3 – Numerical result for σ_0^t with $\sqrt{s} = 13 \text{ TeV}$

Before applying the cross section formula to actual proton-proton collisions, the parton distribution inside the protons has to be taken into account. The momentum carried by a quark q^μ inside the proton with momentum p^μ is $q^\mu = x \cdot p^\mu$. The average momentum fraction of a valence quark (u and d) is $\langle x_V \rangle \approx 0.12$, whereas sea-quarks (the remaining types of quarks and anti-quarks) carry the fraction $\langle x_S \rangle \approx 0.04$ in average [47]. For the t -channel process we can have different quarks involved in the interaction, namely d and \bar{u} at each W -vertex. Thus, we have to take all combinations into account; dropping the sub- and superscript of σ_λ^t we have:

$$\begin{aligned} \sigma(s) &= \sigma_{dd}(s) + \sigma_{\bar{u}\bar{u}}(s) + \sigma_{d\bar{u}}(s) + \sigma_{\bar{u}d}(s) \\ &= \sigma_{dd}(s) + \sigma_{\bar{u}\bar{u}}(s) + 2\sigma_{d\bar{u}}(s) \\ &\approx \sigma(0.12^2 s_{pp}) + \sigma(0.04^2 s_{pp}) + 2\sigma(0.12 \cdot 0.04 s_{pp}). \end{aligned} \quad (\text{B.21})$$

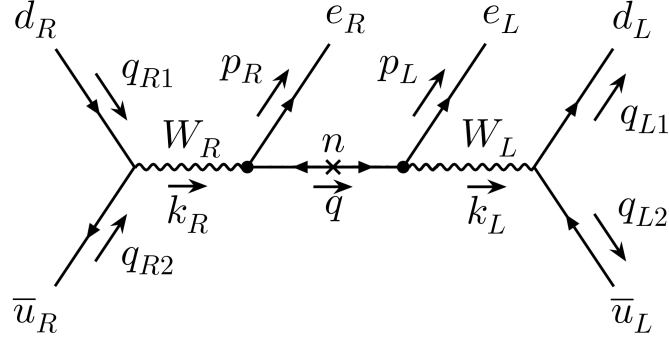


Fig. B.4 – s -channel processes of the λ diagram with right-handed initial quarks.

B.2 s -channel cross section with left-handed final state quarks

Now we want to consider the s -channel interaction with two right-handed quarks in the initial state, interacting to form a heavy W_R boson as shown in Figure B.4. This situation is particularly simple, as we will see below.

We start with Expression (B.3), which has to be slightly modified. Namely, the propagators have to be replaced by the correct expressions to avoid the poles $q^2 = M_i^2$, $k_L^2 = m_L^2$ and $k_R^2 = m_R^2$. Thus we make the replacement

$$\frac{i(\not{p} + m)}{p^2 - m^2} \rightarrow \frac{i(\not{p} + m)}{p^2 - m^2 + i\Gamma m}, \quad (\text{B.22})$$

with $p = q, k_L, k_R, m = M_i, m_L, m_R$ and the decay width $\Gamma = \Gamma_i, \Gamma_L, \Gamma_R$, respectively. Γ_i and Γ_R are given in Chapter A above, and from the SM we have $\Gamma_L \approx 2.1 \text{ GeV}$.

Essentially the same steps as in the case of the t -channel have to be performed now. However, two crucial points are different here: the W_R boson carries the complete energy of the process, i.e. $k_R^2 = s$, and because of the proportionality $\mathcal{A} \propto (k_L^2 - m_L^2)^{-1}$, the amplitude is enhanced for $k_L^2 \approx m_L^2$. Restricting ourselves to the high energy case $s \gg m_L^2$, we can therefore assume $k_L^2 = m_L^2$ in our calculations.⁴ Then, it is straight

⁴ In other words: contributions with $k_L^2 \neq m_L^2$ are negligible as they are suppressed by $s - m_L^2$.

forward to write down the following expression for the amplitude:

$$\mathcal{A} = \frac{1}{\Gamma_L m_L} \frac{s}{s - m_R^2 + i \Gamma_R m_R} \times \left(\sum_{\substack{i=1 \\ \text{light}}}^3 U_{ei} T_{ei}^* + \sum_{\substack{i=1 \\ \text{heavy}}}^3 S_{ei} V_{ei}^* \frac{q^2}{q^2 - M_i^2 + i \Gamma_i M_i} \right) \times \mathcal{A}_0 \left(\frac{q^2}{s}, \frac{m_L^2}{s}, \frac{m_R^2}{s} \right). \quad (\text{B.23})$$

The dependency of \mathcal{A}_0 on m_R^2/s is very weak and we can already neglect it here.⁵ Analogously to Equation (B.11) the cross section is then given as

$$d\sigma = \frac{s^3}{(s - m_R^2)^2 + \Gamma_R^2 m_R^2} \left| \sum_{\substack{i=1 \\ \text{light}}}^3 U_{ei} T_{ei}^* + \sum_{\substack{i=1 \\ \text{heavy}}}^3 S_{ei} V_{ei}^* \frac{q^2}{q^2 - M_i^2 + i \Gamma_i M_i} \right|^2 \times \frac{1}{\Gamma_L^2 m_L^2} G \left(\frac{q^2}{s}, \frac{m_L^2}{s} \right) \frac{dq^2}{s}. \quad (\text{B.24})$$

However, the simulations show that $G(q^2/s, m_L^2/s) \propto s^{-\frac{3}{2}}$; therefore we can define

$$G \left(\frac{q^2}{s}, \frac{m_L^2}{s} \right) \simeq a(s) \frac{\Gamma_L^2 m_L^2}{\sqrt{s^3} \text{GeV}} f_\lambda^{sRL} \left(\frac{q^2}{s} \right) \quad \text{with} \quad (\text{B.25})$$

$$a(s) = 1.08 - 0.88 \frac{s}{13 \text{ TeV}^2},$$

$$f_\lambda^{sRL}(x) = a_0 \frac{e^{-\frac{b_0}{x}}}{(x + c_0)^4}, \quad \text{with } x = q^2/s \text{ and} \quad (\text{B.26})$$

$$a_0 = 0.0136 \text{ GeV}^2 \text{ pb}, \quad b_0 = 2.7 \times 10^{-3}, \quad c_0 = 0.133.$$

Neglecting the W_R decay width in the denominator, the cross section for the s -channel

⁵ It turns out that $\overline{u_R} \gamma^{\nu'} P_R d_R \left(\eta_{\nu\nu} - \frac{k_{R\nu'} k_{R\nu}}{m_R^2} \right) \approx \overline{u_R} \gamma^{\nu'} P_R d_R \eta_{\nu\nu}$ due to the structure of the weak interaction.

process with LH final state quarks is given by⁶

$$\sigma_\lambda^{sRL} = \frac{a(s) \sqrt{s^3} \text{ GeV}^{-1}}{(s - m_R^2)^2} \int_0^\infty f_\lambda^{sRL} \left(\frac{q^2}{s} \right) \times \left| \sum_{\substack{i=1 \\ \text{light}}}^3 U_{ei} T_{ei}^* + \sum_{\substack{i=1 \\ \text{heavy}}}^3 S_{ei} V_{ei}^* \frac{q^2}{q^2 - M_i^2 + i \Gamma_i M_i} \right|^2 \frac{dq^2}{s}. \quad (\text{B.27})$$

As in the case of the t -channel diagram, the parton distribution function has to be taken into account when applying this result to proton-proton collisions. Again we use the average for the momentum fraction carried by the quarks. In the s -channel one down-type quark has to interact with one anti-up quark in order to produce a W_R^- boson. Furthermore we get a factor of two which accounts for the exchange of the interacting d - and \bar{u} -quarks with respect to the protons⁷:

$$s = \langle x_d x_{\bar{u}} \rangle s_{pp} \approx 4.8 \times 10^{-3} s_{pp}, \quad (\text{B.28})$$

$$\sigma_\lambda^{sRL}(s) \approx 2\sigma_\lambda^{sRL}(4.8 \times 10^{-3} s_{pp}), \quad (\text{B.29})$$

with s the center of mass energy of the quarks as used in the cross section formulae and s_{pp} the center of mass energy of the protons; $\langle x_d \rangle \approx 0.12$ and $\langle x_{\bar{u}} \rangle \approx 0.04$ [47].

Continuing with the bare quark-quark interaction, the cross section can be further simplified if only light neutrinos are involved in the process:

$$\sigma_\lambda^{sRL} = \frac{a(s) \sqrt{s^3} \text{ GeV}^{-1} |R_{11}|^2}{(s - m_R^2)^2} \int_0^\infty f_\lambda^{sRL} \left(\frac{q^2}{s} \right) \frac{dq^2}{s} \approx 1.62 |R_{11}|^2 \frac{a(s) \sqrt{s^3} \text{ GeV}^{-1}}{(s - m_R^2)^2}, \quad (\text{B.30})$$

where we used $\sum_{i=1}^3 U_{ei} T_{ei}^* \approx |R_{11}|$ and $\int_0^\infty f_\lambda^{1s}(x) dx \approx 1.62$.

For a single heavy neutrino N_i with the mixing matrix element $S_{ei} V_{ei}^*$ and a mass

⁶ Γ_R is small compared to m_R , see Figure A.1; if the case $s \approx m_R^2$ is considered, it has to be reinserted.

⁷ I.e. the d -quark in the first proton can interact with the \bar{u} -quark in the second proton and vice versa.

$M_i \lesssim \sqrt{s}$ mediating the process, we can write⁸

$$\sigma_\lambda^{sRL} = |S_{ei} V_{ei}^*|^2 \times \frac{a(s) \sqrt{s^3} \text{ GeV}^{-1}}{(s - m_R^2)^2} \int_0^\infty f_\lambda^{sRL} \left(\frac{q^2}{s} \right) \frac{q^4}{(q^2 - M_i^2)^2 + \Gamma_i^2 M_i^2} \frac{dq^2}{s} \quad (\text{B.31})$$

$$\approx |S_{ei} V_{ei}^*|^2 \frac{a(s) \sqrt{s^3} \text{ GeV}^{-1}}{(s - m_R^2)^2} \frac{M_i^3}{\Gamma_i} f_\lambda^{sRL} \left(\frac{M_i^2}{s} \right). \quad (\text{B.32})$$

In the last step the integral was evaluated around the maximum and then multiplied by $\Gamma_i M_i$, as is appropriate for a Lorentz curve.

Finally, if all three heavy and light neutrinos take part in the interaction, i.e. if $M_i \lesssim \sqrt{s}$ for $i = 1, 2, 3$, we can make use of the unitarity of the mixing matrix W in Equation (2.61) and rewrite the mixing matrix elements as $U_{ei} T_{ei}^* = -S_{ei} V_{ei}^*$. If we additionally assume that the masses of the heavy neutrinos are not too close to each other, the Lorentz curves do not overlap and we can neglect interference between the N_i . In this case, the cross section becomes

$$\sigma_\lambda^{sRL} = \frac{a(s) \sqrt{s^3} \text{ GeV}^{-1}}{(s - m_R^2)^2} \times \sum_{i=1}^3 |S_{ei} V_{ei}^*|^2 \int_0^\infty f_\lambda^{sRL} \left(\frac{q^2}{s} \right) \left| \frac{q^2}{q^2 - M_i^2 + i \Gamma_i M_i} - 1 \right|^2 \frac{dq^2}{s} \quad (\text{B.33})$$

$$= \frac{a(s) \sqrt{s^3} \text{ GeV}^{-1}}{(s - m_R^2)^2} \times \sum_{i=1}^3 |S_{ei} V_{ei}^*|^2 \int_0^\infty f_\lambda^{sRL} \left(\frac{q^2}{s} \right) \frac{|M_i^2 - i \Gamma_i M_i|^2}{(q^2 - M_i^2)^2 + \Gamma_i^2 M_i^2} \frac{dq^2}{s} \quad (\text{B.34})$$

$$\approx \frac{a(s) \sqrt{s^3} \text{ GeV}^{-1}}{(s - m_R^2)^2} \sum_{i=1}^3 |S_{ei} V_{ei}^*|^2 f_\lambda^{sRL} \left(\frac{M_i^2}{s} \right) \frac{M_i^3}{\Gamma_i}. \quad (\text{B.35})$$

Again, the integrals were evaluated at the maxima. Additionally we neglected the small decay width $\Gamma_i \ll M_i$ in the nominator after integration. These results show that the heavy neutrino contribution dominates over the light neutrino contribution if the heavy particles can be produced, i.e. if they are accessible at the energy \sqrt{s} .

⁸ For $M_i > \sqrt{s}$ it can not be produced and its contribution is suppressed compared to the light neutrinos, i.e. it can be neglected.

Appendix C

Mad Graph 5: a monte carlo simulator

C.1 The program

Mad Graph 5 is a Monte Carlo Simulator that allows to calculate cross sections for user defined particle interactions. For the simulations it uses the helicity calculation routine HELAS [53], which generates the events by use of the helicity amplitudes of the interacting particles. Although many features are worth discussing, we restrict ourselves to a short introduction including only the parts which are relevant for our simulations. Information about Mad Graph 5 can be found in [30]; useful tutorials for beginners are given in [54, 55].

First steps: setting up a simulation

After launching the program via command line, it is possible to specify a model file which contains the Lagrangian and specifies the interactions the user wants to investigate.¹ Model files can be generated for example by use of the FeynRules package for Mathematica[54]. In our case we modified the model file of the minimal left right symmetric from [56] in order to incorporate the full neutrino mixing matrix W from Equation (2.59). The necessary changes are documented in the subsequent section.

After the user has selected the desired model, an interaction process can be specified. This can be any kind of n to m scattering process ($n, m \in \mathbb{N}$) or the decay of a particle. The basic syntax for this is as follows:²

```
user$ generate i1 i2 ... in > o1 o2 ... om
```

Here, i_1 to i_n correspond to the incoming particles, e.g. e^-e^+ , and o_1 to o_m to the outgoing particles. Furthermore it is possible to define multi-particles like j for jets or

¹ There are some pre-defined models available of which one is automatically loaded on start-up.

² Note that the preamble 'user\$' does not have to be entered and is included to illustrate the terminal only.

p for protons. This allows Mad Graph to pick anyone of the particles included in the multi-particle definition and thus results in the overall cross section including all those particles.

Having specified the interaction in that way, it is possible to add further interaction channels to the calculation by use of

```
user$ add process i1 ... in > o1 ... om
```

When the full interaction has been entered by the user, the directory for the calculations and results has to be chosen. This is done via

```
user$ ouput path/foldername
```

Mad Graph then prepares the directory for the simulation and provides an useful and illustrative *html*-document there, which displays all possible diagrams contributing to the interaction as well as a summary of the out-carried simulations.

Starting the simulation can be done in different ways. The easiest one is to just type

```
user$ launch
```

Other possibilities are bash-scripts, for example. In any case, it is possible to modify some settings after launching the simulation. However, we will explain later how to change the settings by modifying the corresponding parameter files before launching.

Advanced syntax: excluding particles and channels

It is possible to modify the event-generation command above in order to exclude certain particles from the interaction or force s -channel propagators, for example. The authors of Mad Graph explicitly warn the user to be cautious as these options may result in non Lorentz or Gauge invariant interactions which could be physically meaningless. However, sometimes it may be needed. The command

```
user$ generate i1 ... in > a1 ... am > o1 ... ok
```

forces an intermediate step with exactly the particles a_1 to a_m appearing together. In the case of $m = 1$, this results in a s -channel diagram. By use of

```
user$ generate i1 ... in > o1 ... om /p1 ... pk
```

the particles p_1 to p_k are completely excluded from the interaction, whereas

```
user$ generate i1 ... in > o1 ... om $p1 ... pk
```

excludes the the s -channel appearance of the particles p_1 to p_k only. Another useful command is

```
user$ generate i1 ... in > o1 ... om, oj > p1 ... pk
```

which is used to define decay chains and can be applied various times. Further commands can be found in [54, 55].

For the simulations in this thesis, we used precisely the commands above to generate the desired t - and s -channel simulations with different pattern and different neutrinos involved. For example,

```
user$ generate p p > W- > j j e- e- /hm2 z z2 a h h2 h02 h03 h+ h-
      hp2 hl-- hl++ hr++ hr-- h3 a02 ve vt vm
```

was used to generate the s -channel diagram with all heavy neutrinos in the propagator, but no light neutrinos.³

Changing the simulation parameters

Each model allows to adjust some parameters and Mad Graph also provides some options for the simulation. The main adjustments can be done by modifying the files in the *Cards*-folder of the output directory. The file *param_card.dat* contains the model parameters including masses and decay widths and *run_card.dat* specifies the detector and collider settings like center of mass energy, parton distribution function and detector cuts. Further settings can be made in other files like *plot_card.dat*. For example, for our simulations we turned off the parton distribution function by setting

```
0 = lpp1
0 = lpp2
```

in *run_card.dat*.

³ More precisely, the allowed helicities had to be adjusted as explained below. In that way, the resulting interaction included only the desired λ diagram.

Advanced settings: modifying the python scripts

Mad Graph is written in Python and allows the advanced user to modify its routines. One possibility given is to remove certain helicities for the outgoing particles, thus restricting them to have the helicities that are desired by the user. To do this, the files *matrix1.f*⁴ in the subfolders *SubProcesses/P1_cxcx_dxdxmem*⁵ in the output directory have to be modified.

The authors of [53, 57, 58] explain how the Python script works and how to change the helicity amplitudes. Basically lines like

```
DATA (NHEL(I, 2), I=1,6) / 1,-1,-1, 1,-1, 1/
```

correspond to the final state helicities +1, -1, -1, +1, -1 and +1, for the outgoing particles respectively. Here, the order is given in one of the first lines of the file, e.g.

```
C Process: d c~ > u d~ e- e- WEIGHTED<=8 $$ w- w2- w+ w2+ / hp2 z
```

Removing or commenting these lines by adding a *C* in front of it, will exclude the corresponding outcome from the calculation. This possibility was used to restrict the simulations for this thesis in order to reproduce the λ diagram, which consists of two different helicities in the final state electrons.

Note that the source code should only be changed if the user is aware of what he is doing. For example in certain cases the procedure above would require to change the number in the following line

```
DATA IDEN/72/
```

which specifies the averaging factor needed for example when the colour of quarks involved in the interaction is important.

Evaluating the output

Mad Graph not only provides the cross section of the simulated processes. It furthermore gives a sample of events, that is of the in- and outgoing, as well as intermediate on-shell particles. The desired sample number can be specified in the *run_card.dat*

⁴ Further files like *matrix2.f* etc. could be present, depending on the structure of the specified interaction.

⁵ Each amplitude contributing to the interaction is stored in one folder called *P1_cxcx_dxdxmem* or similarly.

via the parameter *nevents* before starting the simulation.⁶ After the simulation is finished, the events are stored in the file `Events/run_01/unweighted_events.lhe.gz` as Les Houches event files. It contains all parameters of the simulation, as well as the samples. The interesting data is given as tables (see Figure C.1 for an example): Each line corresponds to one particle and the following information are encoded in the rows:

row(s)	1	2	3 & 4	5 & 6	
information	particle type	incoming particle (−1)		mother particles	color charge
	7-9	10	11	12	13
	momentum	energy	mass	unknown	helicity

```
<event>
6 1 0.2196600E-14 0.3230295E+03 0.7818600E-02 0.1293390E+00
3 -1 0 0 501 0 0.00000000000E+00 0.00000000000E+00 0.52755350067E+03 0.52755351034E+03 0.10100000000E+00 0. -1.
3 -1 0 0 502 0 0.00000000000E+00 0.00000000000E+00 -0.55140645962E+03 0.55140646887E+03 0.10100000000E+00 0. 1.
4 1 1 2 501 0 -0.20190276374E+02 0.18431385770E+02 0.13702543647E+03 0.13973169426E+03 0.12700000000E+01 0. -1.
4 1 1 2 502 0 0.11399924813E+03 -0.31360567900E+03 -0.41137397642E+03 0.52969284671E+03 0.12700000000E+01 0. 1.
11 1 1 2 0 0 -0.11347694131E+03 0.24954313752E+03 0.20717629832E+03 0.34361433654E+03 0.51100000000E-03 0. 1.
11 1 1 2 0 0 0.19667969554E+02 0.45631155717E+02 0.43319282677E+02 0.65921101708E+02 0.51100000000E-03 0. -1.
<mgrwt>
<rscale> 0 0.94023864E+02</rscale>
<asrwt></asrwt>
<pdfwrt beam="1"> 1 3 0.81162078E-01 0.27367428E+02</pdfwrt>
<pdfwrt beam="2"> 1 3 0.84831764E-01 0.32302951E+03</pdfwrt>
<totfact> 0.43261442E+00</totfact>
</mgrwt>
</event>
<event>
```

Fig. C.1 – Example *lhe* file containing the simulated particle sample.

The data then can be processed in a user defined way. The author of [55] gives examples using Mathematica and provides routines for this.

C.2 The model file for the Left Right symmetric model

Our studies have been carried out in the framework of the Left Right symmetric model. In particular it was important to be able to simulate different neutrino mixing matrices given by Equation (2.59) as

$$W = \begin{pmatrix} V_L^\nu \\ V_R^\nu \end{pmatrix} = \begin{pmatrix} U & S \\ T & V \end{pmatrix} = \begin{pmatrix} 1 - \frac{1}{2}RR^\dagger & R \\ -R^\dagger & 1 - \frac{1}{2}R^\dagger R \end{pmatrix} \begin{pmatrix} U_L & 0 \\ 0 & U_R \end{pmatrix}, \quad (\text{C.1})$$

with R being an arbitrary 3×3 complex matrix and U_L and U_R being PMNS-like.

The model file we used was is explained by their authors in [56]; it is based on the treatment of the LRSM in [29]. Unfortunately it implements only a very limited way of

⁶ The default is 10.000. It is recommended not to use a sample number much larger than 50.000 by the developers of Mad Graph. It results in long-during simulations.

neutrino mixing, the possible parameters given in the model file allowed for the following neutrino mixing matrix with real entries:

$$W = \begin{pmatrix} V_L^\nu \\ V_R^\nu \end{pmatrix} = \begin{pmatrix} U_L & V \\ -V & \mathbb{1} \end{pmatrix}, \quad V = \begin{pmatrix} VK_e & 0 & 0 \\ 0 & VK_\mu & 0 \\ 0 & 0 & VK_\tau \end{pmatrix}. \quad (\text{C.2})$$

Thus we modified the file to implement the full neutrino mixing as given in Equation (C.1). Therefore we removed the parameters VK_e , VK_μ and VK_τ and added 18 parameters for the complex matrix R and 4 parameters for the matrix U_R instead. For reproductive purpose, we list the lines that we removed in C.1 and the new lines and modified lines are shown in C.2 and C.2, respectively. The model file was compiled by use of FeynRules [54].

Code C.1 – Modifications of the MLRSM model file: removed code

```
VKe == {ParameterType -> External, BlockName -> KLRBLOCK,
  ↪ OrderBlock -> 1, Definitions -> {VKe ->
  ↪ Sqrt[0.00001]}, TeX -> Subscript[KLRmix, e],
  ↪ Description -> "Lepton mixing parameter e"},
VKmu == {ParameterType -> External, BlockName -> KLRBLOCK,
  ↪ OrderBlock -> 2, Definitions -> {VKmu ->
  ↪ Sqrt[0.00001]}, TeX -> Subscript[KLRmix, mu],
  ↪ Description -> "Lepton mixing parameter mu"},
VKta == {ParameterType -> External, BlockName -> KLRBLOCK,
  ↪ OrderBlock -> 3, Definitions -> {VKta ->
  ↪ Sqrt[0.00001]}, TeX -> Subscript[KLRmix, ta],
  ↪ Description -> "Lepton mixing parameter ta"},
```

Code C.2 – Modifications of the MLRSM model file: additional code

```
sR12 == {ParameterType -> External, BlockName ->
  ↪ RPMNSBLOCK, OrderBlock -> 1, Value -> 0.549898, TeX ->
  ↪ Subscript[sR, 12], Description -> "sR12"},
sR23 == {ParameterType -> External, BlockName ->
  ↪ RPMNSBLOCK, OrderBlock -> 2, Value -> 0.642788, TeX ->
  ↪ Subscript[sR, 23], Description -> "sR23"},
sR13 == {ParameterType -> External, BlockName ->
  ↪ RPMNSBLOCK, OrderBlock -> 3, Value -> 0.150571, TeX ->
  ↪ Subscript[sR, 13], Description -> "sR13"},
CPR == {ParameterType -> External, BlockName ->
  ↪ RPMNSBLOCK, OrderBlock -> 4, Value -> 0, TeX ->
  ↪ delta_R, Description -> "CP del R"},
```

```

rR11 == {ParameterType -> External , BlockName -> KLRBLOCK,
  ⇨ OrderBlock -> 1, Value -> 0, TeX -> Subscript[rKLRmix,
  ⇨ 11], Description -> "Left - Right - Mixing - Matrix
  ⇨ (real part)"},
rR12 == {ParameterType -> External , BlockName -> KLRBLOCK,
  ⇨ OrderBlock -> 2, Value -> 0, TeX -> Subscript[rKLRmix,
  ⇨ 12], Description -> "Left - Right - Mixing - Matrix
  ⇨ (real part)"},
rR13 == {ParameterType -> External , BlockName -> KLRBLOCK,
  ⇨ OrderBlock -> 3, Value -> 0, TeX -> Subscript[rKLRmix,
  ⇨ 13], Description -> "Left - Right - Mixing - Matrix
  ⇨ (real part)"},
rR21 == {ParameterType -> External , BlockName -> KLRBLOCK,
  ⇨ OrderBlock -> 4, Value -> 0, TeX -> Subscript[rKLRmix,
  ⇨ 21], Description -> "Left - Right - Mixing - Matrix
  ⇨ (real part)"},
rR22 == {ParameterType -> External , BlockName -> KLRBLOCK,
  ⇨ OrderBlock -> 5, Value -> 0, TeX -> Subscript[rKLRmix,
  ⇨ 22], Description -> "Left - Right - Mixing - Matrix
  ⇨ (real part)"},
rR23 == {ParameterType -> External , BlockName -> KLRBLOCK,
  ⇨ OrderBlock -> 6, Value -> 0, TeX -> Subscript[rKLRmix,
  ⇨ 23], Description -> "Left - Right - Mixing - Matrix
  ⇨ (real part)"},
rR31 == {ParameterType -> External , BlockName -> KLRBLOCK,
  ⇨ OrderBlock -> 7, Value -> 0, TeX -> Subscript[rKLRmix,
  ⇨ 31], Description -> "Left - Right - Mixing - Matrix
  ⇨ (real part)"},
rR32 == {ParameterType -> External , BlockName -> KLRBLOCK,
  ⇨ OrderBlock -> 8, Value -> 0, TeX -> Subscript[rKLRmix,
  ⇨ 32], Description -> "Left - Right - Mixing - Matrix
  ⇨ (real part)"},
rR33 == {ParameterType -> External , BlockName -> KLRBLOCK,
  ⇨ OrderBlock -> 9, Value -> 0, TeX -> Subscript[rKLRmix,
  ⇨ 33], Description -> "Left - Right - Mixing - Matrix
  ⇨ (real part)"},
iR11 == {ParameterType -> External , BlockName -> KLRBLOCK,
  ⇨ OrderBlock -> 10, Value -> 0, TeX ->
  ⇨ Subscript[iKLRmix, 11], Description -> "Left - Right
  ⇨ - Mixing - Matrix (imaginary part)"},
iR12 == {ParameterType -> External , BlockName -> KLRBLOCK,
  ⇨ OrderBlock -> 11, Value -> 0, TeX ->

```

```

    ↪ Subscript[iKLRmix, 12], Description → "Left - Right
    ↪ - Mixing - Matrix (imaginary part)"}},
iR13 == {ParameterType → External, BlockName → KLRBLOCK,
    ↪ OrderBlock → 12, Value → 0, TeX →
    ↪ Subscript[iKLRmix, 13], Description → "Left - Right
    ↪ - Mixing - Matrix (imaginary part)"}},
iR21 == {ParameterType → External, BlockName → KLRBLOCK,
    ↪ OrderBlock → 13, Value → 0, TeX →
    ↪ Subscript[iKLRmix, 21], Description → "Left - Right
    ↪ - Mixing - Matrix (imaginary part)"}},
iR22 == {ParameterType → External, BlockName → KLRBLOCK,
    ↪ OrderBlock → 14, Value → 0, TeX →
    ↪ Subscript[iKLRmix, 22], Description → "Left - Right
    ↪ - Mixing - Matrix (imaginary part)"}},
iR23 == {ParameterType → External, BlockName → KLRBLOCK,
    ↪ OrderBlock → 15, Value → 0, TeX →
    ↪ Subscript[iKLRmix, 23], Description → "Left - Right
    ↪ - Mixing - Matrix (imaginary part)"}},
iR31 == {ParameterType → External, BlockName → KLRBLOCK,
    ↪ OrderBlock → 16, Value → 0, TeX →
    ↪ Subscript[iKLRmix, 31], Description → "Left - Right
    ↪ - Mixing - Matrix (imaginary part)"}},
iR32 == {ParameterType → External, BlockName → KLRBLOCK,
    ↪ OrderBlock → 17, Value → 0, TeX →
    ↪ Subscript[iKLRmix, 32], Description → "Left - Right
    ↪ - Mixing - Matrix (imaginary part)"}},
iR33 == {ParameterType → External, BlockName → KLRBLOCK,
    ↪ OrderBlock → 18, Value → 0, TeX →
    ↪ Subscript[iKLRmix, 33], Description → "Left - Right
    ↪ - Mixing - Matrix (imaginary part)"}},

```

Code C.3 – Modifications of the MLRSM model file: modified code

```

KL == {
  ParameterType → Internal,
  Indices       → {Index[Gen2], Index[Generation]},
  Value        → {
    KL[1,1] → (1 + (-(((−I)*iR11 + rR11)*(I*iR11 +
    ↪ rR11)) − ((−I)*iR12 + rR12)*(I*iR12 + rR12) −
    ↪ ((−I)*iR13 + rR13)*(I*iR13 + rR13))/2)*Sqrt[1
    ↪ − sL12^2]*Sqrt[1 − sL13^2] + ((−(((−I)*iR11 +
    ↪ rR11)*(I*iR21 + rR21)) − ((−I)*iR12 +
    ↪ rR12)*(I*iR22 + rR22) − ((−I)*iR13 +

```

$$\begin{aligned}
&\hookrightarrow rR13) * (I * iR23 + rR23)) * (- (sL12 * Sqrt[1 - \\
&\hookrightarrow sL23 ^ 2]) - Sqrt[1 - \\
&\hookrightarrow sL12 ^ 2] * sL13 * sL23 * (Cos[CPL] - I * Sin[CPL])) / 2 \\
&\hookrightarrow + ((- (((- I) * iR11 + rR11) * (I * iR31 + rR31)) - \\
&\hookrightarrow ((- I) * iR12 + rR12) * (I * iR32 + rR32) - \\
&\hookrightarrow ((- I) * iR13 + rR13) * (I * iR33 + rR33)) * (sL12 * sL23 \\
&\hookrightarrow - Sqrt[1 - sL12 ^ 2] * sL13 * Sqrt[1 - \\
&\hookrightarrow sL23 ^ 2] * (Cos[CPL] - I * Sin[CPL])) / 2 ,
\end{aligned}$$

$$\begin{aligned}
KL[1,2] \rightarrow &((- ((I * iR11 + rR11) * ((- I) * iR21 + rR21)) \\
&\hookrightarrow - (I * iR12 + rR12) * ((- I) * iR22 + rR22) - (I * iR13 \\
&\hookrightarrow + rR13) * ((- I) * iR23 + rR23)) * Sqrt[1 - \\
&\hookrightarrow sL12 ^ 2] * Sqrt[1 - sL13 ^ 2]) / 2 + (1 + \\
&\hookrightarrow (- (((- I) * iR21 + rR21) * (I * iR21 + rR21)) - \\
&\hookrightarrow ((- I) * iR22 + rR22) * (I * iR22 + rR22) - \\
&\hookrightarrow ((- I) * iR23 + rR23) * (I * iR23 + \\
&\hookrightarrow rR23)) / 2) * (- (sL12 * Sqrt[1 - sL23 ^ 2]) - Sqrt[1 - \\
&\hookrightarrow sL12 ^ 2] * sL13 * sL23 * (Cos[CPL] - I * Sin[CPL])) + \\
&\hookrightarrow (- (((- I) * iR21 + rR21) * (I * iR31 + rR31)) - \\
&\hookrightarrow ((- I) * iR22 + rR22) * (I * iR32 + rR32) - \\
&\hookrightarrow ((- I) * iR23 + rR23) * (I * iR33 + rR33)) * (sL12 * sL23 \\
&\hookrightarrow - Sqrt[1 - sL12 ^ 2] * sL13 * Sqrt[1 - \\
&\hookrightarrow sL23 ^ 2] * (Cos[CPL] - I * Sin[CPL])) / 2 ,
\end{aligned}$$

$$\begin{aligned}
KL[1,3] \rightarrow &((- ((I * iR11 + rR11) * ((- I) * iR31 + rR31)) \\
&\hookrightarrow - (I * iR12 + rR12) * ((- I) * iR32 + rR32) - (I * iR13 \\
&\hookrightarrow + rR13) * ((- I) * iR33 + rR33)) * Sqrt[1 - \\
&\hookrightarrow sL12 ^ 2] * Sqrt[1 - sL13 ^ 2]) / 2 + ((- ((I * iR21 + \\
&\hookrightarrow rR21) * ((- I) * iR31 + rR31)) - (I * iR22 + \\
&\hookrightarrow rR22) * ((- I) * iR32 + rR32) - (I * iR23 + \\
&\hookrightarrow rR23) * ((- I) * iR33 + rR33)) * (- (sL12 * Sqrt[1 - \\
&\hookrightarrow sL23 ^ 2]) - Sqrt[1 - \\
&\hookrightarrow sL12 ^ 2] * sL13 * sL23 * (Cos[CPL] - I * Sin[CPL])) / 2 \\
&\hookrightarrow + (1 + (- (((- I) * iR31 + rR31) * (I * iR31 + rR31)) \\
&\hookrightarrow - ((- I) * iR32 + rR32) * (I * iR32 + rR32) - \\
&\hookrightarrow ((- I) * iR33 + rR33) * (I * iR33 + \\
&\hookrightarrow rR33)) / 2) * (sL12 * sL23 - Sqrt[1 - \\
&\hookrightarrow sL12 ^ 2] * sL13 * Sqrt[1 - sL23 ^ 2] * (Cos[CPL] - \\
&\hookrightarrow I * Sin[CPL])) ,
\end{aligned}$$

$$\begin{aligned}
KL[2,1] \rightarrow &(1 + (- (((- I) * iR11 + rR11) * (I * iR11 + \\
&\hookrightarrow rR11)) - ((- I) * iR12 + rR12) * (I * iR12 + rR12) -
\end{aligned}$$

$$\begin{aligned}
&\hookrightarrow ((-I)^* iR13 + rR13) * (I^* iR13 + \\
&\hookrightarrow rR13) / 2) * sL12 * Sqrt[1 - sL13^2] + \\
&\hookrightarrow (((-I)^* iR11 + rR11) * (I^* iR21 + rR21)) - \\
&\hookrightarrow ((-I)^* iR12 + rR12) * (I^* iR22 + rR22) - \\
&\hookrightarrow ((-I)^* iR13 + rR13) * (I^* iR23 + rR23)) * (Sqrt[1 - \\
&\hookrightarrow sL12^2] * Sqrt[1 - sL23^2] - \\
&\hookrightarrow sL12 * sL13 * sL23 * (Cos[CPL] - I * Sin[CPL])) / 2 + \\
&\hookrightarrow (((-I)^* iR11 + rR11) * (I^* iR31 + rR31)) - \\
&\hookrightarrow ((-I)^* iR12 + rR12) * (I^* iR32 + rR32) - \\
&\hookrightarrow ((-I)^* iR13 + rR13) * (I^* iR33 + rR33)) * (- (Sqrt[1 \\
&\hookrightarrow - sL12^2] * sL23) - sL12 * sL13 * Sqrt[1 - \\
&\hookrightarrow sL23^2] * (Cos[CPL] - I * Sin[CPL])) / 2,
\end{aligned}$$

$$\begin{aligned}
KL[2,2] \rightarrow &(((I^* iR11 + rR11) * ((-I)^* iR21 + rR21)) \\
&\hookrightarrow - (I^* iR12 + rR12) * ((-I)^* iR22 + rR22) - (I^* iR13 \\
&\hookrightarrow + rR13) * ((-I)^* iR23 + rR23)) * sL12 * Sqrt[1 - \\
&\hookrightarrow sL13^2] / 2 + (1 + (-(((-I)^* iR21 + \\
&\hookrightarrow rR21) * (I^* iR21 + rR21)) - ((-I)^* iR22 + \\
&\hookrightarrow rR22) * (I^* iR22 + rR22) - ((-I)^* iR23 + \\
&\hookrightarrow rR23) * (I^* iR23 + rR23)) / 2) * (Sqrt[1 - \\
&\hookrightarrow sL12^2] * Sqrt[1 - sL23^2] - \\
&\hookrightarrow sL12 * sL13 * sL23 * (Cos[CPL] - I * Sin[CPL])) + \\
&\hookrightarrow (((-I)^* iR21 + rR21) * (I^* iR31 + rR31)) - \\
&\hookrightarrow ((-I)^* iR22 + rR22) * (I^* iR32 + rR32) - \\
&\hookrightarrow ((-I)^* iR23 + rR23) * (I^* iR33 + rR33)) * (- (Sqrt[1 \\
&\hookrightarrow - sL12^2] * sL23) - sL12 * sL13 * Sqrt[1 - \\
&\hookrightarrow sL23^2] * (Cos[CPL] - I * Sin[CPL])) / 2,
\end{aligned}$$

$$\begin{aligned}
KL[2,3] \rightarrow &(((I^* iR11 + rR11) * ((-I)^* iR31 + rR31)) \\
&\hookrightarrow - (I^* iR12 + rR12) * ((-I)^* iR32 + rR32) - (I^* iR13 \\
&\hookrightarrow + rR13) * ((-I)^* iR33 + rR33)) * sL12 * Sqrt[1 - \\
&\hookrightarrow sL13^2] / 2 + (((-I)^* iR21 + rR21) * ((-I)^* iR31 + \\
&\hookrightarrow rR31)) - (I^* iR22 + rR22) * ((-I)^* iR32 + rR32) - \\
&\hookrightarrow (I^* iR23 + rR23) * ((-I)^* iR33 + rR33)) * (Sqrt[1 - \\
&\hookrightarrow sL12^2] * Sqrt[1 - sL23^2] - \\
&\hookrightarrow sL12 * sL13 * sL23 * (Cos[CPL] - I * Sin[CPL])) / 2 + \\
&\hookrightarrow (1 + (-(((-I)^* iR31 + rR31) * (I^* iR31 + rR31)) - \\
&\hookrightarrow ((-I)^* iR32 + rR32) * (I^* iR32 + rR32) - \\
&\hookrightarrow ((-I)^* iR33 + rR33) * (I^* iR33 + \\
&\hookrightarrow rR33)) / 2) * (- (Sqrt[1 - sL12^2] * sL23) - \\
&\hookrightarrow sL12 * sL13 * Sqrt[1 - sL23^2] * (Cos[CPL] - \\
&\hookrightarrow I * Sin[CPL])),
\end{aligned}$$

$$\begin{aligned}
\text{KL}[3,1] &\rightarrow ((-(((-I)^*iR11 + rR11)^*(I^*iR21 + rR21))) \\
&\hookrightarrow - ((-I)^*iR12 + rR12)^*(I^*iR22 + rR22) - \\
&\hookrightarrow ((-I)^*iR13 + rR13)^*(I^*iR23 + rR23))^* \text{Sqrt}[1 - \\
&\hookrightarrow sL13^2]^*sL23)/2 + ((-(((-I)^*iR11 + \\
&\hookrightarrow rR11)^*(I^*iR31 + rR31)) - ((-I)^*iR12 + \\
&\hookrightarrow rR12)^*(I^*iR32 + rR32) - ((-I)^*iR13 + \\
&\hookrightarrow rR13)^*(I^*iR33 + rR33))^* \text{Sqrt}[1 - sL13^2]^* \text{Sqrt}[1 \\
&\hookrightarrow - sL23^2])/2 + (1 + (-(((-I)^*iR11 + \\
&\hookrightarrow rR11)^*(I^*iR11 + rR11)) - ((-I)^*iR12 + \\
&\hookrightarrow rR12)^*(I^*iR12 + rR12) - ((-I)^*iR13 + \\
&\hookrightarrow rR13)^*(I^*iR13 + rR13))/2)^*sL13*(\text{Cos}[\text{CPL}] + \\
&\hookrightarrow I^*\text{Sin}[\text{CPL}]),
\end{aligned}$$

$$\begin{aligned}
\text{KL}[3,2] &\rightarrow (1 + (-(((-I)^*iR21 + rR21)^*(I^*iR21 + \\
&\hookrightarrow rR21)) - ((-I)^*iR22 + rR22)^*(I^*iR22 + rR22) - \\
&\hookrightarrow ((-I)^*iR23 + rR23)^*(I^*iR23 + rR23))/2)^* \text{Sqrt}[1 \\
&\hookrightarrow - sL13^2]^*sL23 + ((-(((-I)^*iR21 + \\
&\hookrightarrow rR21)^*(I^*iR31 + rR31)) - ((-I)^*iR22 + \\
&\hookrightarrow rR22)^*(I^*iR32 + rR32) - ((-I)^*iR23 + \\
&\hookrightarrow rR23)^*(I^*iR33 + rR33))^* \text{Sqrt}[1 - sL13^2]^* \text{Sqrt}[1 \\
&\hookrightarrow - sL23^2])/2 + ((-((I^*iR11 + rR11)^*((-I)^*iR21 \\
&\hookrightarrow + rR21)) - (I^*iR12 + rR12)^*((-I)^*iR22 + rR22) \\
&\hookrightarrow - (I^*iR13 + rR13)^*((-I)^*iR23 + \\
&\hookrightarrow rR23))^*sL13*(\text{Cos}[\text{CPL}] + I^*\text{Sin}[\text{CPL}]))/2,
\end{aligned}$$

$$\begin{aligned}
\text{KL}[3,3] &\rightarrow ((-((I^*iR21 + rR21)^*((-I)^*iR31 + rR31))) \\
&\hookrightarrow - (I^*iR22 + rR22)^*((-I)^*iR32 + rR32) - (I^*iR23 \\
&\hookrightarrow + rR23)^*((-I)^*iR33 + rR33))^* \text{Sqrt}[1 - \\
&\hookrightarrow sL13^2]^*sL23)/2 + (1 + (-(((-I)^*iR31 + \\
&\hookrightarrow rR31)^*(I^*iR31 + rR31)) - ((-I)^*iR32 + \\
&\hookrightarrow rR32)^*(I^*iR32 + rR32) - ((-I)^*iR33 + \\
&\hookrightarrow rR33)^*(I^*iR33 + rR33))/2)^* \text{Sqrt}[1 - \\
&\hookrightarrow sL13^2]^* \text{Sqrt}[1 - sL23^2] + ((-((I^*iR11 + \\
&\hookrightarrow rR11)^*((-I)^*iR31 + rR31)) - (I^*iR12 + \\
&\hookrightarrow rR12)^*((-I)^*iR32 + rR32) - (I^*iR13 + \\
&\hookrightarrow rR13)^*((-I)^*iR33 + rR33))^*sL13*(\text{Cos}[\text{CPL}] + \\
&\hookrightarrow I^*\text{Sin}[\text{CPL}]))/2,
\end{aligned}$$

$$\begin{aligned}
\text{KL}[4,1] &\rightarrow ((-I)^*iR11 + rR11)^* \text{Sqrt}[1 - \\
&\hookrightarrow sR12^2]^* \text{Sqrt}[1 - sR13^2] + ((-I)^*iR12 + \\
&\hookrightarrow rR12)^*(-(sR12^* \text{Sqrt}[1 - sR23^2]) - \text{Sqrt}[1 -
\end{aligned}$$

$$\begin{aligned}
 &\hookrightarrow sR12^2 * sR13 * sR23 * (\text{Cos}[CPR] - I * \text{Sin}[CPR]) + \\
 &\hookrightarrow ((-I) * iR13 + rR13) * (sR12 * sR23 - \text{Sqrt}[1 - \\
 &\hookrightarrow sR12^2] * sR13 * \text{Sqrt}[1 - sR23^2] * (\text{Cos}[CPR] - \\
 &\hookrightarrow I * \text{Sin}[CPR])),
 \end{aligned}$$

$$\begin{aligned}
 \text{KL}[4,2] &\rightarrow ((-I) * iR21 + rR21) * \text{Sqrt}[1 - \\
 &\hookrightarrow sR12^2] * \text{Sqrt}[1 - sR13^2] + ((-I) * iR22 + \\
 &\hookrightarrow rR22) * (-(sR12 * \text{Sqrt}[1 - sR23^2]) - \text{Sqrt}[1 - \\
 &\hookrightarrow sR12^2] * sR13 * sR23 * (\text{Cos}[CPR] - I * \text{Sin}[CPR])) + \\
 &\hookrightarrow ((-I) * iR23 + rR23) * (sR12 * sR23 - \text{Sqrt}[1 - \\
 &\hookrightarrow sR12^2] * sR13 * \text{Sqrt}[1 - sR23^2] * (\text{Cos}[CPR] - \\
 &\hookrightarrow I * \text{Sin}[CPR])),
 \end{aligned}$$

$$\begin{aligned}
 \text{KL}[4,3] &\rightarrow ((-I) * iR31 + rR31) * \text{Sqrt}[1 - \\
 &\hookrightarrow sR12^2] * \text{Sqrt}[1 - sR13^2] + ((-I) * iR32 + \\
 &\hookrightarrow rR32) * (-(sR12 * \text{Sqrt}[1 - sR23^2]) - \text{Sqrt}[1 - \\
 &\hookrightarrow sR12^2] * sR13 * sR23 * (\text{Cos}[CPR] - I * \text{Sin}[CPR])) + \\
 &\hookrightarrow ((-I) * iR33 + rR33) * (sR12 * sR23 - \text{Sqrt}[1 - \\
 &\hookrightarrow sR12^2] * sR13 * \text{Sqrt}[1 - sR23^2] * (\text{Cos}[CPR] - \\
 &\hookrightarrow I * \text{Sin}[CPR])),
 \end{aligned}$$

$$\begin{aligned}
 \text{KL}[5,1] &\rightarrow ((-I) * iR11 + rR11) * sR12 * \text{Sqrt}[1 - \\
 &\hookrightarrow sR13^2] + ((-I) * iR12 + rR12) * (\text{Sqrt}[1 - \\
 &\hookrightarrow sR12^2] * \text{Sqrt}[1 - sR23^2] - \\
 &\hookrightarrow sR12 * sR13 * sR23 * (\text{Cos}[CPR] - I * \text{Sin}[CPR])) + \\
 &\hookrightarrow ((-I) * iR13 + rR13) * (-(\text{Sqrt}[1 - sR12^2] * sR23) - \\
 &\hookrightarrow sR12 * sR13 * \text{Sqrt}[1 - sR23^2] * (\text{Cos}[CPR] - \\
 &\hookrightarrow I * \text{Sin}[CPR])),
 \end{aligned}$$

$$\begin{aligned}
 \text{KL}[5,2] &\rightarrow ((-I) * iR21 + rR21) * sR12 * \text{Sqrt}[1 - \\
 &\hookrightarrow sR13^2] + ((-I) * iR22 + rR22) * (\text{Sqrt}[1 - \\
 &\hookrightarrow sR12^2] * \text{Sqrt}[1 - sR23^2] - \\
 &\hookrightarrow sR12 * sR13 * sR23 * (\text{Cos}[CPR] - I * \text{Sin}[CPR])) + \\
 &\hookrightarrow ((-I) * iR23 + rR23) * (-(\text{Sqrt}[1 - sR12^2] * sR23) - \\
 &\hookrightarrow sR12 * sR13 * \text{Sqrt}[1 - sR23^2] * (\text{Cos}[CPR] - \\
 &\hookrightarrow I * \text{Sin}[CPR])),
 \end{aligned}$$

$$\begin{aligned}
 \text{KL}[5,3] &\rightarrow ((-I) * iR31 + rR31) * sR12 * \text{Sqrt}[1 - \\
 &\hookrightarrow sR13^2] + ((-I) * iR32 + rR32) * (\text{Sqrt}[1 - \\
 &\hookrightarrow sR12^2] * \text{Sqrt}[1 - sR23^2] - \\
 &\hookrightarrow sR12 * sR13 * sR23 * (\text{Cos}[CPR] - I * \text{Sin}[CPR])) + \\
 &\hookrightarrow ((-I) * iR33 + rR33) * (-(\text{Sqrt}[1 - sR12^2] * sR23) -
 \end{aligned}$$

$$\begin{aligned} &\hookrightarrow sR12 * sR13 * \text{Sqrt}[1 - sR23^2] * (\text{Cos}[CPR] - \\ &\hookrightarrow I * \text{Sin}[CPR]), \end{aligned}$$

$$\begin{aligned} \text{KL}[6,1] &\rightarrow ((-I) * iR12 + rR12) * \text{Sqrt}[1 - \\ &\hookrightarrow sR13^2] * sR23 + ((-I) * iR13 + rR13) * \text{Sqrt}[1 - \\ &\hookrightarrow sR13^2] * \text{Sqrt}[1 - sR23^2] + ((-I) * iR11 + \\ &\hookrightarrow rR11) * sR13 * (\text{Cos}[CPR] + I * \text{Sin}[CPR]), \end{aligned}$$

$$\begin{aligned} \text{KL}[6,2] &\rightarrow ((-I) * iR22 + rR22) * \text{Sqrt}[1 - \\ &\hookrightarrow sR13^2] * sR23 + ((-I) * iR23 + rR23) * \text{Sqrt}[1 - \\ &\hookrightarrow sR13^2] * \text{Sqrt}[1 - sR23^2] + ((-I) * iR21 + \\ &\hookrightarrow rR21) * sR13 * (\text{Cos}[CPR] + I * \text{Sin}[CPR]), \end{aligned}$$

$$\begin{aligned} \text{KL}[6,3] &\rightarrow ((-I) * iR32 + rR32) * \text{Sqrt}[1 - \\ &\hookrightarrow sR13^2] * sR23 + ((-I) * iR33 + rR33) * \text{Sqrt}[1 - \\ &\hookrightarrow sR13^2] * \text{Sqrt}[1 - sR23^2] + ((-I) * iR31 + \\ &\hookrightarrow rR31) * sR13 * (\text{Cos}[CPR] + I * \text{Sin}[CPR]) \\ &\hookrightarrow \}, \end{aligned}$$

```

TeX          -> Superscript[V,KL],
Description -> "Left-handed-leptonic-mixing-Matrix",
KR == {
ParameterType -> Internal,
Indices       -> {Index[Gen2], Index[Generation]},
Value        -> {
  KR[1,1] -> -(((-I) * iR11 + rR11) * Sqrt[1 -
    \hookrightarrow sL12^2] * Sqrt[1 - sL13^2]) - ((-I) * iR21 +
    \hookrightarrow rR21) * (-sL12 * Sqrt[1 - sL23^2]) - Sqrt[1 -
    \hookrightarrow sL12^2] * sL13 * sL23 * (Cos[CPL] + I * Sin[CPL])) -
    \hookrightarrow ((-I) * iR31 + rR31) * (sL12 * sL23 - Sqrt[1 -
    \hookrightarrow sL12^2] * sL13 * Sqrt[1 - sL23^2]) * (Cos[CPL] +
    \hookrightarrow I * Sin[CPL])),
  KR[1,2] -> -(((-I) * iR12 + rR12) * Sqrt[1 -
    \hookrightarrow sL12^2] * Sqrt[1 - sL13^2]) - ((-I) * iR22 +
    \hookrightarrow rR22) * (-sL12 * Sqrt[1 - sL23^2]) - Sqrt[1 -
    \hookrightarrow sL12^2] * sL13 * sL23 * (Cos[CPL] + I * Sin[CPL])) -
    \hookrightarrow ((-I) * iR32 + rR32) * (sL12 * sL23 - Sqrt[1 -
    \hookrightarrow sL12^2] * sL13 * Sqrt[1 - sL23^2]) * (Cos[CPL] +
    \hookrightarrow I * Sin[CPL])),

```

$$\begin{aligned}
 \text{KR}[1,3] &\rightarrow -(((-I) * iR13 + rR13) * \text{Sqrt}[1 - \\
 &\hookrightarrow sL12^2] * \text{Sqrt}[1 - sL13^2]) - ((-I) * iR23 + \\
 &\hookrightarrow rR23) * (-sL12 * \text{Sqrt}[1 - sL23^2]) - \text{Sqrt}[1 - \\
 &\hookrightarrow sL12^2] * sL13 * sL23 * (\text{Cos}[\text{CPL}] + I * \text{Sin}[\text{CPL}]) - \\
 &\hookrightarrow ((-I) * iR33 + rR33) * (sL12 * sL23 - \text{Sqrt}[1 - \\
 &\hookrightarrow sL12^2] * sL13 * \text{Sqrt}[1 - sL23^2]) * (\text{Cos}[\text{CPL}] + \\
 &\hookrightarrow I * \text{Sin}[\text{CPL}]),
 \end{aligned}$$

$$\begin{aligned}
 \text{KR}[2,1] &\rightarrow -(((-I) * iR11 + rR11) * sL12 * \text{Sqrt}[1 - \\
 &\hookrightarrow sL13^2]) - ((-I) * iR21 + rR21) * (\text{Sqrt}[1 - \\
 &\hookrightarrow sL12^2] * \text{Sqrt}[1 - sL23^2] - \\
 &\hookrightarrow sL12 * sL13 * sL23 * (\text{Cos}[\text{CPL}] + I * \text{Sin}[\text{CPL}])) - \\
 &\hookrightarrow ((-I) * iR31 + rR31) * (-\text{Sqrt}[1 - sL12^2] * sL23) - \\
 &\hookrightarrow sL12 * sL13 * \text{Sqrt}[1 - sL23^2] * (\text{Cos}[\text{CPL}] + \\
 &\hookrightarrow I * \text{Sin}[\text{CPL}]),
 \end{aligned}$$

$$\begin{aligned}
 \text{KR}[2,2] &\rightarrow -(((-I) * iR12 + rR12) * sL12 * \text{Sqrt}[1 - \\
 &\hookrightarrow sL13^2]) - ((-I) * iR22 + rR22) * (\text{Sqrt}[1 - \\
 &\hookrightarrow sL12^2] * \text{Sqrt}[1 - sL23^2] - \\
 &\hookrightarrow sL12 * sL13 * sL23 * (\text{Cos}[\text{CPL}] + I * \text{Sin}[\text{CPL}])) - \\
 &\hookrightarrow ((-I) * iR32 + rR32) * (-\text{Sqrt}[1 - sL12^2] * sL23) - \\
 &\hookrightarrow sL12 * sL13 * \text{Sqrt}[1 - sL23^2] * (\text{Cos}[\text{CPL}] + \\
 &\hookrightarrow I * \text{Sin}[\text{CPL}]),
 \end{aligned}$$

$$\begin{aligned}
 \text{KR}[2,3] &\rightarrow -(((-I) * iR13 + rR13) * sL12 * \text{Sqrt}[1 - \\
 &\hookrightarrow sL13^2]) - ((-I) * iR23 + rR23) * (\text{Sqrt}[1 - \\
 &\hookrightarrow sL12^2] * \text{Sqrt}[1 - sL23^2] - \\
 &\hookrightarrow sL12 * sL13 * sL23 * (\text{Cos}[\text{CPL}] + I * \text{Sin}[\text{CPL}])) - \\
 &\hookrightarrow ((-I) * iR33 + rR33) * (-\text{Sqrt}[1 - sL12^2] * sL23) - \\
 &\hookrightarrow sL12 * sL13 * \text{Sqrt}[1 - sL23^2] * (\text{Cos}[\text{CPL}] + \\
 &\hookrightarrow I * \text{Sin}[\text{CPL}]),
 \end{aligned}$$

$$\begin{aligned}
 \text{KR}[3,1] &\rightarrow -(((-I) * iR21 + rR21) * \text{Sqrt}[1 - \\
 &\hookrightarrow sL13^2] * sL23) - ((-I) * iR31 + rR31) * \text{Sqrt}[1 - \\
 &\hookrightarrow sL13^2] * \text{Sqrt}[1 - sL23^2] - ((-I) * iR11 + \\
 &\hookrightarrow rR11) * sL13 * (\text{Cos}[\text{CPL}] - I * \text{Sin}[\text{CPL}]),
 \end{aligned}$$

$$\begin{aligned}
 \text{KR}[3,2] &\rightarrow -(((-I) * iR22 + rR22) * \text{Sqrt}[1 - \\
 &\hookrightarrow sL13^2] * sL23) - ((-I) * iR32 + rR32) * \text{Sqrt}[1 - \\
 &\hookrightarrow sL13^2] * \text{Sqrt}[1 - sL23^2] - ((-I) * iR12 + \\
 &\hookrightarrow rR12) * sL13 * (\text{Cos}[\text{CPL}] - I * \text{Sin}[\text{CPL}]),
 \end{aligned}$$

$$\begin{aligned}
\text{KR}[3,3] &\rightarrow -(((-I) * iR23 + rR23) * \text{Sqrt}[1 - \\
&\hookrightarrow sL13^2] * sL23) - ((-I) * iR33 + rR33) * \text{Sqrt}[1 - \\
&\hookrightarrow sL13^2] * \text{Sqrt}[1 - sL23^2] - ((-I) * iR13 + \\
&\hookrightarrow rR13) * sL13 * (\text{Cos}[\text{CPL}] - I * \text{Sin}[\text{CPL}]), \\
\text{KR}[4,1] &\rightarrow (1 + (-(((-I) * iR11 + rR11) * (I * iR11 + \\
&\hookrightarrow rR11)) - ((-I) * iR21 + rR21) * (I * iR21 + rR21) - \\
&\hookrightarrow ((-I) * iR31 + rR31) * (I * iR31 + rR31)) / 2) * \text{Sqrt}[1 \\
&\hookrightarrow - sR12^2] * \text{Sqrt}[1 - sR13^2] + ((-(((-I) * iR11 + \\
&\hookrightarrow rR11) * (I * iR12 + rR12)) - ((-I) * iR21 + \\
&\hookrightarrow rR21) * (I * iR22 + rR22) - ((-I) * iR31 + \\
&\hookrightarrow rR31) * (I * iR32 + rR32)) * (- (sR12 * \text{Sqrt}[1 - \\
&\hookrightarrow sR23^2]) - \text{Sqrt}[1 - \\
&\hookrightarrow sR12^2] * sR13 * sR23 * (\text{Cos}[\text{CPR}] + I * \text{Sin}[\text{CPR}])) / 2 \\
&\hookrightarrow + ((-(((-I) * iR11 + rR11) * (I * iR13 + rR13)) - \\
&\hookrightarrow ((-I) * iR21 + rR21) * (I * iR23 + rR23) - \\
&\hookrightarrow ((-I) * iR31 + rR31) * (I * iR33 + rR33)) * (sR12 * sR23 \\
&\hookrightarrow - \text{Sqrt}[1 - sR12^2] * sR13 * \text{Sqrt}[1 - \\
&\hookrightarrow sR23^2] * (\text{Cos}[\text{CPR}] + I * \text{Sin}[\text{CPR}])) / 2, \\
\text{KR}[4,2] &\rightarrow ((-((I * iR11 + rR11) * ((-I) * iR12 + rR12)) \\
&\hookrightarrow - (I * iR21 + rR21) * ((-I) * iR22 + rR22) - (I * iR31 \\
&\hookrightarrow + rR31) * ((-I) * iR32 + rR32)) * \text{Sqrt}[1 - \\
&\hookrightarrow sR12^2] * \text{Sqrt}[1 - sR13^2]) / 2 + (1 + \\
&\hookrightarrow (-(((-I) * iR12 + rR12) * (I * iR12 + rR12)) - \\
&\hookrightarrow ((-I) * iR22 + rR22) * (I * iR22 + rR22) - \\
&\hookrightarrow ((-I) * iR32 + rR32) * (I * iR32 + \\
&\hookrightarrow rR32)) / 2) * (- (sR12 * \text{Sqrt}[1 - sR23^2]) - \text{Sqrt}[1 - \\
&\hookrightarrow sR12^2] * sR13 * sR23 * (\text{Cos}[\text{CPR}] + I * \text{Sin}[\text{CPR}])) + \\
&\hookrightarrow ((-(((-I) * iR12 + rR12) * (I * iR13 + rR13)) - \\
&\hookrightarrow ((-I) * iR22 + rR22) * (I * iR23 + rR23) - \\
&\hookrightarrow ((-I) * iR32 + rR32) * (I * iR33 + rR33)) * (sR12 * sR23 \\
&\hookrightarrow - \text{Sqrt}[1 - sR12^2] * sR13 * \text{Sqrt}[1 - \\
&\hookrightarrow sR23^2] * (\text{Cos}[\text{CPR}] + I * \text{Sin}[\text{CPR}])) / 2, \\
\text{KR}[4,3] &\rightarrow ((-((I * iR11 + rR11) * ((-I) * iR13 + rR13)) \\
&\hookrightarrow - (I * iR21 + rR21) * ((-I) * iR23 + rR23) - (I * iR31 \\
&\hookrightarrow + rR31) * ((-I) * iR33 + rR33)) * \text{Sqrt}[1 - \\
&\hookrightarrow sR12^2] * \text{Sqrt}[1 - sR13^2]) / 2 + ((-((I * iR12 + \\
&\hookrightarrow rR12) * ((-I) * iR13 + rR13)) - (I * iR22 + \\
&\hookrightarrow rR22) * ((-I) * iR23 + rR23) - (I * iR32 + \\
&\hookrightarrow rR32) * ((-I) * iR33 + rR33)) * (- (sR12 * \text{Sqrt}[1 -
\end{aligned}$$

$$\begin{aligned}
 &\hookrightarrow sR23^2) - \text{Sqrt}[1 - \\
 &\hookrightarrow sR12^2]^*sR13^*sR23^*(\text{Cos}[CPR] + I*\text{Sin}[CPR]))/2 \\
 &\hookrightarrow + (1 + (-(((-I)^*iR13 + rR13)^*(I*iR13 + rR13))) \\
 &\hookrightarrow - ((-I)^*iR23 + rR23)^*(I*iR23 + rR23) - \\
 &\hookrightarrow ((-I)^*iR33 + rR33)^*(I*iR33 + \\
 &\hookrightarrow rR33))/2)^*(sR12*sR23 - \text{Sqrt}[1 - \\
 &\hookrightarrow sR12^2]^*sR13^*\text{Sqrt}[1 - sR23^2]^*(\text{Cos}[CPR] + \\
 &\hookrightarrow I*\text{Sin}[CPR])),
 \end{aligned}$$

$$\begin{aligned}
 \text{KR}[5,1] \rightarrow &(1 + (-(((-I)^*iR11 + rR11)^*(I*iR11 + \\
 &\hookrightarrow rR11)) - ((-I)^*iR21 + rR21)^*(I*iR21 + rR21) - \\
 &\hookrightarrow ((-I)^*iR31 + rR31)^*(I*iR31 + \\
 &\hookrightarrow rR31))/2)^*sR12^*\text{Sqrt}[1 - sR13^2] + \\
 &\hookrightarrow ((-(((-I)^*iR11 + rR11)^*(I*iR12 + rR12)) - \\
 &\hookrightarrow ((-I)^*iR21 + rR21)^*(I*iR22 + rR22) - \\
 &\hookrightarrow ((-I)^*iR31 + rR31)^*(I*iR32 + rR32))^*(\text{Sqrt}[1 - \\
 &\hookrightarrow sR12^2]^*\text{Sqrt}[1 - sR23^2] - \\
 &\hookrightarrow sR12^*sR13^*sR23^*(\text{Cos}[CPR] + I*\text{Sin}[CPR]))/2 + \\
 &\hookrightarrow ((-(((-I)^*iR11 + rR11)^*(I*iR13 + rR13)) - \\
 &\hookrightarrow ((-I)^*iR21 + rR21)^*(I*iR23 + rR23) - \\
 &\hookrightarrow ((-I)^*iR31 + rR31)^*(I*iR33 + rR33))^*(-(\text{Sqrt}[1 \\
 &\hookrightarrow - sR12^2]^*sR23) - sR12^*sR13^*\text{Sqrt}[1 - \\
 &\hookrightarrow sR23^2]^*(\text{Cos}[CPR] + I*\text{Sin}[CPR]))/2,
 \end{aligned}$$

$$\begin{aligned}
 \text{KR}[5,2] \rightarrow &((-((I*iR11 + rR11)^*((-I)^*iR12 + rR12)) \\
 &\hookrightarrow - (I*iR21 + rR21)^*((-I)^*iR22 + rR22) - (I*iR31 \\
 &\hookrightarrow + rR31)^*((-I)^*iR32 + rR32))^*sR12^*\text{Sqrt}[1 - \\
 &\hookrightarrow sR13^2])/2 + (1 + (-(((-I)^*iR12 + \\
 &\hookrightarrow rR12)^*(I*iR12 + rR12)) - ((-I)^*iR22 + \\
 &\hookrightarrow rR22)^*(I*iR22 + rR22) - ((-I)^*iR32 + \\
 &\hookrightarrow rR32)^*(I*iR32 + rR32))/2)^*(\text{Sqrt}[1 - \\
 &\hookrightarrow sR12^2]^*\text{Sqrt}[1 - sR23^2] - \\
 &\hookrightarrow sR12^*sR13^*sR23^*(\text{Cos}[CPR] + I*\text{Sin}[CPR])) + \\
 &\hookrightarrow ((-(((-I)^*iR12 + rR12)^*(I*iR13 + rR13)) - \\
 &\hookrightarrow ((-I)^*iR22 + rR22)^*(I*iR23 + rR23) - \\
 &\hookrightarrow ((-I)^*iR32 + rR32)^*(I*iR33 + rR33))^*(-(\text{Sqrt}[1 \\
 &\hookrightarrow - sR12^2]^*sR23) - sR12^*sR13^*\text{Sqrt}[1 - \\
 &\hookrightarrow sR23^2]^*(\text{Cos}[CPR] + I*\text{Sin}[CPR]))/2,
 \end{aligned}$$

$$\begin{aligned}
 \text{KR}[5,3] \rightarrow &((-((I*iR11 + rR11)^*((-I)^*iR13 + rR13)) \\
 &\hookrightarrow - (I*iR21 + rR21)^*((-I)^*iR23 + rR23) - (I*iR31 \\
 &\hookrightarrow + rR31)^*((-I)^*iR33 + rR33))^*sR12^*\text{Sqrt}[1 -
 \end{aligned}$$

$$\begin{aligned}
&\hookrightarrow sR13^2)/2 + ((-(I*iR12 + rR12)*((-I)*iR13 + \\
&\hookrightarrow rR13)) - (I*iR22 + rR22)*((-I)*iR23 + rR23) - \\
&\hookrightarrow (I*iR32 + rR32)*((-I)*iR33 + rR33))*(\text{Sqrt}[1 - \\
&\hookrightarrow sR12^2]*\text{Sqrt}[1 - sR23^2] - \\
&\hookrightarrow sR12*sR13*sR23*(\text{Cos}[CPR] + I*\text{Sin}[CPR]))/2 + \\
&\hookrightarrow (1 + (((-I)*iR13 + rR13)*(I*iR13 + rR13)) - \\
&\hookrightarrow ((-I)*iR23 + rR23)*(I*iR23 + rR23) - \\
&\hookrightarrow ((-I)*iR33 + rR33)*(I*iR33 + \\
&\hookrightarrow rR33))/2)*(-\text{Sqrt}[1 - sR12^2]*sR23) - \\
&\hookrightarrow sR12*sR13*\text{Sqrt}[1 - sR23^2]*(\text{Cos}[CPR] + \\
&\hookrightarrow I*\text{Sin}[CPR]),
\end{aligned}$$

$$\begin{aligned}
\text{KR}[6,1] &\rightarrow (((-I)*iR11 + rR11)*(I*iR12 + rR12)) \\
&\hookrightarrow -((-I)*iR21 + rR21)*(I*iR22 + rR22) - \\
&\hookrightarrow ((-I)*iR31 + rR31)*(I*iR32 + rR32))*\text{Sqrt}[1 - \\
&\hookrightarrow sR13^2]*sR23)/2 + (((-I)*iR11 + \\
&\hookrightarrow rR11)*(I*iR13 + rR13)) - ((-I)*iR21 + \\
&\hookrightarrow rR21)*(I*iR23 + rR23) - ((-I)*iR31 + \\
&\hookrightarrow rR31)*(I*iR33 + rR33))*\text{Sqrt}[1 - sR13^2]*\text{Sqrt}[1 \\
&\hookrightarrow -sR23^2])/2 + (1 + (((-I)*iR11 + \\
&\hookrightarrow rR11)*(I*iR11 + rR11)) - ((-I)*iR21 + \\
&\hookrightarrow rR21)*(I*iR21 + rR21) - ((-I)*iR31 + \\
&\hookrightarrow rR31)*(I*iR31 + rR31))/2)*sR13*(\text{Cos}[CPR] - \\
&\hookrightarrow I*\text{Sin}[CPR]),
\end{aligned}$$

$$\begin{aligned}
\text{KR}[6,2] &\rightarrow (1 + (((-I)*iR12 + rR12)*(I*iR12 + \\
&\hookrightarrow rR12)) - ((-I)*iR22 + rR22)*(I*iR22 + rR22) - \\
&\hookrightarrow ((-I)*iR32 + rR32)*(I*iR32 + rR32))/2)*\text{Sqrt}[1 \\
&\hookrightarrow -sR13^2]*sR23 + (((-I)*iR12 + \\
&\hookrightarrow rR12)*(I*iR13 + rR13)) - ((-I)*iR22 + \\
&\hookrightarrow rR22)*(I*iR23 + rR23) - ((-I)*iR32 + \\
&\hookrightarrow rR32)*(I*iR33 + rR33))*\text{Sqrt}[1 - sR13^2]*\text{Sqrt}[1 \\
&\hookrightarrow -sR23^2])/2 + (((I*iR11 + rR11)*((-I)*iR12 \\
&\hookrightarrow + rR12)) - (I*iR21 + rR21)*((-I)*iR22 + rR22) \\
&\hookrightarrow - (I*iR31 + rR31)*((-I)*iR32 + \\
&\hookrightarrow rR32))*sR13*(\text{Cos}[CPR] - I*\text{Sin}[CPR])/2,
\end{aligned}$$

$$\begin{aligned}
\text{KR}[6,3] &\rightarrow (((-I)*iR12 + rR12)*((-I)*iR13 + rR13)) \\
&\hookrightarrow - (I*iR22 + rR22)*((-I)*iR23 + rR23) - (I*iR32 \\
&\hookrightarrow + rR32)*((-I)*iR33 + rR33))*\text{Sqrt}[1 - \\
&\hookrightarrow sR13^2]*sR23)/2 + (1 + (((-I)*iR13 + \\
&\hookrightarrow rR13)*(I*iR13 + rR13)) - ((-I)*iR23 +
\end{aligned}$$

$$\begin{aligned}
 &\hookrightarrow rR23) * (I * iR23 + rR23) - ((-I) * iR33 + \\
 &\hookrightarrow rR33) * (I * iR33 + rR33) / 2) * \text{Sqrt}[1 - \\
 &\hookrightarrow sR13^2] * \text{Sqrt}[1 - sR23^2] + ((-((I * iR11 + \\
 &\hookrightarrow rR11) * ((-I) * iR13 + rR13)) - (I * iR21 + \\
 &\hookrightarrow rR21) * ((-I) * iR23 + rR23) - (I * iR31 + \\
 &\hookrightarrow rR31) * ((-I) * iR33 + rR33)) * sR13 * (\text{Cos}[CPR] - \\
 &\hookrightarrow I * \text{Sin}[CPR]) / 2\},
 \end{aligned}$$

TeX \rightarrow Superscript[V,KR],
 Description \rightarrow "Right-handed-leptonic-mixing-Matrix"

Bibliography

- [1] The CMS Collaboration. “Observation of a new boson at a mass of 125 GeV with the CMS experiment at the LHC”. In: (July 2012). DOI: 10.1016/j.physletb.2012.08.021. arXiv: 1207.7235.
- [2] The ATLAS The ATLAS Collaboration. “Observation of a new particle in the search for the Standard Model Higgs boson with the ATLAS detector at the LHC”. In: (July 2012). DOI: 10.1016/j.physletb.2012.08.020. arXiv: 1207.7214.
- [3] *The 1979 Nobel Prize in Physics - Press Release*. [Online; accessed 02-March-2017]. 1979. URL: http://www.nobelprize.org/nobel_prizes/physics/laureates/1979/press.html.
- [4] M. Goldhaber, L. Grodzins, and A. W. Sunyar. “Helicity of Neutrinos”. In: *Phys. Rev.* 109 (3 Feb. 1958), pp. 1015–1017. DOI: 10.1103/PhysRev.109.1015.
- [5] John N. Bahcall. “Solar Neutrinos”. In: *Phys. Rev. Lett.* 17 (7 Aug. 1966), pp. 398–401. DOI: 10.1103/PhysRevLett.17.398.
- [6] J.N. Bahcall. “The solar neutrino problem”. In: *Nuclear Instruments and Methods* 110 (1973), pp. 381–384. ISSN: 0029-554X. DOI: [http://dx.doi.org/10.1016/0029-554X\(73\)90715-5](http://dx.doi.org/10.1016/0029-554X(73)90715-5).
- [7] Y. Fukuda et al. “Measurements of the solar neutrino flux from Super-Kamiokande’s first 300 days”. In: *Phys. Rev. Lett.* 81 (1998). [Erratum: *Phys. Rev. Lett.* 81,4279(1998)], pp. 1158–1162. DOI: 10.1103/PhysRevLett.81.1158. arXiv: hep-ex/9805021 [hep-ex].
- [8] S. Abe et al. “Precision Measurement of Neutrino Oscillation Parameters with KamLAND”. In: *Phys. Rev. Lett.* 100 (22 June 2008), p. 221803. DOI: 10.1103/PhysRevLett.100.221803.
- [9] The KamLAND Collaboration. “Constraints on θ_{13} from A Three-Flavor Oscillation Analysis of Reactor Antineutrinos at KamLAND”. In: (2010). DOI: 10.1103/PhysRevD.83.052002. eprint: arXiv:1009.4771.
- [10] K2K Collaboration and M. H. Ahn. “Measurement of Neutrino Oscillation by the K2K Experiment”. In: (2006). DOI: 10.1103/PhysRevD.74.072003. eprint: arXiv: hep-ex/0606032.
- [11] B. Pontecorvo. “Mesonium and anti-mesonium”. In: *Sov. Phys. JETP* 6 (1957). [*Zh. Eksp. Teor. Fiz.* 33,549(1957)], p. 429.

- [12] B. Pontecorvo. “Inverse beta processes and nonconservation of lepton charge”. In: *Sov. Phys. JETP* 7 (1958). [Zh. Eksp. Teor. Fiz.34,247(1957)], pp. 172–173.
- [13] Q. R. Ahmad et al. “Direct Evidence for Neutrino Flavor Transformation from Neutral-Current Interactions in the Sudbury Neutrino Observatory”. In: *Phys. Rev. Lett.* 89 (1 June 2002), p. 011301. DOI: 10.1103/PhysRevLett.89.011301.
- [14] *The 2015 Nobel Prize in Physics - Press Release*. [Online; accessed 18-February-2017]. 2015. URL: http://www.nobelprize.org/nobel_prizes/physics/laureates/2015/press.html.
- [15] Ch. Kraus et al. “Final Results from phase II of the Mainz Neutrino Mass Search in Tritium β Decay”. In: (2004). DOI: 10.1140/epjc/s2005-02139-7. eprint: arXiv:hep-ex/0412056.
- [16] V. M. Lobashev. “Direct search for the neutrino mass in the beta decay of tritium: Status of the “Troitsk ν -mass” experiment”. In: *Physics of Atomic Nuclei* 63.6 (2000), pp. 962–968. ISSN: 1562-692X. DOI: 10.1134/1.855732.
- [17] Steven Weinberg. “Baryon- and Lepton-Nonconserving Processes”. In: *Phys. Rev. Lett.* 43 (21 Nov. 1979), pp. 1566–1570. DOI: 10.1103/PhysRevLett.43.1566.
- [18] F. del Aguila and J. A. Aguilar-Saavedra. “Distinguishing seesaw models at LHC with multi-lepton signals”. In: *Nuclear Physics B* 813.1-2 (2009), pp. 22–90. ISSN: 05503213. DOI: 10.1016/j.nuclphysb.2008.12.029. arXiv: 0808.2468.
- [19] Mattias Blennow et al. “Neutrinoless double beta decay in seesaw models”. In: *Journal of High Energy Physics* 2010.7 (July 2010), p. 96. ISSN: 1029-8479. DOI: 10.1007/JHEP07(2010)096. arXiv: 1005.3240.
- [20] J. D. Vergados, H Ejiri, and F Šimkovic. “Theory of neutrinoless double-beta decay”. In: *Reports on Progress in Physics* 75.10 (2012), p. 106301. ISSN: 0034-4885. DOI: 10.1088/0034-4885/75/10/106301. arXiv: 1205.0649.
- [21] James Barry and Werner Rodejohann. “Lepton number and flavour violation in TeV-scale left-right symmetric theories with large left-right mixing”. In: *Journal of High Energy Physics* 2013.9 (2013). ISSN: 10298479. DOI: 10.1007/JHEP09(2013)153. arXiv: 1303.6324.
- [22] V. Lozza. “The SNO+ Experiment for Neutrinoless Double-Beta Decay”. In: *Nuclear and Particle Physics Proceedings* 273–275 (2016). 37th International Conference on High Energy Physics (ICHEP), pp. 1836–1841. ISSN: 2405-6014. DOI: <http://dx.doi.org/10.1016/j.nuclphysbps.2015.09.296>.
- [23] M. Agostini et al. “Search of Neutrinoless Double Beta Decay with the {GERDA} Experiment”. In: *Nuclear and Particle Physics Proceedings* 273–275 (2016). 37th International Conference on High Energy Physics (ICHEP), pp. 1876–1882. ISSN: 2405-6014. DOI: <http://dx.doi.org/10.1016/j.nuclphysbps.2015.09.303>.

-
- [24] R. Arnold et al. “Probing New Physics Models of Neutrinoless Double Beta Decay with SuperNEMO”. In: (2010). DOI: 10.1140/epjc/s10052-010-1481-5. eprint: arXiv:1005.1241.
- [25] Jogesh C. Pati and Abdus Salam. “Lepton number as the fourth ”color””. In: *Phys. Rev. D* 10 (1 July 1974), pp. 275–289. DOI: 10.1103/PhysRevD.10.275.
- [26] R. N. Mohapatra and J. C. Pati. “”Natural” left-right symmetry”. In: *Phys. Rev. D* 11 (9 May 1975), pp. 2558–2561. DOI: 10.1103/PhysRevD.11.2558.
- [27] G. Senjanovic and R. N. Mohapatra. “Exact left-right symmetry and spontaneous violation of parity”. In: *Phys. Rev. D* 12 (5 Sept. 1975), pp. 1502–1505. DOI: 10.1103/PhysRevD.12.1502.
- [28] Vladimir Tello. “Connections between the high and low energy violation of Lepton and Flavor numbers in the minimal left-right symmetric model”. PhD thesis. SISSA, Trieste, 2012. URL: <http://hdl.handle.net/1963/6272>.
- [29] P. Duka, J. Gluza, and M. Zralek. “Quantization and renormalization of the manifest left-right symmetric model of electroweak interactions”. In: (1999). DOI: 10.1006/aphy.1999.5988. arXiv: 9910279 [hep-ph].
- [30] Johan Alwall et al. “MadGraph 5: Going beyond”. In: *Journal of High Energy Physics* 2011.6 (2011). ISSN: 11266708. DOI: 10.1007/JHEP06(2011)128. arXiv: 1106.0522.
- [31] Masataka Fukugita and T. Yanagida. *Physics of neutrinos. and application to astrophysics ; with 64 tabl.* eng. Physics and astronomy online library. Includes bibliographical references and index. Berlin ; Heidelberg [u.a.]: Springer, 2003, XII, 593 S. ISBN: 3-540-43800-9 and 978-3-540-43800-7.
- [32] Carlo Giunti and Chung Wook Kim. *Fundamentals of neutrino physics and astrophysics.* eng. 1. publ. Oxford [u.a.]: Oxford Univ. Press, 2007, XVI, 710 S. ISBN: 978-0-19-850871-7.
- [33] G. Senjanović. “Neutrino mass: From LHC to grand unification”. In: *Rivista del Nuovo Cimento* 34.1 (2011), pp. 1–68. ISSN: 0393697X. DOI: 10.1393/ncr/i2011-10061-8.
- [34] P. S Bhupal Dev et al. “125 GeV Higgs boson and the type-II seesaw model”. In: *Journal of High Energy Physics* 2013.3 (2013). ISSN: 11266708. DOI: 10.1007/JHEP03(2013)150. arXiv: 1301.3453.
- [35] F. del Aguila et al. “Electroweak constraints on see-saw messengers and their implications for LHC”. In: (June 2008). arXiv: 0806.1023.
- [36] Walter Grimus and Luís Lavoura. “The seesaw mechanism at arbitrary order: disentangling the small scale from the large scale”. In: *Journal of High Energy Physics* 2000.11 (Nov. 2000), pp. 042–042. ISSN: 1029-8479. DOI: 10.1088/1126-6708/2000/11/042. arXiv: 0008179 [hep-ph].

- [37] Tao Han et al. “Lepton Number Violation and W ’ Chiral Couplings at the LHC”. In: (2012), pp. 1–44. DOI: 10.1103/PhysRevD.87.035011. arXiv: 1211.6447.
- [38] Rabindra N. Mohapatra. “Limits on the mass of the right-handed Majorana neutrino”. In: *Phys. Rev. D* 34 (3 Aug. 1986), pp. 909–910. DOI: 10.1103/PhysRevD.34.909.
- [39] Yue Zhang et al. “General CP violation in minimal left-right symmetric model and constraints on the right-handed scale”. In: *Nuclear Physics B* 802.1-2 (2008), pp. 247–279. ISSN: 05503213. DOI: 10.1016/j.nuclphysb.2008.05.019. arXiv: 0712.4218.
- [40] Stefano Bertolini, Alessio Maiezza, and Fabrizio Nesti. “Present and future K and B meson mixing constraints on TeV scale left-right symmetry”. In: *Physical Review D - Particles, Fields, Gravitation and Cosmology* 89.9 (2014). ISSN: 15502368. DOI: 10.1103/PhysRevD.89.095028. arXiv: 1403.7112.
- [41] A. Ibarra, E. Molinaro, and S. T. Petcov. “Low energy signatures of the TeV scale seesaw mechanism”. In: *Physical Review D - Particles, Fields, Gravitation and Cosmology* 84.1 (2011). ISSN: 15507998. DOI: 10.1103/PhysRevD.84.013005. arXiv: 1103.6217.
- [42] A Marrone et al. “Three-neutrino mixing: status and prospects”. In: *Journal of Physics: Conference Series* 718.6 (2016), p. 62042. URL: <http://stacks.iop.org/1742-6596/718/i=6/a=062042>.
- [43] Anupama Atre et al. “The search for heavy Majorana neutrinos”. In: *Journal of High Energy Physics* 2009.05 (2009), pp. 030–030. ISSN: 1029-8479. DOI: 10.1088/1126-6708/2009/05/030. arXiv: 0901.3589.
- [44] Georges Azuelos, K. Benslama, and J. Ferland. “Prospects for the search for a doubly charged Higgs in the left–right symmetric model with ATLAS”. In: *Journal of Physics G: Nuclear and Particle Physics* 32.2 (2006), pp. 73–91. ISSN: 0954-3899. DOI: 10.1088/0954-3899/32/2/002. arXiv: 0503096 [hep-ph].
- [45] F Del Águila, Ja Aguilar-Saavedra, and R Pittau. “Neutrino physics at large colliders”. In: *Journal of Physics: Conference Series* 53.D (2006), pp. 506–527. ISSN: 1742-6588. DOI: 10.1088/1742-6596/53/1/032. arXiv: 0606198 [hep-ph].
- [46] KamLAND-Zen Collaboration. “Search for Majorana Neutrinos near the Inverted Mass Hierarchy Region with KamLAND-Zen”. In: (2016). DOI: 10.1103/PhysRevLett.117.082503. eprint: arXiv:1605.02889.
- [47] Bogdan Povh et al. *Teilchen und Kerne. Eine Einführung in die physikalischen Konzepte*. ger. 9. Aufl. 2014. SpringerLink : Bücher. Berlin, Heidelberg: Springer Spektrum, 2014, Online-Ressource (XII, 467 S. 160 Abb, online resource). ISBN: 978-364-23782-2-5. DOI: 10.1007/978-3-642-37822-5. URL: <http://dx.doi.org/10.1007/978-3-642-37822-5>.

- [48] Francisco Del Aguila, Juan Antonio Aguilar-Saavedra, and Roberto Pittau. “Heavy neutrino signals at large hadron colliders”. In: *Journal of High Energy Physics* 2007.10 (2007), pp. 047–047. ISSN: 1029-8479. DOI: 10.1088/1126-6708/2007/10/047. arXiv: 0703261 [hep-ph].
- [49] P. S Bhupal Dev and R. N. Mohapatra. “Unified Explanation of the $eejj$, Diboson, and Dijet Resonances at the LHC”. In: *Physical Review Letters* 115.18 (2015), pp. 1–7. ISSN: 10797114. DOI: 10.1103/PhysRevLett.115.181803. arXiv: 1508.02277.
- [50] Chien Yi Chen, P. S Bhupal Dev, and R. N. Mohapatra. “Probing heavy-light neutrino mixing in left-right seesaw models at the LHC”. In: *Physical Review D - Particles, Fields, Gravitation and Cosmology* 88.3 (2013), pp. 1–6. ISSN: 15507998. DOI: 10.1103/PhysRevD.88.033014. arXiv: 1306.2342.
- [51] H.E. Haber and G.L. Kane. “The search for supersymmetry: Probing physics beyond the standard model”. In: *Physics Reports* 117.2 (1985), pp. 75–263. ISSN: 0370-1573. DOI: [http://dx.doi.org/10.1016/0370-1573\(85\)90051-1](http://dx.doi.org/10.1016/0370-1573(85)90051-1).
- [52] Michael Edward Peskin and Daniel V. Schroeder. *An introduction to quantum field theory*. eng. Student economy edition. The advanced book program. [Boulder]: Westview Press, a member of the Perseus Books Group, 2016, xxii, 842 Seiten. ISBN: 0-8133-5019-0 and 978-0-8133-5019-6.
- [53] H. Murayama, I. Watanabe, and Kaoru Hagiwara. “HELAS: HELicity amplitude subroutines for Feynman diagram evaluations”. In: (1992). URL: <https://inspirehep.net/record/336604/>.
- [54] Stefan Ask et al. “From Lagrangians to Events: Computer Tutorial at the MC4BSM - 2012 Workshop”. In: (2012), p. 58. arXiv: 1209.0297.
- [55] Flip Tanedo. *Monte Carlo with Madgraph - Personal notes and how-to guide*. <http://www.physics.uci.edu/~tanedo/files/notes/ColliderMadgraph.pdf>; Tools: <http://www.physics.uci.edu/~tanedo/files/code/LHC0Tools.nb>. Aug. 2011.
- [56] Aviad Roitgrund, Gad Eilam, and Shaouly Bar-Shalom. “Implementation of the manifest left-right symmetric model in FeynRules”. In: *Computer Physics Communications* 203 (2015). LRSM model file available from https://drive.google.com/folderview?id=0BxMAGX_T1pi9X0RUZW9tS2RaQ0E&usp=sharing, p. 21. ISSN: 00104655. DOI: 10.1016/j.cpc.2015.12.009. arXiv: 1401.3345.
- [57] Tilman Plehn. *Lectures on LHC physics*. Vol. 886. 2015, pp. 1–340. ISBN: 9783319059419. DOI: 10.1007/978-3-319-05942-6. arXiv: 0910.4182.
- [58] Tilman Plehn. “LHC Phenomenology for Physics Hunters”. In: (2008). arXiv: 0810.2281.

Statement of authorship

Ich versichere, dass ich diese Arbeit selbstständig verfasst habe und keine anderen als die angegebenen Quellen und Hilfsmittel benutzt habe.

I assure, that this work was written independently and no other than the quoted references and tools were used.

Heidelberg, March 7, 2017

.....